MECHANISM OF OXLDL CAUSING CHOP ACTIVATION DURING ER STRESS AND ITS INHIBITION BY MACROPHAGE ANTIOXIDANT 7, 8-DIHYDRONEOPTERIN IN U937 CELLS.

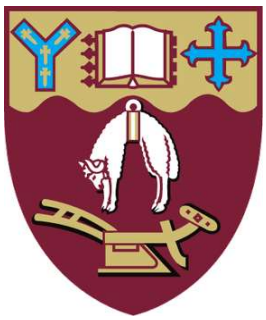

A thesis submitted in partial fulfillment of the requirements for the degree of Master of Science in Cellular and Molecular Biology.

School of Biological Sciences

University of Canterbury

New Zealand

Anurup Balpande

2018

Contents

List of figures

List of Tables

Abstract

Endoplasmic Reticulum stress (ER) and oxidative stress are two related processes which can cause the death of macrophages within the artery wall. Atherosclerosis is a chronic inflammatory disease caused by the abnormal deposition of cholesterol ester filled macrophages within the inner arterial wall so limiting flow of oxygenated blood to various organs of the body. Scavenger receptors such as CD36 are responsible for the absorption of heavily oxidized low density lipoprotein (oxLDL) forming atherosclerotic plaque in the artery wall. The macrophage antioxidant 7, 8-dihydroneopterin downregulate macrophage CD36 so preventing cholesterol esters accumulations in the cells. The ER-stress triggered by free unesterified cholesterol accumulation causes perturbations in ER function resulting in incorrectly folded proteins. ER stress causes activation of three ER proteins resulting in signaling pathways that lower ER stress as a part of Unfolded Protein Response (UPR). However, unresolved ER-stress leads to the activation of the CHOP (C/EBP-homologous protein) protease which causes mitochondrial-mediated cell death. The research investigated the effect of oxLDL causing CHOP activation in U937 cell line and its inhibition by 7, 8-dihydroneopterin.

Thapsigargin (TG), an ER calcium agonist, was found to be a suitable positive control of ER stress-mediated cell death in U937 cells. TG was very cytotoxic causing a 70% loss on cell viability when treated with at only 100 nM. The mitochondrial membrane potential surprisingly increased with TG treatment but at the same time there was a large loss of intact cells which may have masked the loss of mitochondrial potential.

Western blot analysis showed 50 nM TG caused maximum expression of ER-stress marker CHOP in U937 cells. The expression increased with increasing concentrations of TG suggesting the potential of TG in triggering CHOP activation through the unresolved ER-stress-UPR pathway. Cu-oxLDL caused CHOP expression in U937 cells with increasing concentrations with activation occurring within 3 hours with maximum levels seen by 24 hours.

The addition of the macrophage generated antioxidant 7, 8-dihydroneopterin reduced the CHOP expression in U937 cells. Treatment with 200 μM 7, 8-dihydroneopterin reduced the levels of CHOP to 57.67% of control.

ACAT inhibitor (Sandoz 580-35) was expected to trigger ER-stress through the buildup of free cholesterol. Instead the inhibitor caused an increase in cell survival when the U937 cells treated with a sub-lethal dose of oxLDL. The inhibitor prevented cell death at lower concentrations of 10 μg/mL. However, it was observed that the ACAT inhibitor is lethal to cells when given at 25 μg/mL and above concentrations in the absence of oxLDL.

The results confirm that TG and oxLDL induced cell death in U937 cells through ER-stress pathway by CHOP activation. The results showed the potential of macrophage antioxidant 7, 8-dihydroneopterin in downregulating CHOP expression suggesting the suppression of CHOP-induced ER-stress in the cells. The research also demonstrated that ACAT inhibitor at lower concentrations can increase the cell survival rates during oxLDL induced cell death in U937 cells.

Acknowledgements

Firstly, I would like to express my sincere gratitude to my supervisor Associate Professor Steven Gieseg for the continuous support for my master's study and related research, his patience, motivation and deep knowledge. His unwavering enthusiasm for biochemistry and heart research kept me constantly engaged with my research and his personal generosity helped make my time at University of Canterbury enjoyable. His cheerful personality, guidance, support and advice helped me in all the time of research and writing of this thesis. I could not have imagined having a better mentor for my master's study.

I would like to thank Blood Service NZ Riccarton Branch for their continuous supply of blood from haemochromatosis patients, ensuring to maintain human monocyte cultures. A big thank you to plasma donors and nurses at University of Canterbury for LDL supply. It was an honor to be trusted by these donors. I would also like to acknowledge University of Canterbury for providing me exciting research facilities for this project.

My sincere thanks also goes to my co-supervisor and associate supervisors Professor Mark Hampton and Associate Professor Ashley Garrill for their much-appreciated inputs, their insightful comments, encouragements and advices but also for the hard questions which incented me to widen my research from various perspectives. I would also like to take my time to thank Dr. Barry Hock for taking out his valuable time teaching, solving problems related to flow cytometry and western blotting whenever I was in trouble.

My appreciations also extends to my fellow lab members of Plaques and Recreation team; Gregory Baxter-Parker, Hannah Prebble, Sean Cross, Joe Healey, Nina Steyn, Nooshin Ghodsian (Maria), Anthony Yeandle and Cris Kaldor for stimulating discussions and for all the fun we had in last 2 years. With you all I never felt that I am thousand miles away from my home and country, you guys have always been my family here. Thank you for being there during my highlights and lowlights, without your help, advices and suggestions this thesis would have not been possible. A special thank you to Nooshin Ghodsian (Maria) and Gregory Baxter-Parker for sharing their wisdom and expertise in western blotting and culturing human monocytes.

A massive thank you to our wonderful, cheerful, generous and kindhearted 4th floor laboratory technician Craig Galilee for always being there when needed and for providing the continuous and smooth supply of Ethanol throughout my entire research. You have been an inspiration to me when it came to health and safety measures while working and maintaining the laboratory.

Last but not the least I would like to thank my Mom, Dad and my younger brother Swapnil who always encouraged me and helped pursue my dream. Without your unflattering support and endless love during these years I would have never reached this far.

Abbreviations

ΔΨm	Mitochondrial membrane potential
7, 8-DNP	7, 8-Dihydroneopterin
7, 8-DXP	7, 8-Dihydroxanthopterin
7-KC	7-Ketocholesterol
AAPH	2,2'-azobis-2-methyl-propanimidamide, dihydrochloride.
ABCA1/G1	ATP binding cassette A1/G1
ACAT	acyl coenzyme A: cholesterol acyltransferase
acLDL	acetylated low-density lipoprotein
agLDL	Aggregated low-density lipoprotein
ANOVA	Analysis of variance
ANT	Adenine nucleotide translocase
Apaf-1	Apoptotic protease activating factor-1
ApoB100	Apolipoprotein B-100
ATF4	Activating transcription factor 4
ATP	Adenosine triphosphate
BA	Bongkrekic acid
BAK	BCL-2 antagonist killer
BAX	BCL-2 associated X
BCA	Bicinchoninic acid
BCL-2	B-cell lymphoma 2
BH3	BCL-2 homology 3
BID	BCL-2 homology 3 interacting domain
BSA	Bovine serum albumin
C/EBP	CCAAT/enhancer binding protein
CaMKII	Ca2+/calmodulin dependent kinase II
Caspase	Cysteine-aspartic proteases

CCCP	Carbonyl cyanide m-chlorophenyl hydrazone
CD36	Cluster of differentiation 36
CE	Cholesterol ester
CHOP	C/EBP-homologous protein
$CuCl_2$	Copper chloride
Cu-oxLDL	Copper oxidized low-density lipoprotein
cyPD	Cyclophilin D
DDIT3	DNA damage inducible transcript 3
DEX	Dexamethasone
DiOC6(3)	3,3'-Dihexyloxacarbocyanine Iodide
DMSO	Dimethyl sulphoxide
DNA	Deoxyribose nucleic acid
DR	Death receptor
EC	Endothelial cell
EDTA	Ethylenediaminetetraacetic acid
ERAD	Endoplasmic reticulum associated degradation
ERO1α	Endoplasmic reticulum oxidase 1 alpha
ER	Endoplasmic reticulum
FBS	Fetal bovine serum
FC	Free cholesterol
FADD	FAS-associated death domain
GADD153	Growth arrest and DNA damage inducible protein 153
GM-CSF	Granulocyte macrophage-colony stimulating factor
GRP78	Glucose-related protein
GTP	Guanosine-5'-triphosphate
H_20_2	Hydrogen peroxide
HCl	Hydrochloric acid
HDL	High density lipoprotein

HMDM	Human monocyte derived macrophages
HOCl	Hypochlorite
HOCl-oxLDL	Hypochlorite oxidized low density lipoprotein
HRP	Hydrogen peroxidase
HS	Human serum
IgGκ-BP	Immunoglobulin G kappa-binding protein
IMM	Inner mitochondrial membrane
INFγ	Interferon γ
IRE1α	Inositol-requiring enzyme 1 alpha
IP3R	Inositol-1,4,5-triphosphate receptor
KBr	Potassium bromide
KH_2PO_4	Potassium dihydrogen phosphate
LDL	Low density lipoprotein
LOX-1	Lectin-like oxidative low-density lipoprotein-1
LPS	Lipopolysaccharide
M-β-CD	Methyl-beta-cyclodextrin
mLDL	Minimally oxidized low-density lipoprotein
MOMP	Mitochondrial outer membrane permealization
MOPS	3-morpholinopropane-1-sulfonic acid
mRNA	Messenger ribose nucleic acid
MTT	3-[4,5-dimethylthiazol-2-yl]-2,5-diphenyl-tetrazolium bromide
NaCl	Sodium chloride
NADPH	Nicotine adenine dinucleotide phosphate
NaH_2PO_4	Sodium dihydrogen phosphate
NaOH	Sodium hydroxide
NC	Nitrocellulose
NO	Nitrous oxide

NOX	NADPH oxidase
NRF2	Nuclear factor (erythroid-derived2)-like 2
OMM	Outer mitochondrial membrane
oxLDL	Oxidized low density lipoprotein
PBS	Phosphate buffered saline
PDI	Protein disulfide isomerase
PERK	Protein kinase-like ER kinase
PI	Propidium iodide
PMA	phorbol-12-myristate-13-acetate.
PPAR-γ	Peroxisome proliferator activator receptor-gamma
PS	Phosphatidyl serine
PT	Pore transition
PTP	Permeability transition pore
RCT	Reverse cholesterol transport
RIDD	Regulated IRE1-dependent mRNA decay
RNA	Ribose nucleic acid
RNase	Ribonuclease
ROS	Reactive oxygen species
RPMI 1640	Roswell Park Memorial Institute 1640
S 58-035	Sandoz 58-035
SDS	Sodium dodecyl sulphate
SDS-PAGE	Sodium dodecyl sulphate-polyacryl amide gel electrophoresis
SERCA	Sarco/endoplasmic reticulum calcium ATPase
siRNA	Small interfering ribonucleic acid
SMCs	Smooth muscle cells
SP1	Site protease 2
SR-A, B	Scavenger receptor A, B
TBS	Tris buffered saline
TBSM	Tris buffered saline in Milk powder

TG	Thapsigargin
TLR4	Toll-like receptor 4
TMRM	Tetramethylrhodamine methyl ester
TNFα	Tumor necrotic factor α
UPR	Unfolded protein response
UPS	Ubiquitin proteasome system
VDAC	Voltage-dependent anion channel
XBP1	X box-binding protein 1
XBP1s	X box-binding protein 1 spliced

CHAPTER 1

1 INTRODUCTION

1.1 Atherosclerosis

Atherosclerosis is a chronic inflammatory disease caused by the accumulation of cholesterol-esters filled macrophages (atherosclerotic plaque) in the inner arterial wall which limits the flow of oxygenated blood to various organs of the body (Ross, 1999; Shoenfeld, Sherer, & Harats, 2001). The disease pathologically happens to start when the monocytes start migrating into the arterial lumen and differentiate into macrophages (Libby, Ridker, & Maseri, 2002). These macrophages start taking up the oxidized form of low density lipoproteins (oxLDL) through cell surface receptors (called scavenger receptors) (Moore & Freeman, 2006) leading to the formation of foam cells which drive events in the development of atherosclerosis. The interaction of these scavenger receptors and oxLDL also triggers an immune response which induces cytokine secretion, recruiting immune cells infiltrating in the arterial lumen and provoking an inflammatory response (Jiang et al., 2012). The foam cells undergo physiological changes (discussed in 1.1.1) with the progression of atherosclerosis as these scavenger receptors causes macrophages to starts accumulating oxLDL in larger amounts resulting in the hardening of plaque through calcification over time, obstructing the arteries and diminishing the flow of oxygenated blood to various organs of the body (Anderson, 1999) (Libby, 2006; Libby et al., 2002). Hardened plaque not only contains calcium phosphate but also contains lipids, cholesterol, and fatty acids (Libby et al., 2002) (Anderson, 1999) and its position in the arteries distinguishes it in different types (Dobmeyer, Lohrmann, & Feussner, 1996; Stary et al., 1995). Plaque formation characterizes coronary artery disease in the coronary artery which results in angina or chest pain (Hansson, 2005). Carotid artery disease is marked by the build-up of plaque in the carotid artery which can lead to a stroke when ruptured (Sobieszczyk & Beckman, 2006). The peripheral arterial disease is a result of plaque accumulation in arteries supplying blood to legs, arms, pelvis,

etc. (Ouriel, 2001) and chronic kidney disease is caused by plaque development in renal arteries (Schiffrin, Lipman, & Mann, 2007).

1.1.1 Pathogenesis of atherosclerosis

A normal arterial wall is surrounded by the three distinct concentric layers bounded by the arterial lumen. The intima consists of smooth muscle cells (SMCs) and endothelial cells is adjoined by the arterial lumen. The middle layer media is composed of mainly SMCs that are organized in layers depending upon the arterial size. Lastly, the arterial adventitia, the outermost layer typically consists loose matrix of elastin, SMCs, fibroblasts, and collagen.

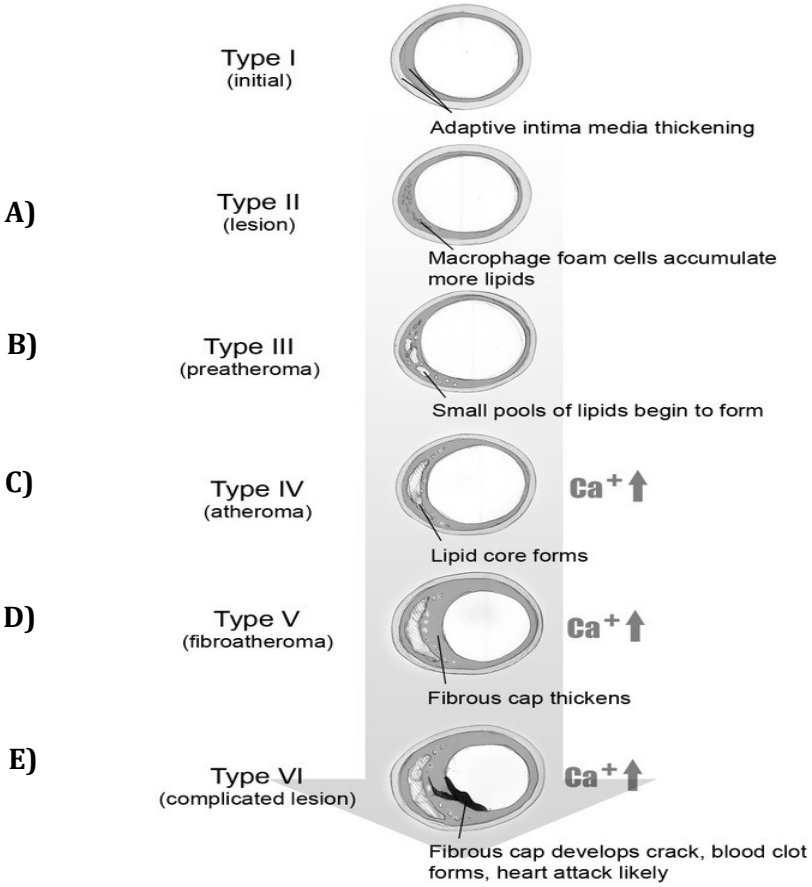

Figure 1: Stages in atherosclerotic plaque formation.

Lesion-prone arterial sites are marked by the intimal thickening which is considered among the first histological changes. Atherosclerotic lesions are demarcated into

different stages depending upon development, and progression of the lesion. The occurrence of lipid-loaded foam cells in the intima of the artery is the peculiarity of atherosclerosis and is referred as type II lesions (Figure 1A). Foam cell formation occurs when the scavenger receptors present on the surface of macrophages gathers modified form of low density lipoproteins (LDL) known as oxLDL (Discussed in 1.1.2) and migrated into the intima. Occurrence of foam cells from the macrophages in the lesson marks the initial event in atherosclerosis (Boullier et al., 2001). As the formation of foam cells continues; the macrophages start developing necrotic core producing type III lesions or preatheroma (Figure 1B) which consist of small pools of lipid. With the progression of the lesion, type III lesion advances to type IV lesion or atheroma (Figure 1C) by separating thin tissue of lipid core from the arterial lumen whereas, Type V lesions or fibroatheroma (Figure 1D) are characterized by the occurrence of fibrous cap thickening. Type VI lesions (Figure 1E) are the matured lesions that often exhibit the framework which is more complicated and is distinguished by the development of calcified fibrous areas.

There have been countless efforts to demystify the complex events related to atherosclerosis advancement which has resulted in the development of three distinct hypotheses; 1) The response–to–injury, 2) The response–to–retention and 3) oxidative modification. These hypotheses are not irreconcilable but are preferably different notions that are essential and adequate to uphold the atherosclerotic lesions enhancement. The response–to–injury hypothesis proposes a primordial step in atherogenesis is endothelial denudation that results in various compensatory counter-responses that modify the normal vascular homeostatic properties (Ross, 1993). William and Tabas suggested Response-to-retention theory in 1995 (Williams & Tabas, 1995) which proposed that plaque development is activated as a result of diffusion and retention of lipoprotein molecules present within the sub-endothelial layer of the intima, binding to proteoglycan chains with high affinity. Long carbohydrate chains of glycosaminoglycans (GAGs) covalently attached to core protein via glycosidic linkages are the classic feature of proteoglycans. The theory lies upon the concept of repeating disaccharide units of GAGs containing negatively charged sulphate or carbohydrate groups attracted to the positively charged lysine groups of ApoB100 resulting in adherance to GAG matrix as the LDL moves through the sub-endothelial space (Evanko,

Raines, Ross, Gold, & Wight, 1998; Libby, Ridker, & Hansson, 2009). Rentention and accumulation of LDL in the intima further causes its oxidative modification by oxidants resulting in its uptake by macrophages via scavenger receptors resulting in foam cell formation. However, oxidative modification hypothesis emphasizes more on the concept that LDL is atherogenic when is taken by the macrophages in the modified form rather than native form by so-called "Scavenger Receptor" pathway (Napoli et al., 1997; Rosenfeld, 1996). During this process the LDL is oxidized to oxLDL and is readily taken up by the scavenger receptors (Discussed in 1.1.2), converting them into cholesterol-loaden foam cells which further carry the process of atherogenesis.

1.1.2 Oxidative low-density lipoproteins as a contributor to cell death

OxLDL is believed to be a major contributor to the death of macrophage cell within the plaque through a combination of factors which include the presence of cytotoxic levels of oxLDL (Moore & Freeman, 2006). OxLDL binding occurs through several receptors present on the surface of macrophages which include Scavenger Receptor–A1, A2 (SR-A1, A2), cluster of differentiation 36 (CD36), scavenger receptor–B (SR-B) and lectin-like oxidized low-density lipoprotein-1 (LOX-1) (Levitan, Volkov, & Subbaiah, 2010) (Figure 2). Among the receptors aforementioned, LOX-1 is a major oxLDL receptor that has been identified in endothelial cells (ECs) (Sawamura et al., 1997) whereas SR-A and CD36 are the main scavenger receptors identified in macrophages that play a critical role in foam cell formation and development of atherosclerotic lesion (Boullier et al., 2001; Collot-Teixeira, Martin, McDermott-Roe, Poston, & McGregor, 2007; Huh, Pearce, Yesner, Schindler, & Silverstein, 1996; Park, 2014).

Since cholesterol levels do not regulate uptake of oxLDL by CD36, therefore the oxLDL taken up by the macrophages gathers a more significant quantity of cholesterol converting them into "foam cells" which in later stages results in plaque formation (Goldstein, Ho, Basu, & Brown, 1979). The appearance of foam cells originating from macrophages or SMCs in atherosclerotic lesions represents the initial event in atherogenesis (Ira Tabas, Williams, & Borén, 2007) (Figure 1). (T. Chang, Chang, & Cheng, 1997). Uptake of oxLDL by the macrophages causes excess cholesterol accumulation

(Moore & Tabas, 2011). This excess cholesterol present in the foam cells undergoes efflux on HDL by ATP binding cassette A1 and G1 (ABCA1 And G1) transporters and is then transported to the liver for further excretion. This process is known as reverse cholesterol transport. 7-ketocholesterol (7-KC), being a major oxysterol in oxLDL, is also known to impair ABCA1 transporter, as a result FC is prevented from moving out of the cell. This causes membrane vesicles which are filled with CE to accumulate in the cytoplasm (Brown & Jessup, 1999).

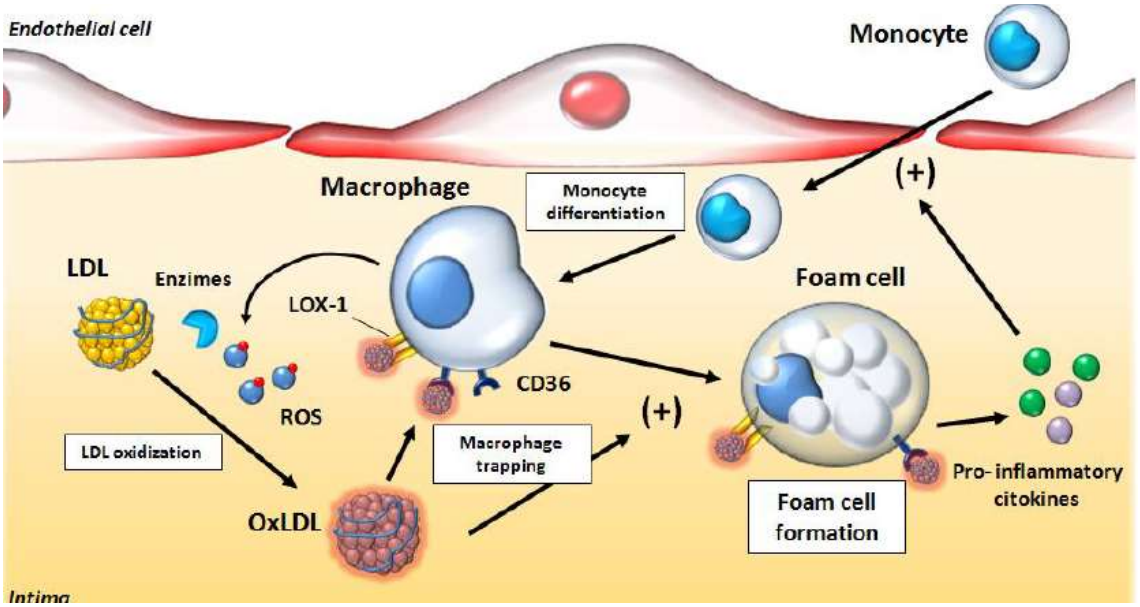

Figure 2: Role of oxLDL in foam cell formation taken from (Kathryn J. Moore, and, & Fisher, 2013)

1.1.3 Role of scavenger receptors in foam cell formation and atherosclerosis.

OxLDL uptake and atherosclerosis progression are mainly driven by CD36 and SR-A therefore; these receptors have been of interest for atherosclerotic studies. OxLDL products such as phospholipids and oxysterols are being generated when oxLDL is internalized by CD36 by the action of lipoxygenase (LPO) (Febbraio, Hajjar, & Silverstein, 2001; Rahaman et al., 2006; Steinberg, 2002). These oxidized lipids generated within the oxLDL also serves as a ligand for nuclear hormone receptor peroxisome proliferator

activated receptor-γ (PPAR-γ), upregulating the expression of CD36 which further facilitates the uptake of oxLDL (Nagy, Tontonoz, Alvarez, Chen, & Evans, 1998; Tontonoz, Nagy, Alvarez, Thomazy, & Evans, 1998). This increases expression of CD36 receptors on the surface of macrophages causes higher uptake of oxLDL and atherosclerotic foam cell formation (Febbraio et al., 2001; Rahaman et al., 2006). A study performed on $Apoe^{-/-}$ mice lacking CD36 demonstrated a reduction in atherosclerotic lesion area by 76% indicating the importance of CD36 mediated oxLDL uptake by macrophages is necessary for foam cell formation and atherosclerotic lesion development (Febbraio et al., 2000).

SR-B1 share high homology and ligand repertoire to that of CD36 (S. Acton et al., 1996; S. L. Acton, Scherer, Lodish, & Krieger, 1994; Webb, De Villiers, Connell, de Beer, & van der Westhuyzen, 1997), however, both the receptors differ in functions of lipid metabolism. CD36 binds oxLDL in large amount leading to macrophage foam cell formation whereas SR-B1, which is mainly present on the liver, play a crucial role in binding high-density lipoproteins (HDL) and reverse cholesterol transport by facilitating cholesterol from and transferring it back to HDL (S. Acton et al., 1996). SR-B1 is expressed in liver, macrophages and steroidogenic tissues such as ovaries, adrenal gland and testis (S. Acton et al., 1996). However, in macrophages SR-B1 mediates the re-uptake of cholesterol esters by inhibiting ATP-binding cassette 1 (ABCA1) facilitated cholesterol efflux (Chen, Silver, Smith, & Tall, 2000; Van Eck, Pennings, Hoekstra, Out, & Van Berkel, 2005) indicating the protective role played by SR-B1 in arterial wall (A. C. Li & Glass, 2002).

LOX-1 has been identified as the first major oxLDL receptor in endothelial cells (Sawamura et al., 1997) and is expressed on macrophages and smooth muscle cells (SMCs) (Draude, Hrboticky, & Lorenz, 1999). LOX-1 is not only expressed in ECs in early stages of atherogenesis but is highly expressed in intimal SMCs and macrophages in carotid atherosclerotic plaque (Kataoka et al., 1999), suggesting the involvement of LOX-1 in endothelial activation and formation of foam cells. LOX-1 is also known to bind mildly oxidized LDL, highly oxidized LDL (such as Cu-oxLDL) and delipidated oxLDL suggesting its capability of binding and recognizing modified forms of oxidized lipoproteins (Levitan et al., 2010). LOX-1 binds oxLDL by activating NADPH oxidase (NOX) leading to the rapid elevation in intracellular ROS such as superoxides, hydrogen peroxide (H_2O_2), and hypochlorite (HOCl). NOX is an important producer of ROS in the macrophages and is

believed to be a principle superoxide-generating enzyme, which is highly essential in redox signalling (Dworakowski, Anilkumar, Zhang, & Shah, 2006). In later stages of atherosclerosis, these ROS reacts with intracellular nitrous oxide (NO) which causes a decrease in NO levels and upregulation of LOX-1; culminating the excess production of ROS (Ou et al., 2010). According to the pathway proposed by (Hong et al., 2014), upregulation of LOX-1 by oxLDL and intracellular NOX levels triggers three ER–stress (Endoplasmic Reticulum–Stress) pathways which further leads to activation of proapoptotic mediators such as CHOP, Bcl-2, and caspase-12 eventually leading to apoptosis in endothelial cells. We hypothesize that oxLDL induction alone is sufficient to induce ER-stress marker CHOP and initiate ER-stress mediated cell death in macrophages.

1.2 Endoplasmic reticulum (ER) and atherosclerosis.

The endoplasmic reticulum is a complex eukaryotic organelle consisting of extended membrane network with supplied machinery for protein folding and maturation. The ER lumen contains higher calcium concentration and dedicated enzymes for protein glycosylation. It facilitates the maintenance and reducing on redox potential that promotes disulfide bond formation for secretory protein maturation. These conditions are essential for optimum function of ER–chaperones such as glucose-related protein 78 (GRP78/BiP) and enzymes such as protein disulphide isomerase (PDI), calnexin, calreticulin, and peptidylprolyl isomerase that are required for protein folding, their transportation, and post-translational modification (Ma & Hendershot, 2004; Tu & Weissman, 2004).

1.2.1 ER-stress and atherosclerosis.

ER function affects the course of atherosclerosis in several ways. The first way involves the disturbances in the homeostatic processes of ER leading to the unfolding of proteins entering ER and forcing the organelle to undergo ER-stress. Upon the induction of ER-stress, the organelle responds by triggering specific measures that ensure the proper folding of proteins by the process known as unfolded protein response (UPR) (See 1.2.2) which is governed by three principal ER-membrane proteins viz. inositol-requiring enzyme 1 α (IRE1α) (see 1.2.2.1), protein kinase-like ER kinase (PERK) (See 1.2.2.2) and

activating transcription factor-6 (ATF-6) (see 1.2.2.3). Altogether these proteins help in reduction of overall protein load and increase the folding capacity of ER, so resolving ER-stress. However, the failure of these transmembrane proteins, due to increased protein load, leads to activation of downstream effectors and apoptotic signals causing cellular death (Discussed in 1.2.3). The second mechanism involves the failure of cholesterol esterase enzyme, acyl-coenzyme A: cholesterol acyltransferase (ACAT). ACAT is a primary enzyme that converts free cholesterol (FC) to cholesterol esters (CE). However, its failure leads to the accumulation of FC into the ER which usually is normally in low cholesterol, so the increasing cholesterol causes ER stress and potential cell death (discussed in 1.2.4).

The disturbances in homeostasis processes such as calcium balance, oxidative stress and chronic inflammation result in the dysfunctioning of ER, which leads to the state in which the protein misfolds or delayed folding in ER by the mechanism known as ER-stress (Hotamisligil, 2010). These stimuli activate various signals that enhance the formation of new proteins to deal with stress and at the same time reducing the load of general protein synthesis (Hetz, Chevet, & Oakes, 2015; Ron & Walter, 2007). This mechanism of activating the series of responses to ensure the correct folding of proteins is termed as UPR (Unfolded Protein Response) (Ron & Walter, 2007). The second mechanism by which the UPR repairs the homeostasis is by the process termed as ER-associated degradation (ERAD) (Meusser, Hirsch, Jarosch, & Sommer, 2005; Travers et al., 2000). ERAD ensures translocation of the unfolded proteins from ER to the cytoplasm. In the cytoplasm, the degradation of these unfolded proteins takes place via ubiquitin-proteasome system (UPS) (Meusser et al., 2005; Travers et al., 2000). Another mechanism by which ERAD carries protein degradation is stimulated is through autophagy (Meusser et al., 2005).

1.2.2 Unfolded Protein Response (UPR) and Transmembrane proteins.

When the endoplasmic reticulum experiences imbalance in the homeostasis processes such as oxidative stress, chronic inflammation and calcium balance, it leads to misfolding of proteins creating stress on endoplasmic reticulum (ER-stress). Corresponding to ER-

stress, the ER membrane proteins triggers series of responses to ensure the correct protein folding thereby reducing the load of misfolded proteins on the endoplasmic reticulum. This mechanism of ensuring and repairing the correct protein folding is termed as unfolded protein response (UPR). The UPR is operated by three main ER resident proteins. **i)** Inositol-requiring enzyme 1 alpha, (IRE1 α) **ii).** Protein Kinase-like ER kinase (PERK) and **iii)** Activating Transcription Factor–6 (ATF-6). These proteins bind to chaperone GRP78/BiP that dwell in ER membrane monitoring the health of ER and ensuring the proteins are folded correctly (Shutong Yao, 2014). However, upon continuous induction of ER–stress, these transmembrane proteins, and their downstream effectors induce cell death at different levels.

1.2.2.1 Inositol–Requiring Enzyme 1 α (IRE1α)

IRE1α, an ER transmembrane protein consists of kinase and endoribonuclease domains (which carries kinase and RNase activities) on its cytosolic surface (Wang et al., 1998). RNA degradation is performed by RNase which reduces the synthesis of proteins by a process known as regulated IRE1–dependent mRNA decay (RIDD) (Hollien & Weissman, 2006). However, RNase activity of IRE1α is sequence-specific under low–activation conditions. They are involved in the regulation of mRNA of specific genes, particularly XBP1 (X box–binding protein 1). Upon the activation of IRE1α, a small intron from XBP1 mRNA gets removed to undergo frameshift which leads to the formation of spliced XBP1 (XBP1s). This splicing is a marker of UPR activation (Cawley, Deegan, Samali, & Gupta, 2011), but besides being a marker it also acts as an essential controller of UPR as it is responsible for activation of number of genes that are transcriptionally needed for reviving protein folding capacity of ER (Acosta-Alvear et al., 2007).

1.2.2.2 Protein kinase–Like ER Kinase (PERK)

PERK is another ER transmembrane protein which participates in UPR by regulating oxidative stress and lowering protein translation. PERK not only phosphorylates and activates transcription factor NRF2 (Nuclear factor (erythroid-derived 2)-like 2) which induces antioxidant proteins (Cullinan et al., 2003), but also helps in phosphorylation of initiation factor 2α(eIF2α) (Harding, Zhang, & Ron, 1999), blocking translation and initiating cell survival by reducing the accumulation of unfolded or misfolded proteins thereby relieving ER stress. However, if eIF2α is inhibited, ATF4 (Activating

Transcription factor 4) which is belongs to CCAAT/enhancer binding protein family (C/EBP), family of transcription factors; is induced, and activates certain genes which functions in protein synthesis and their secretion, amino acid metabolism and transport, and antioxidant stress stimuli (J. Han et al., 2013; Harding et al., 2003). ATF4 also plays a significant role in the induction of cell death through activation of CHOP/GADD153 (C/EBP–homologous protein/Growth Arrest and DNA damage-inducible protein 153) (Discussed in 1.2.3).

1.2.2.3 Activating Transcription Factor–6 (ATF–6)

Activating Transcription Factor–6 (ATF–6) is a third transmembrane ER–protein, but it acts as a transcription factor when cleaved. Upon ER–stress, ATF–6 translocates to Golgi and gets cleaved by proteases Site protease 1 (SP1) and Site protease 2 (SP2) releasing the active form of ATF–6 into the cytosol (Shen, Chen, Hendershot, & Prywes, 2002; Ye et al., 2000). ATF–6 in its active form increases the transcription of XBP1 mRNA which targets IRE1α (Yoshida, Matsui, Yamamoto, Okada, & Mori, 2001).

1.2.3 CHOP and CHOP-mediated apoptosis

CHOP/GADD153 protein expressed by DNA Damage-inducible transcript 3 (DDIT3) gene was a first protein to be identified as a member of CCAAT/enhancer binding proteins (C/EBP) family. CHOP is expressed by ER-resident proteins (Figure 3) with binding sites for ATF–6, ATF–4, and XBPs enclosed within its promoters. These binding sites are highly essential to initiate ER–stress-induced apoptosis through different signalling pathways, which are both mitochondrial-dependent and independent.

CHOP mediates cell death either by altering transcription of genes involved in apoptosis and oxidative stress or by replacing PERK mediated translation inhibition (Marciniak et al., 2004; Oyadomari & Mori, 2004). CHOP initiates apoptotic cell death through different signalling pathways. One mechanism links interaction of CHOP with the members of BCL–2 family proteins which further involves BH3–only proteins (Figure 3). When BH3–only proteins are involved, they further activate BAX and BAK and initiates apoptosis through caspase–12 activation (Timmins et al., 2009).

However, the other mechanism involves the fundamental function of NOX. NOX is a main ROS producer in the macrophages and is believed to be a dominant superoxide-

generating enzyme which is highly essential in redox signalling (Dworakowski et al., 2006). OxLDL triggers NOX activation in macrophages and vasculature enhancing the progression of atherosclerosis (Meyer & Schmitt, 2000; Pongnimitprasert, 2009). NOX facilitates the excess formation of (ROS), favouring oxidative stress and calcium signalling pathways through activation of CHOP–dependent ER–oxidase 1α (ERO1α) and initiating release of calcium through activation of ER calcium channel IP3R1 (Figure 3) (G. Li, Scull, Ozcan, & Tabas, 2010). Later, calcium in the cytoplasm triggers CaMKII (CaMKII is Serine/threonine-specific protein kinase regulated by Ca^{2+}/Calmodulin complex and is essential for calcium homeostasis) which is the calcium-sensing enzyme (Figure 3). CaMKII further activates some downstream apoptotic pathways which include initiation of Fas death receptor and release of apoptogens from mitochondria (Scull & Tabas, 2011). Therefore, NOX plays a critical role in ER–stress-CHOP–IP3R activation–ER–Calcium release–CaMKII activation–NOX activation–oxidative stress, which is a bidirectional pathway. Reduction in peroxide accumulation and apoptosis in NOX2 $^{-/-}$ mice indicated that NOX is centrally involved in oxidative stress and apoptosis under ER–stress conditions (G. Li et al., 2010). NOX activation also causes membrane depolarization resulting in outer membrane permeabilization and releasing pro-apoptotic factors mainly cytochrome c causing mitochondrial-mediated apoptosis in ER-stressed macrophages. This suggests that antioxidant may inhibit CHOP-induced cell death.

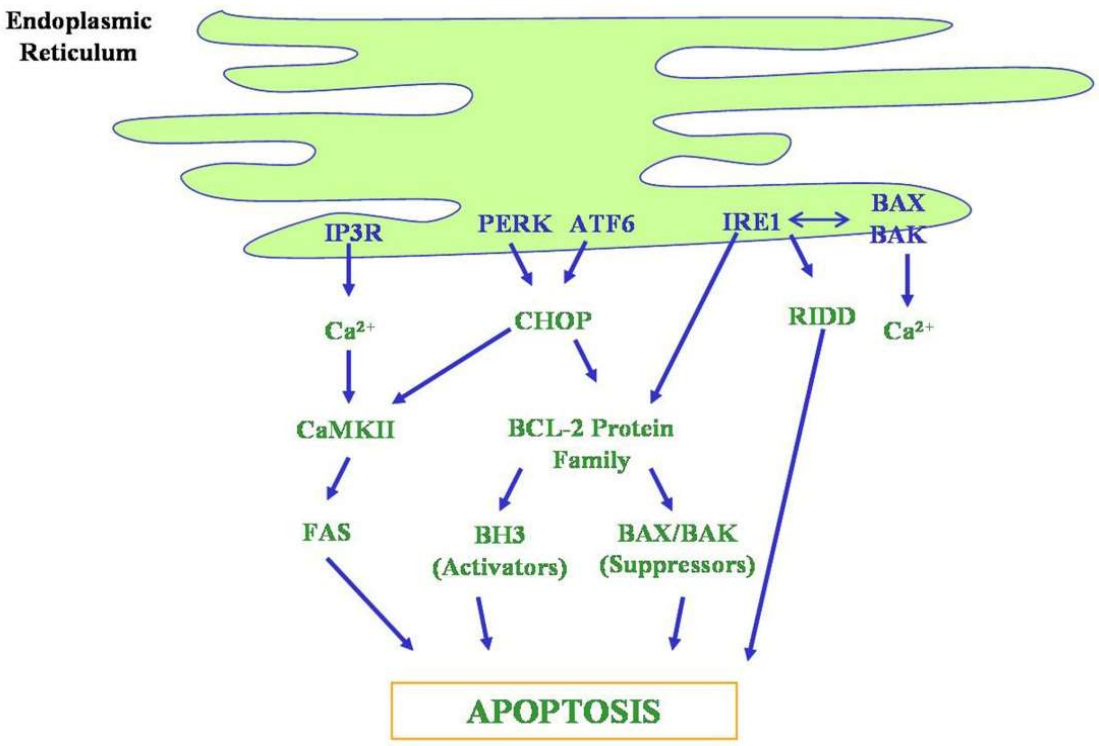

Figure 3: ER-stress and unfolded protein response malfunction induced apoptosis taken from (Stacchiotti, Favero, & Rezzani, 2013).

1.2.4 ACAT dysfunction and ER-stress.

The microsomal enzyme acyl -coenzyme A: cholesterol acyltransferase (ACAT) regulates cholesterol homeostasis by modulating increasing levels of cholesterol by an esterifying excess of free cholesterol (FC) into cholesterol esters (CE). This enzyme is known to occur in two isoforms, ACAT-1 and ACAT-2. ACAT-1 is expressed only in macrophages and SMCs, whereas ACAT1 and ACAT2 is expressed in the liver as well as intestine (Buhman, Accad, & Farese, 2000). With the progression of the atherosclerotic lesion, FC starts accumulating in macrophages and SMCs, as a result of ACAT, ABCA1 and ABCG1 transporter malfunction (Moore & Tabas, 2011). The intracellular accumulation of excess FC causes macrophage death via endoplasmic reticulum-mediated cell apoptosis (Bo Feng et al., 2003; I Tabas, 2004). As the ER is the site of low cholesterol content, the accumulation of excess FC in the ER can cause membrane dysfunction and ultimately the ER stress causing dysfunctioning in unfolded protein response (UPR) pathways.

Dysfunction in unfolded protein response pathways further initiates apoptosis in macrophages proliferated by fas and CHOP-mediated apoptosis (I Tabas, 2004). In some animal models, it has been observed that the ACAT inhibitors effective in reducing the atheroma formation (Bocan et al., 1993). Inhibitors of ACAT-1 are capable of blocking esterification of cholesterol, prevent the transformation of macrophages into cholesterol loaded foam cells and slowing the progression of atherosclerosis (Bocan et al., 2000; Bocan et al., 1993; Kusunoki et al., 2001). However, we postulate that ACAT inhibitor (Sandoz 580-35) along with oxLDL would block the FC conversion to CE and mediate FC into the ER to initiate UPR which would further trigger apoptosis in U937 and human monocytes.

1.3 Types of Cell Death

1.3.1 Apoptosis

Apoptosis is programmed cell death that takes place in multicellular organisms and is dependent on BCL-2 family proteins including pro-apoptotic and anti-apoptotic proteins which regulate the correlation between the ER and mitochondria. Cell shrinkage, nuclear fragmentation, chromatin condensation and membrane blebbing are some morphological characteristics of apoptotic cell death due to the proteolytic activity of caspase proteases (Kerr, Wyllie, & Currie, 1972; Taylor, Cullen, & Martin, 2008).

Apoptosis proceeds via the intrinsic and extrinsic pathway. The intrinsic pathway initiates with mitochondrial outer membrane permeabilization (MOMP) which causes mitochondria to release cytochrome c (Scorrano et al., 2003; Scull & Tabas, 2011). Cytochrome c later binds to Apaf–1 and undergo a conformational change to form a complex known as apoptosome which activates initiator caspase, caspase-9. The initiator caspase further activates executioner caspases, caspase-3 and caspase-7 causing apoptotic cell death. However, in the extrinsic pathway (also known as death receptor (DR) Pathway), ligation of cell surface death receptors causes the recruitment of adaptor molecules like FAS-associated death domain protein (FADD) which binds and activates initiator caspase–8, which further cleaves and activates executioner caspases–7 and–9, and initiates apoptosis without mitochondrial outer membrane permeabilization (MOMP). Crosstalk between intrinsic and extrinsic pathway also occurs through caspase–

8. Caspase–8 cleaves and activates BID (BCL-2 homology 3 (BH3) interacting domain) and MOMP, which further results in activating executioner caspases-3 and -7 further resulting in apoptosis (Tait & Green, 2010).

1.3.2 Necrosis

Necrosis, also referred to as accidental cell death, is portrayed by the loss of ion homeostasis which results in internal organelle structure degradation, cell swelling, disruption of nuclear membrane and rupture of the plasma membrane (Syntichaki & Tavernarakis, 2003). It has also been reported that ATP levels play a distinguishing role between apoptosis and necrosis; apoptosis is observed when the cells have a higher amount of ATP while necrosis is observed when ATP levels are low (Eguchi, Shimizu, & Tsujimoto, 1997; Los et al., 2002). Disruption of mitochondrial integrity prevents the production of ATP, and at the same time, disruption of plasma membrane causes the release of cellular contents which includes denatured proteins, DNA fragments, and other cellular debris into the extracellular compartment of the cell.

However, depending upon the cell type, oxLDL-mediated cell death may be either caspase-dependent or -independent apoptotic pathways or via necrosis (Baird, Hampton, & Gieseg, 2004). Previous studies led by this laboratory discovered that THP-1 undergo caspase-mediated apoptosis whereas U937 cells depicted necrotic cell death due to the absence of caspase and no phosphatidylserine (PS) exposure (Baird et al., 2004). Moreover, a study done on HMDM cells revealed caspase-3 independent necrotic cell death (S. P. Gieseg, Amit, Yang, Shchepetkina, & Katouah, 2010; Shchepetkina, 2013). However, with the current research, we assume that oxLDL mediated–CHOP activation in U937 cells and human monocytes may lead to caspase-dependent or mitochondrial-dependent apoptosis. We also question the ability of macrophage antioxidant 7,8–dihydroneopterin (7,8-DNP) (Discussed in 1.7) in downregulating CHOP activation and preventing oxLDL–CHOP–mediated cell death in both cell lines.

1.4 Mitochondria and mitochondrial membrane potential.

Mitochondria play a central role in cellular death mechanisms as it is the primary organelle involved in the cell's response to apoptosis and signal transduction cascade (Green & Reed, 1998; Johnson & Boise, 1999). Mitochondrial membrane dysfunction is an early process before the changes in nuclear and plasma membranes. Mitochondria are responsible for translocating cytochrome c from the inner mitochondrial membrane (IMM) to the cytosol is an essential process in apoptotic signalling (Green & Reed, 1998; Majno & Joris, 1995; Patrice Xavier Petit et al., 1997; Tait & Green, 2010; Taylor et al., 2008). Further release of cytochrome c activates caspases, causing apoptosis (detailed in 1.3.1). The release of cytochrome c is related with the loss in mitochondrial membrane potential and permeability transition (PT) (Marzo et al., 1998; Patrice Xavier Petit et al., 1997; Shimizu, Narita, & Tsujimoto, 1999).

The changes in membrane dysfunctioning are marked by the increase in mitochondrial membrane permeability and loss in mitochondrial membrane potential ($\Delta\Psi m$). Mitochondrial permeability transition pore (PTP) is the central regulator of loss in membrane potential ($\Delta\Psi m$) and membrane permeability (Green & Reed, 1998). PTP complex is referred megachannel comprised of voltage-dependent anion channel (VDAC), inner membrane Adenine nucleotide translocators, i.e. adenine nucleotide translocase (ANT), cyclophilin D (cyPD) and peripheral benzodiazepine receptors (Figure 4) (Green & Reed, 1998; Patrice Xavier Petit et al., 1997). Cooperation of these multichannel proteins leads to the formation of large conductance channels which are accountable for mitochondrial permeability transition (PT) that may provoke apoptosis. The term was first coined by Hunter and Haworth in 1970s (Haworth & Hunter, 1979; Hunter, Haworth, & Southard, 1976; Hunter & Haworth, 1979). PT is described as a sudden elevation in inner mitochondrial membrane permeability to solutes (Ca^{2+}, Mg^{2+}, K^{+} ions) of molecular mass <1.5 kDa as a result the charge difference between mitochondrial matrix and cytosol (Bernardi, 1996; Gunter & Pfeiffer, 1990; Ichas & Mazat, 1998; Zoratti & Szabò, 1995). As the PTP pore is opened, the solutes and water cause the mitochondrial matrix to swell, repturing outer mitochondrial membrane (OMM) along with mitochondrial proteins

(Kroemer, 1997). This quick change in the permeability is conjugated with PT resulting in depolarization of membrane, uncoupled oxidative photophosphorylation, the release of intramitochondrial ions, metabolic intermediates and large swelling of mitochondria (Green & Reed, 1998; Patrice Xavier Petit et al., 1997; Zoratti & Szabò, 1995).

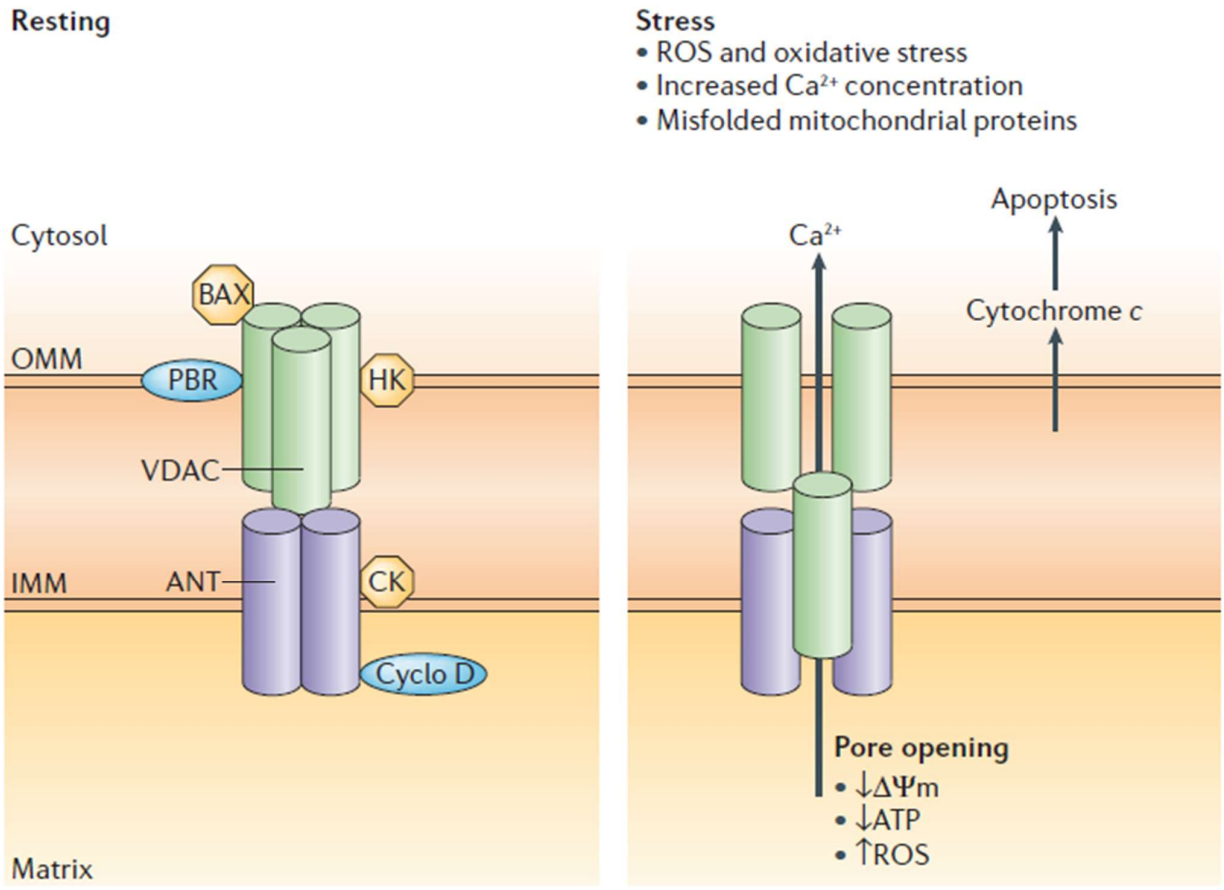

Figure 4: Mitochondrial permeability transition pore (PTP) regulation taken from (Abou-Sleiman, Muqit, & Wood, 2006).

1.5 Mitochondrial permeability transition pore (PTP) regulation.

The opening of PTP is controlled by mitochondrial membrane potential (ΔΨm) and the pH of the mitochondrial matrix. The chances of opening pore increase when the mitochondrial matrix undergo acidification with the reduction in pH below 7.0 and decrease in ΔΨm (Bernardi et al., 1992). The PTP is administered in 3 different

conditions; **i)** closed condition where ΔΨm is integrated, **ii)** low conductance state, where the pore is partially opened, permeable to molecules <300 Da followed by the reversible decrease in ΔΨm and **iii)** high conductance state, a condition characterised by the irreversible flip in the pore from the state of high conductance to state of low conductance accompanied by the irreversible collapse in ΔΨm allowing permeability to molecules <1.5 kDa (Bernardi et al., 1992). During normal functioning of mitochondria, the PTP is impermeable in such a way that proper ΔΨm is maintained for cell survival as it is responsible for ATP synthesis and oxidative phosphorylation (Gottlieb, 2001). This state of high conductance is essential for initiation of apoptosis (Zamzami et al., 1995).

1.5.1 PTP opening models and cytochrome c release causing apoptosis.

Several models of PTP opening have been proposed that dismantle ΔΨm that are involved in the cytochrome c release so causing apoptosis via caspase activation.

1.5.1.1 PTP induced mitochondrial swelling model (VDAC opening model)

The model is characterized by the swelling and rupturing of the outer mitochondrial membrane that has been observed with different inducing agents (Scarlett & Murphy, 1997; Zamzami et al., 1995) (Figure 5). Apoptosis inducers are directly linked with PTP causing the pore to open along with rapid depolarization and mitochondrial matrix swelling (Waring & Beaver, 1996).

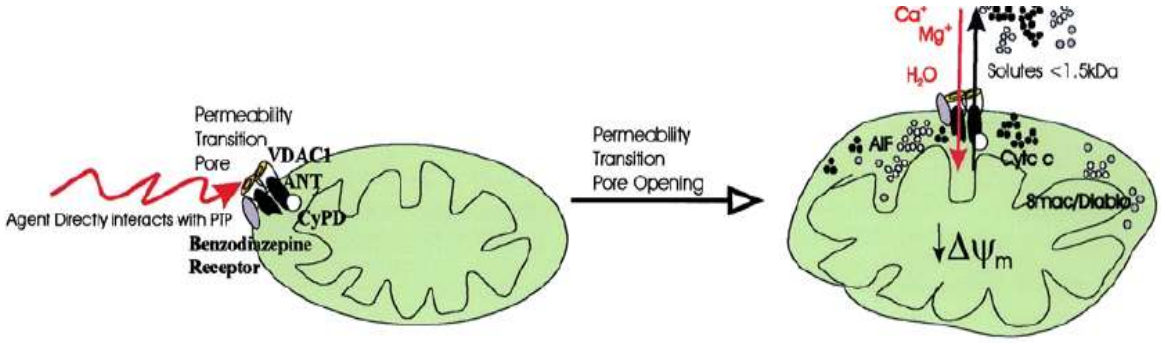

Figure 5: VDAC opening model taken from (Ly, Grubb, & Lawen, 2003).

1.5.1.2 PTP non-swelling model.

The model suggests that low concentrations of Bax or Bid can induce mitochondria to release cytochrome c without mitochondrial matrix swelling or its rupture (Jürgensmeier et al., 1998). It was also observed that PTP opening without mitochondrial matrix swelling causes ΔΨm to collapse through proton degeneration pathway causing Bax to undergo conformational change and its translocation to mitochondrial membrane to release cytochrome c and trigger apoptosis (Jürgensmeier et al., 1998; Pastorino et al., 1999) (Figure 6).

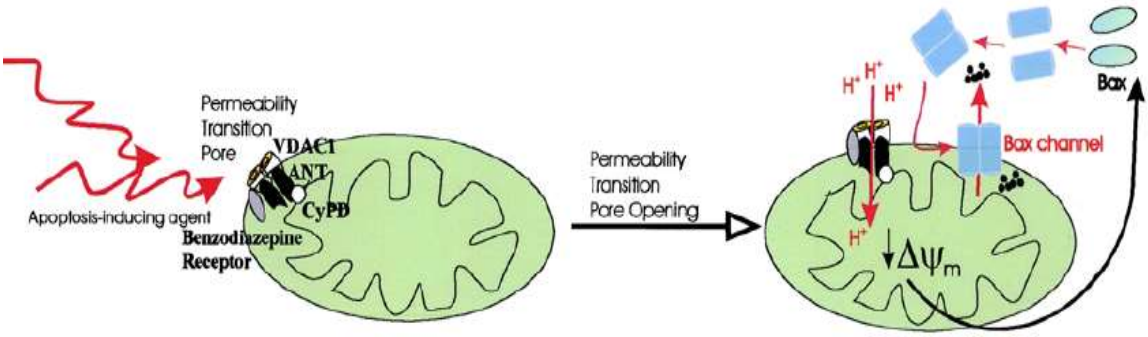

Figure 6: PTP non-swelling model taken from (Ly et al., 2003).

1.5.1.3 Formation of conducting channels.

Numerous studies suggested the formation of conducting channels along with a non-specific rupture of the outer membrane causes apoptosis (ANTONSSON, MONTESSUIT, LAUPER, ESKES, & MARTINOU, 2000; De Giorgi et al., 2002). The model also illustrates that the mitochondrial membrane rupture is a result of specific apoptotic proteins which later causes mitochondria to release cytochrome c. It is also known that this model system leads to the formation of the Bax-lipidic pore and Bax-VDAC channels (ANTONSSON et al., 2000; De Giorgi et al., 2002; Marzo et al., 1998; Shimizu, Ide, Yanagida, & Tsujimoto, 2000) (Figure 7).

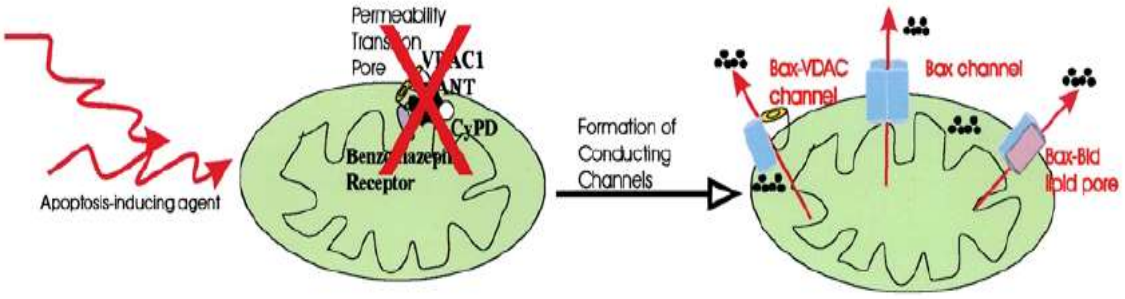

Figure 7: Formation of conducting channels taken from (Ly et al., 2003).

1.6 Mitochondrial membrane potential (ΔΨm) and apoptosis.

1.6.1 Calcium and mitochondrial membrane potential (ΔΨm).

Cellular metabolism and apoptosis regulation are the critical roles played by mitochondria and the alterations in the cellular functions maintained by mitochondria is associated with apoptosis. This includes the collapse in of ΔΨm, ROS accumulation, membrane PT and release of apoptotic factors (BCL-2 family protein members) into mitochondrial membrane and intermembranal space (cytochrome c) (Gottlieb, 2001). Mitochondria have long known to play an essential role in handling calcium load and are capable of sequestering Ca^{2+} through mitochondrial uniporter, using mitochondrial membrane potential to enhance the uptake of Ca^{2+} in higher amounts (De Stefani, Raffaello, Teardo, Szabò, & Rizzuto, 2011; Kirichok, Krapivinsky, & Clapham, 2004; Lawrie, Rizzuto, Pozzan, & Simpson, 1996). Due to their role in calcium homeostasis, they are also referred as capacitors.

Alterations in the calcium homeostasis can lead to an elevation in cytosolic free calcium and lead to apoptosis through classical pore transition (PT) (Crompton, 1999; Rasola & Bernardi, 2007). Ca^{2+} overload in mitochondria can activate the opening of mitochondrial permeability transition pore (PTP) that further causes mitochondrial permeability transition (PT). Therefore when the apoptosis-inducing agents are introduced into the cellular system, the intracellular cytoplasmic Ca^{2+} levels are elevated resulting in primitive dispersion of ΔΨm prior to the activation of caspases (Koya et al., 2000; I.

Kruman, Guo, & Mattson, 1998; I. I. Kruman & Mattson, 1999). Apoptosis induced calcium ionophores or TG can be blocked by intracellular calcium chelators by decreasing the calcium concentration below the concentration that is required to activate PTP (Koya et al., 2000; I. I. Kruman & Mattson, 1999). Izani (2015) observed that the cytosolic Ca^{2+} elevation induced by the calcium ionophore A2318 (BrA) resulted in loss of cell viability when the cells were incubated with 5 μM BrA and above. The following loss in cell viability was also observed by Yang (2009) when the BrA concentration was 5μM and above decreasing the viable cells up to 50% compared to cell only control within 5 minutes of treatment. However, when the lower concentrations of BrA (3 μM) was introduced, it did not cause any significant loss in cell viability within 24 hours of treatment suggesting that intracellular concentration of Ca^{2+} in the cytosol is required to cause the cellular death.

1.6.2 Mitochondrial membrane potential (ΔΨm) and cytochrome c release.

Mitochondrial potential and PT play a vital role in the release of cytochrome c. However, PT inhibitors inhibit both apoptosis and cytochrome c release. The role of PT in apoptosis is still debated and is suggested that cytochrome c release and no loss in ΔΨm is also an event responsible for cell death processes (J. Yang et al., 1997). However, there are evidences that directly supports the involvement of loss of ΔΨm in releasing cytochrome c. Various studies suggested that PT and cytochrome c release are highly associated processes and the cytochrome c release occurs via PT through mitochondrial swelling and subsequent rupture of OMM (Patrice X Petit et al., 1998; Scarlett & Murphy, 1997). Rat hepatocytes underwent apoptosis induced by microstatin-LT during which a substantial loss in ΔΨm was observed along with cytochrome c release and PT activation (Ding, Shen, & Ong, 2002). This was also observed in cultured cortical neurons which activated PT, rupturing OMM and releasing cytochrome c (Brustovetsky, Brustovetsky, Jemmerson, & Dubinsky, 2002). A drop in ΔΨm and cytochrome c release was observed in PC6 cells when treated with Staurosporine (Heiskanen, Bhat, Wang, Ma, & Nieminen, 1999). However, when ΔΨm was inhibited by Bongkrekic acid (BA), it prevented cytochrome c release from dexamethasone (DEX) treated thymocytes suggesting correlation of ΔΨm with cytochrome c release (Yoshino et al., 2001).

In contrast, there are also evidences that suggested the cytochrome c release is independent of changes or loss of mitochondrial membrane potential. This finding was supported by the study done on human monocyte-like THP-1 cells where cytochrome c release occurred before outer mitochondrial membrane rupture (Zhuang, Dinsdale, & Cohen, 1998). This was also followed by the finding in a cell-free system where cytochrome c release was not accompanied by changes in ΔΨm during apoptosis suggesting that there was no involvement of PT activation (Kluck, Bossy-Wetzel, Green, & Newmeyer, 1997). Interestingly, involvement of Bcl-2 family member proteins (BH3-only, Bid and Bik) resulted in cytochrome c release without any changes in ΔΨm and PT activation (Shimizu & Tsujimoto, 2000; Von Ahsen et al., 2000). Overall these evidences suggests that the ΔΨm play the role of a double-edged sword in releasing cytochrome c and further activating PT leading apoptotic cell death.

1.7 7, 8–dihydroneopterin (7, 8–DNP)

1.7.1 Neopterin and 7,8-DNP Synthesis.

7, 8–DNP is a pterin synthesized by ϒ–interferon (INF-γ) activated macrophages (Figure 8) (Müller, Curtius, Herold, & Huber, 1991) and its oxidation leads to the formation of different products including neopterin (Figure 8). Plasma neopterin is a highly fluorescent compound whose quantity in plasma has been used as a potential marker of inflammation (S. P. Gieseg, Crone, Flavall, & Amit, 2008) and a reliable indicator of plaque stability and prognosis (Liu & Li, 2013), in vascular disease (S. P. Gieseg et al., 2010; Janmale et al., 2015). Both neopterin and 7,8-DNP belong to a class of pteridines which are characterised by the presence of pyrazino-2,3-pyrimidine bicyclic nitrogen ring system (Wachter et al., 1992). Upon further classification, pteridines can be sub-classified depending on the oxidation state into fully reduced tetrahydropterins and partially reduced dihydroneopterins and aromatic pterins (K Oettl & Reibnegger, 2002).

All members of pteridine class of compounds are synthesized from guanosine triphosphate (GTP). Upon stimulation of INF-γ, the enzyme GTP cyclohydrolase 1 metabolises GTP into 7,8-NP triphosphate (Werner et al., 1990). Further, 7,8-DNP is generated from 7,8-NP triphosphate by the action of phosphatase enzymes (Wachter et al., 1992). Synthesis is also enhanced upon co-stimulation of tumor necrotic factor-α

(TNF-α), dexamethasone (DEX) or lipopolysaccharides (LPS) although not as stong as stimulated by TNF-α (Werner-Felmayer et al., 1995; Werner-Felmayer et al., 1990). Later, breakdown of 7,8-NP after its reaction with oxidant species results formation of neopterin, 7,8-dihydroxanthopterin and xanthopterin.

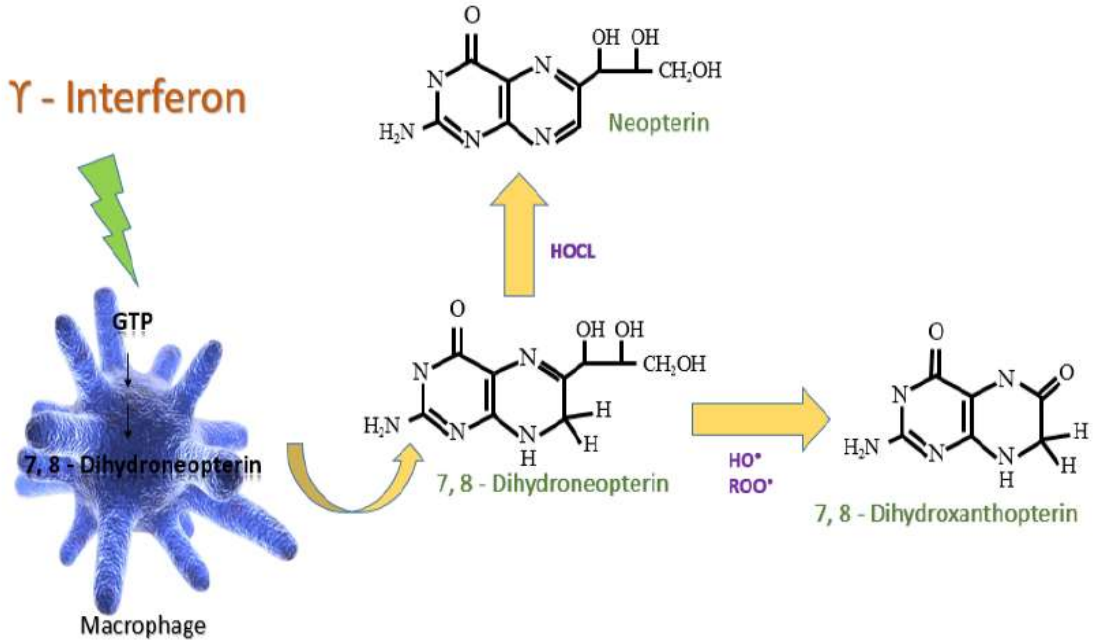

Figure 8: Synthesis of 7, 8-DNP.

1.7.2 Antioxidant potential of 7,8-DNP.

Reduced pteridines such as 7, 8-DNP are well-known for their antioxidant potential (Rezk, Haenen, van der Vijgh, & Bast, 2003) and are produced by the macrophages in the plaque. In vitro studies have shown the ability of 7, 8-DNP in inhibiting LDL oxidation (S. P. Gieseg, Reibnegger, Wachter, & Esterbauer, 1995), inhibiting ROS mediated reactions (Karl Oettl, Greilberger, Dikalov, & Reibnegger, 2004), and preventing free radical damage including hydroxyl and peroxyl radicals (Duggan, Rait, Platt, & Gieseg, 2002); suggesting the antioxidant effect of 7, 8-DNP. 7, 8-DNP is an efficient scavenger of superoxide and peroxyl radicals generated by 2,2'-azobis-2-methyl-propanimidamide, dihydrochloride (AAPH) (Karl Oettl et al., 2004) while also reacting with hydrogen peroxide (H_2O_2) and chlorine species such as chloramine-T (Weiss et al., 1993). The reaction rate of 7, 8-DNP with AAPH which nears its rate of diffusion makes it a good

inhibitor of peroxyl radical damage (Duggan et al., 2002; S. Gieseg, Duggan, & Gebicki, 2000). 7, 8-DNP has also been shown the inhibition of AAPH driven oxidation of polyunsaturated omega-6 fatty acid linoleate along with the formation of diene on LDL molecules during AAPH as well as copper mediated LDL oxidation (S. P. Gieseg et al., 1995). 7, 8-DNP protects bovine serum albumin (BSA) against AAPH-driven oxidation (S. P. Gieseg et al., 1995).

7, 8-DNP can also inhibit erythrocyte lysis caused by HOCl, H_2O_2 and AAPH treatments (S. P. Gieseg, Maghzal, & Glubb, 2001; Y. T. Yang, Whiteman, & Gieseg, 2012). The degree of protection varied as 7, 8-DNP provided a complete protection during AAPH mediated oxidation, while providing partial protection (40%) when oxidation was driven by H_20_2 (S. P. Gieseg et al., 2001). Further studies confirmed this effect of 7, 8-DNP in protein hydroxide and lipid peroxide formation on LDL slowed down in HMDM and THP-1 cells (Firth, Crone, Flavall, Roake, & Gieseg, 2008). Overall the evidence suggests that 7, 8-DNP can act as an antioxidant which is capable of protecting cells from oxidative damage.

1.7.3 Role of 7, 8-DNP on cell survival and viability.

The research studies carried by this laboratory over the years targeted at determining whether the antioxidant potential of 7, 8-DNP is sufficient for cell survival and viability. A biologically relevant study has demonstrated the protective role of 7, 8-DNP on oxLDL induced cytotoxicity on the cells from myelocytic origins. It has also been reported that micromolar concentrations of 7, 8-DNP inhibited oxLDL toxicity to U937 cells (Baird, Reid, Hampton, & Gieseg, 2005), THP-1 and HMDM cells (S. P. Gieseg & Cato, 2003).

Conversely, other studies also found the non-protective effect of 7,8-DNP where high 7,8-DNP concentrations induced apoptotic cell death. The study reported that L2 cells experienced 17% and 13% apoptosis when treated with 100 μM 7,8-DNP and neopterin (Schobersberger et al., 1996) while exibiting higher cytokines TNF-α and INF-γ to get the effect. It was also observed that cells underwent apoptosis when treated with 5 mM 7,8-DNP (Wirleitner, Baier-Bitterlich, Böck, Widner, & Fuchs, 1998). Later it was suggested that 7,8-DNP generated by overproduction of free radicals might be a possible factor for its apoptotic effects (Wirleitner et al., 2001).

In contrast to above evidences, a study led by Bratslavsta *et. al* (2007) showed that neopterin and 7, 8-DNP had no effect on cell viability in Hep-G2 cells (Bratslavska, Platace, Miklaševičs, Fuchs, & Martinsons, 2007). However, no adverse effect of 7, 8-DNP (upto 300 μM) on cell viability of U937, THP-1 or HMDM cells was observed in our laboratory. The described effects may be determined by the tolerance of different cell lines responding to the disturbances in the intracellular redox balance.

Based on the following activities of 7,8-DNP, we also hypothesize that macrophage antioxidant 7, 8–DNP would block macrophage activation of CHOP and prevent CHOP–mediated cell death in U937 cells in the presence of oxLDL as NOX activation appears to be a crucial part of unfolded protein response.

1.8 Research Goals

Endoplasmic reticulum stress is a well-studied mechanism which causes cell death through activation of various pathways (Oyadomari & Mori, 2004; Scull & Tabas, 2011; Tu & Weissman, 2004; Xu, Bailly-Maitre, & Reed, 2005). In this research, we aimed at observing the expression of an essential ER-stress marker CHOP (Oyadomari & Mori, 2004) in mediating cell death. It is also known that oxidized LDL is also known to trigger CHOP mediated cell death (Shutong Yao, 2014; Tao et al., 2009). Hence one of the critical goals of the research is to observe oxLDL mediated CHOP activation in U937 cells.

The initial section of **Chapter Three (3.1)** will determine the toxic effect of Cu-oxLDL on U937 cell viability. The cell viability obtained from different Cu-oxLDL batches will help in examining the LC_{50} concentrations throughout the research, and further objectives will be carried out based on LC_{50} concentrations obtained. The viability will be examined by both PI flow cytometry and MTT colorimetric assay.

The second part of the study will focus on determining the cytotoxic effect of SERCA inhibitor Thapsigargin (TG) on U937 cells. The cytotoxic effect of TG will again be determined using PI flow cytometry, and MTT colorimetry assay and LC_{50} concentration will be calculated **(3.2)**. Thapsigargin is also known to activate apoptotic cell death in various cell lines, so to investigate this, the research will further assess the changes in mitochondrial membrane potential by staining the cells by TMRM which will be analyzed by flow cytometry **(3.3).** The next section of **Chapter 3 (3.4)** will investigate the potency

of ER-stress inducer TG in triggering CHOP activation in U937 cells. CHOP is main ER-stress marker and is expressed when the cell experiences ER-stress. Western blotting will investigate the expression of TG-induced ER-stress.

Numerous studies till date have shown the capacity of 7, 8-DNP to protect the cells from cytotoxic effect of oxLDL (Baird et al., 2005; S. P. Gieseg et al., 2010; S. P. Gieseg et al., 2001). However, the effect of 7, 8-DNP on CHOP upregulation/downregulation is not yet seen. Based on the protective effect of 7, 8-DNP we will examine the effect of antioxidant 7, 8-DNP neopterin CHOP activation in U937 cells. **3.5** part of **Chapter 3** will emphasize the antioxidant effect of macrophage stimulated antioxidant 7, 8-DNP on CHOP activation by western blotting technique.

One of the principal goals of the research program is to investigate the potential of oxLDL in inducing Cu-oxLDL-induced CHOP expression in U937 cells. This part of **Chapter 3 (3.6)** will examine the role of Cu-oxLDL in triggering CHOP activation in Dose **(3.6)** and time-dependent manner **(3.7)**. Western blotting will examine the investigation of CHOP expression.

ACAT (cholesterol esterase enzyme) is the responsible enzyme for the conversion of FC to CE. ACAT inhibitors have reported reducing foam cell and atheroma formation (Bocan et al., 2000; Bocan et al., 1993; Kusunoki et al., 2001). The present study has utilized the novel ACAT inhibitor Sandoz 58-035. **3.8** and **3.9** sections of Chapter Three to determine the effectiveness of ACAT inhibitor on Cu-oxLDL **(3.8)** treated cells and the toxicity of ACAT inhibitor alone **(3.9)** using PI flow cytometry and MTT colorimetric assay.

The last part of **Chapter 3** will address some preliminary work investigations looking at the effect of TG and oxLDL on human monocytes.

CHAPTER 2

2 MATERIALS AND METHODS

2.1 Materials

2.1.1 Reagents

Experiments throughout the research were carried out using reagents of analytical grade or better. Water was deionized and ultra-filtered using a Milli-Q filtration water system and all solutions were prepared using this nanopure water.

β–mercaptoethanol	Sigma Chemical Co., Missouri, USA
3–[4,5–Dimethylthiazol–2–yl]–2,5–diphenyl-tetrazolium bromide (MTT)	Sigma Chemical Co., Missouri, USA
4–Morpholine–propanesulfonic acid (MOPS)	Sigma Chemical Co., Missouri, USA
7, 8–Dihydroneopterin (7,8–DNP)	Schircks Laboratory, Switzerland
Acetic acid (glacial)	
Acetone	Merck Ltd, Poole, England
Non–fat milk powder	Alpine
Argon gas	BOC Gases, Auckland, NZ
Bicinchoninic acid (BCA) protein determination kit	Pierce, Illinois, USA
Bovine Serum Albumin (BSA)	Gibco, Invitro Corporation, USA
Bromophenol blue	Sigma Chemical Co., Missouri, USA
Chelex 100 resin	Bio – Rad Laboratories, California, USA
Cholesterol reagent	Roche Diagnostics, USA
Copper chloride ($CuCl_2$)	Sigma Chemical Co., Missouri, USA
Coumassie blue R stain	Sigma Chemical Co., Missouri, USA

Dimethyl sulphoxide (DMSO)	BDH Laboratory Supplies Ltd., Poole, England
Dulbecco's Phosphate Buffered Saline (PBS)	Sigma Aldrich, UK
Ethanol	Fisher Chemicals
Ethylenediaminetetraacetic acid (EDTA)	Sigma Chemical Co., Missouri, USA
Hydrochloric acid, fuming 37 %	Merck, Darmstadt, Germany
Isopropanol	Fisher Chemicals
Methanol	Fisher Chemicals
Molecular Weight Marker	Thermofisher Scientific
Nitrogen gas	BOC Gases, Auckland, NZ
NuPAGE 4–12 % Bis–tris Gel, 1.5 mm X 10 well	Invitrogen, Oregon, USA
Ponceau S	Sigma Chemical Co., Missouri, USA
Potassium bromide (KBr)	Sigma Chemical Co., Missouri, USA
Potassium dihydrogen phosphate (KH_2PO_4)	Fisher Chemicals
Propidium Iodide (PI)	Sigma Chemical Co., Missouri, USA
Sandoz 58–035 (ACAT Inhibitor)	Sigma Chemical Co., Missouri, USA
Sodium chloride (NaCl)	VWR, Life technologies Ltd.
Sodium dihydrogen orthophosphate monohydrate ($NaH_2PO_4.H_2O$)	Scharlau, Spain
Sodium dodecyl sulphate (SDS)	Sigma Chemical Co., Missouri, USA
Sodium hydroxide (NaOH)	
Supersignal west Dura chemiluminescence	Pierce Biotechnology Inc., Illinois, USA
Thapsigargin	Sigma Chemical Co., Missouri, USA
Thimerosal	Sigma Chemical Co., Missouri, USA
Tetramethylrhodamine methyl ester (TMRM)	Merck Darmstadt, Germany
Tris	Sigma Chemical Co., Missouri, USA
Triton–X 100	Sigma Chemical Co., Missouri, USA

Trypan blue solution (0.4 %)	Sigma Chemical Co., Missouri, USA
Tween–20	Sigma Chemical Co., Missouri, USA

2.1.2 Media

Fetal bovine serum	Sigma Chemical Co., Missouri, USA
Penicillin/Streptomycin (10000 units/mL Penicillin G and 10000 units/mL Streptomycin)	Gibco by life Technology, USA
Roswell Park Memorial Institute (RPMI)–1640 Media with phenol red	Hyclone, GE Healthcare Life Sciences, Utah
Roswell Park Memorial Institute (RPMI)–1640 Media without phenol red	Gibco by life technology, USA

2.1.3 Antibodies

GADD 153 (B–3) mouse monoclonal $IgG_1 \kappa$	Santa Cruz Biotechnology Inc., USA
Mouse monoclonal against β – actin	Sigma – Aldrich Chemicals Co., USA
Mouse monoclonal m – IgGκ BP – HRP	Santa Cruz Biotechnology Inc., USA

2.2 General solutions and buffers

2.2.1 Phosphate buffered saline (PBS)

Phosphate buffered saline consisted 150 mM sodium chloride (NaCl, MW= 58.44 g/mol) to 10 mM sodium dihydrogen phosphate at pH 7.4 ($NaH_2PO_4.H_2O$, MW= 137.99 g/mol). A liter of PBS was prepared by adding 50 mL of 3M NaCl, 40 mL of 250 mM $NaH_2PO_4.H_2O$ (pH 7.4) to 910 mL of Nano-pure water. PBS solution for cell culture work was vacuum filtered through 0.45 µm membrane and sterilized by autoclaving for 15 minutes, 121^0C and 15 psi. PBS was warmed in water bath at 37^oC in water bath prior to use with cells.

2.2.2 MTT assay solution

MTT (3–[4,5–Dimethylthiazol–2–yl]–2,5–diphenyl-tetrazolium bromide) stock solution was prepared by dissolving MTT powder (Sigma Chemical Co., Missouri, USA) in RPMI 1640 without phenol red to give the final concentration at 5 mg/mL. This solution was filtered sterilized using a 0.22 µm MS® PES syringe filter and stored at -20^0C in the dark until further use. For viability assay, the stock solution was used to give final concentration at 0.5 mg/mL.

A 10% SDS in 0.01 M HCl was made up from 11.44 M HCl and Nano–pure water. Sodium dodecyl sulphate (SDS) powder was added to 0.01 M HCl solution and stirred up slowly to give a final concentration at 10% (w/v) SDS.

2.2.3 ACAT inhibitor stock solution

Sandoz 58–035 (ACAT inhibitor) (Sigma Chemical Co., Missouri, USA) stock solution was prepared by dissolving Sandoz 58–035 powder in DMSO (BDH Laboratory Supplies Ltd., Poole, England) to give the final concentration at 5 mg/mL. The solution was filtered sterilized using a 0.22 µm MS® PES Syringe filter and stored at 4^0C until use.

2.2.4 Propidium iodide stock solution

A 1 mg/mL stock solution was prepared by dissolving propidium iodide (PI) powder (Sigma Chemical Co., Missouri, USA) in sterile nanopure water to give the final concentration of at 1.5 µg/mL. The solution was filtered sterilized using a 0.22 µm MS® PES syringe filter and was stored at 4^0C until further use.

2.2.5 7, 8–dihydroneopterin (7, 8-DNP) solution

A 2 mM stock solution of 7, 8–DNP (MW= 255.2 g/mol) was prepared fresh every time immediately before each experiment. 7, 8-DNP powder (Schircks Laboratory, Switzerland) was dissolved in appropriate medium followed by 10–15 minutes ultrasonication. The 7, 8–DNP solution was then filtered–sterilized using a 0.22 µm MS® PES Syringe filter and diluted to working concentrations before added to cells. The solution was kept on ice at all times.

2.3 Methods

2.3.1 Cell Culture

All cell culture work and experiments were performed in aseptic conditions in Class II biological safety cabinet (ScanLaf, Labgene APS, Denmark). All equipment and plastic wares were supplied sterile, ready to use and disposable. All media and solutions prepared were sterilized either by autoclaving or by filtering through sterile 0.22 µm membrane filter. All equipment and tissue culture items were sprayed thoroughly by 70% ethanol before being used in CII biological safety cabinet. Cells were incubated in an incubator at 37^0C in humified atmosphere containing 5% CO_2.

2.3.2 Cell culture media

Cell culture media with varying chemical compositions were used for cell culture depending on the compatibility of cells and environmental conditions. In the current study, RPMI–1640 medium was used in culture of U937 cell line and human monocytes.

2.3.3 Standard RPMI-1640 media

RPMI-1640 medium with phenol red (Hyclone, GE Healthcare Life Sciences, Utah) supplemented with 100 U/mL penicillin G, 100 U/mL streptomycin and 5% fetal bovine serum (FBS) was utilized for normal U937 cell sustenance. However, for human monocytes, 10% human serum was used as a substitute for FBS for normal cell maintenance.

2.3.4 RPMI–1640 without phenol red

RPMI 1640 without phenol red (Gibco by life technology, USA) was aliquoted in 50 mL falcon tubes and were used for experiments with and without 5% fetal bovine serum as stated for individual procedure.

2.4 Cell culture experimental conditions and protocols

Experiments were performed using either 12–well or 24 well suspension culture plates depending upon the number of treatments or total volumes for both U937 cells (with or without serum) and human monocytes unless otherwise stated. The wells of plates were coated with 1 mL albumin (1.25 mg/mL) (Gibco, Invitro Corporation, USA), were left undisturbed for 2–3 minutes until dried and were later used for experiments when performing experiments in absence of serum.

Cells were counted using a hemocytometer and a light microscope after staining with trypan blue at a ratio of 1: 1 (2 times dilution) for U937 cells whereas 1: 9 (10 times dilution) ratio for human monocytes. The required quantity was cells for the experiments was centrifuged at 500 g for 5 minutes at room temperature and was re-suspended in appropriated experimental medium at 37^0C. The cell concentration was the aliquoted into wells containing the medium at a concentration of either 0.5×10^6 cells/mL or 1×10^6 cells/mL for U937 cells or human monocytes.

2.5 Preparation of culture of human monocytes

Unlinked blood from the healthy consenting haemochromatosis individuals were collected into a 500 mL autologous blood bag containing anticoagulant by New Zealand Blood Service (NZBS) Riccarton branch, Christchurch. The cells were immediately prepared after blood collection or kept for up to 18 hours at 4^0C if processing cannot be carried out on the same day.

The bag of whole blood was inverted gently for 10–12 times to ensure evening mixing and distribution of cells and other components before placing the bag in to the CII safety cabinet aseptically. One of the bag tube was cut opened using scissors and blood was transferred to 50 mL falcon tubes and were centrifuged at 1000 g with fast acceleration and slow deceleration for 20 minutes. After centrifugation, the cells were separated into

few layers consisting of erythrocytes at the bottom, topped with white layer of leucocytes (buffy coat) and overlaid with the plasma layer. The plasma layer was aspirated leaving the leucocytes layer which was removed using a mixing cannula attached to a 10 mL plastic syringe, pooled and mixed with equal volume of Dulbecco's PBS (Sigma Aldrich, UK) by inverting thoroughly. The mixture was then underlaid by 15 mL Lymphoprep® (Lymphoprep) using a mixing cannula attached to a 20 mL syringe before being centrifuged again at 1000 g (with brakes off and soft start) for 20 minutes at room temperature. The resulting white layer of monocytes/lymphocytes was visible halfway down 50 mL tube encircled by clear plasma and Lymphoprep layers. The top layer solution layer was aspirated leaving above the leucocyte layer.

The cells in solution was transferred in new 50 mL falcon tubes using a mixing cannula attached to a syringe and thoroughly re-suspended and evenly divided between a designated number of tubes with each containing approximately 15 mL solution. Later, PBS was topped up to a final volume of 50 mL, was mixed by inverting before being centrifuged at 500 g for 15 minutes. The pellet was re–suspended in 5 mL sterile MiliQ water for 10-12 seconds was topped up again with PBS up to the final volume of 50 mL and was centrifuged again at 500 g for 15 minutes if the pellet consisted of erythrocytes. The washing step with PBS was repeated once more before the cells were re–suspended in the RPMI–1640 media containing Penicillin/streptomycin without serum. The cells were then plated into 6–well suspension plates (CellStar, Greiner Bio-one, Germany) and incubated in the CO_2 incubator for 40 hours.

2.6 Preparation of human serum for cell culture

Human serum from haemochromatosis blood donors was used for cell culture of human monocytes under ethics approval CTY/98/07/069 approved by Upper South (B) regional Ethics committee. Unlinked blood from heathy consenting donors was collected into 450 mL dry bags (without anticoagulant) by New Zealand Blood Service (NZBS) Riccarton branch, Christchurch. The blood bag was left in the vertical position in polypropylene container at room temperature for 2 hours to allow blood clot. The blood bag was later transferred to 4^0C fridge and stored overnight to grant sufficient time for separation of serum from clot.

The blood bag was opened in CII cabinet under sterile conditions and serum was pooled in 50 mL falcon tubes using a mixing cannula attached to a syringe, leaving blood clot at the bottom of bag. The tubes were centrifuged at 1500 g at room temperature for 15 minutes. The centrifugation step was repeated if the serum appeared red after first centrifugation. The serum was transferred into fresh sterile falcon tubes leaving the pellet behind. The serum was then cooled at 4^0C, transferred to -20^0C for freezing and finally to –80^0C for long term storage. This human serum was supplied to human monocytes at 10% final concentration.

2.7 Isolation and oxidation of LDL

2.7.1 Collecting human blood for plasma preparation

Blood (200 mL) was drawn from healthy donor by venipuncture using an 18G butterfly needle and a syringe after an overnight fast. The blood was collected directly into a 50 mL falcon tube with 0.5 mL 10% EDTA pH at 7.4 so that the final concentration of EDTA in blood was 0.1%. The blood was centrifuged at 4,100 g for 20 minutes at 4^0C with a soft start and stop. The supernatant was transferred to white 50 mL high speed centrifuge tubes for a fixed angle rotor followed by centrifugation at 11,000 g for 30 minutes with soft start button on. However, centrifugation was proceeded at 5,000 rpm for first 5 minutes and was later switched to 13,000 rpm for next 20 minutes using a SS34 rotor centrifuge. After the centrifugation, the plasma was pooled and collected into a single cylinder by pouring it from the centrifuge tube leaving the pellet intact in the centrifuge tube. The volume of pooled plasma was recorded and was aliquoted in 32 mL lots in a 50 mL falcon tube. The pooled plasma was cooled at 4^0C, moved to -20^0C for freezing and was finally transferred to –80^0C for long term storage.

2.7.2 LDL preparation from plasma by gradient centrifugation

LDL was prepared using modified Beckman NVTi65 Rotor method as described by Gieseg and Esterbauer (1994). In general, the method separates lipid types based on their gradient. EDTA–plasma tube was defrosted in the running cold water. Centrifuge was cooled at 4^0C until the plasma was defrosted. The plasma was further centrifuged at 4,700 g for 10 minutes at 4^0C. The supernatant was transferred into the beaker placed on the ice, adjusting the plasma density at 1.3 by slowly adding 381.8 mg of KBr per mL of

plasma. The solution was gently stirred to dissolve KBr allowing less amount of froth formation. In meanwhile, 1% EDTA pH 7.4 was degassed for 10 minutes in oxygen free nitrogen and 8 mL of this deoxygenated 1% EDTA was added to each of 8 ultracentrifuge tubes (OptiSeal™, Beckman Coulter, USA) before underlaying with 4 mL of KBr–Plasma using a longer lure–fitting needle attached to a 5 mL syringe. The tubes were transferred to NVTi65 rotor and centrifuged at 60,000 rpm for 2 hours and 4^0C with acceleration and deceleration. A yellow band (Figure 9) was observed was collected using a syringe attached to 90^0C–bent needle.

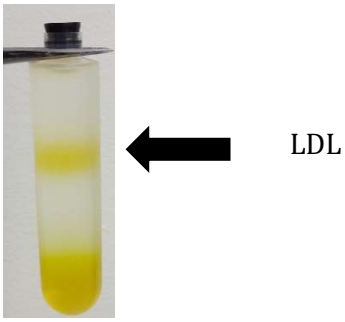

Figure 9: LDL isolation

2.7.3 LDL concentration

LDL was concentrated using ultrafiltration centrifugation cartridges (Amicon, Ultra, Millipore Ireland Ltd., Ireland). Before using tubes for LDL concentration, they were rinsed thrice with nanopure water and then centrifuged with PBS for 2 minutes at 3000 g to wash. After the wash, LDL was placed into these cartridges (20 mL), topped up with PBS and centrifuged at 3000 g at 4^0C for 20 minutes with fast acceleration and deceleration. This process was repeated twice to exclude remaining EDTA from the LDL. The purified LDL was concentrated using the same procedure by centrifuging for 10–20 minutes, however, the centrifugation time varied depending upon the original concentration of the LDL which was later adjusted to final concentration of 10 mg/mL solution (total mass). After use, the membranes were rinsed with nanopure water, centrifuged with nanopure water for 2 minutes, then for 1 minute with 100% ethanol and were stored in 70% ethanol in the fridge.

2.7.4 LDL concentration determination

Determination of LDL concentration was done with respect to the total cholesterol mass which was measured by Cholesterol assay kit (Roche, Germany). The total cholesterol in the LDL was determined by incubating 1 mL of CHOL reagent with 10 µL of native LDL at room temperature. After 10 minutes, the absorbance was measured at 500 nm and LDL concentration was calculated based on estimation that LDL having molecular weight of 2,500 KDa and cholesterol accounts for 31.69% of LDL particle by weight and total LDL mass relates to the mass of apoB–100 as 1:5 (S. P. Gieseg & Esterbauer, 1994).

Calculation of LDL Concentration:

Absorbance × 14.9 = [Cholesterol] (mM)

[Cholesterol] (M) × 368.64 g/mol = [Cholesterol] (g/L)

[Cholesterol] (g/L) × 100/31.69 = [LDL] (g/L or mg/mL)

2.8 Preparation of oxidized LDL

2.8.1 Dialysis tubing preparation for oxidation of LDL

The dialysis membrane tubing (Medical International Ltd., London, England) was cut into 25 cm sections and were boiled in 1 mM EDTA and 5% (w/v) $NaHCO_3$ for 20 minutes. The tubes were washed with nanopure water and boiled again in nanopure water for 20 minutes. The tubes were again washed thoroughly with nanopure water and were stored for long term use in the solution containing water: ethanol (50:50, v/v) at 4^0C. The tubes were rinsed with water and PBS before being used for oxidation of LDL.

2.8.2 LDL oxidation

The concentrated native LDL was mixed with 0.5 mM $CuCl_2$ placed in the double knotted dialysis tubing closed with a zip clip and a knot. The tubing was later placed in a loosely capped bottle containing PBS and 0.5 mM $CuCl_2$, kept in 37^0C in shaking incubator for 24 hours (Satchell & Leake, 2012). The amount of PBS was adjusted accordance to the amount of LDL to comprise 1L buffer/10 mg LDL. During this process, the yellow colored native LDL becomes colorless. After 24 hours, the dialysis bag was transferred to bottle containing 1L PBS and a teaspoon of washed Chelex-100 resins and magnetic flee at 4^0C.

The solution was left stirring for 2 hours at 4^0C after which the bag was transferred to a new bottle containing and Chelex and PBS for 2 more hours. The tubing was left undisturbed overnight after transferring the tubing into the new bottle containing PBS and Chelex. The following day oxLDL was separated from dialysis tubing and was filter-sterilized through a 0.22 μm membrane filter in the CII cabinet, stored at 4^0C and was used within 2 months from time of oxidation.

2.9 Biochemical analysis

2.9.1 Protein concentration determination

Bicincronic acid (BCA) protein analysis kit (Thermo Scientific, Rockford, USA) was used to estimate the protein concentration in the samples. The method is the combination of reduction of Cu^{2+} ions to Cu^{+} ions in alkaline medium and calorimetric determination of Cu+ ions using bicincronic acid.

Sample preparation: The working reagent for BCA assay was freshly prepared by mixing Reagent A and Reagent B of the kit in 50: 1 ratio. 1 mL of working reagent was mixed with 50 μL of diluted sample and incubated at 60^0C for 30 minutes with gentle shaking. The reaction was stopped by either placing samples on ice or partially immersing them in the cool water for no longer than 2 minutes. The protein concentration was determined by reading absorbance at 562 nm (Agilent Technology) and was compared to standard curve prepared by the incubation of known BSA concentrations in 1 mL working reagent.

2.10 Cell viability Assay

2.10.1 MTT reduction Assay

The MTT colorimetric assay determined the ability of viable cells to convert soluble tetrazolium salt (MTT) into insoluble formazan precipitate. Tetrazolium salts accepts electrons from oxidized substrates or appropriate enzymes such as NADH and NADPH. MTT is reduced by ubiquinone, cytochrome b and c sites of mitochondrial electron transport chain and is a result of succinate dehydrogenase activity. This reaction converts yellow salts to blue colored formazan crystals that can be dissolved in an organic solvent whose concentration can be spectrophotometrically determined (Mosmann, 1983).

Trypan blue exclusion assay is another widely used method to determine cell viability. Cell's ability to exclude a colored dye (trypan blue) serves as a measure of membrane integrity thus indicating cell survival.

Sample preparation for U937 cells: 500 µL of U937 suspension cells were seeded at concentration 2.5×10^6 cells/mL into 24 well suspension plates and were directly treated with 50 µL of 5 mg/mL MTT reagent into the treatment wells to obtain the final concentration of 0.5 mg/mL. The plates were incubated in the dark at 37^0C for 1–2 hours to allow sufficient formazan development. The formazan crystals were thoroughly mixed and solubilized by addition of equal volume (500 µL) of 10% (w/v) SDS in 0.01 M HCl into each well and the absorbance was quantified at 570 nm using (Agilent Technology) against the blank containing either the reagents only or nanopure water. The relative percentage of viability was calculated as follows:

$$Viability\ (\%) = \left[\frac{A570\ (Compound)}{A570\ (Control)}\right] \times 100$$

Sample preparation for human monocytes: 500 µL of human monocyte suspension cells were seeded at concentration 0.5×10^6 cells/mL into 24 well suspension plates and were directly treated with 50 µL of 5 mg/mL MTT reagent into the treatment wells to obtain the final concentration of 0.5 mg/mL. The plates were incubated in the dark at 37^0C for 1–2 hours to allow sufficient formazan development. The formazan crystals were thoroughly mixed and solubilized by addition of equal volume (500 µL) of 10% (w/v) SDS in 0.01 M HCl into each well and the absorbance was quantified at 570 nm using (Agilent technology) against the blank containing either the reagents only or nanopure water. The relative percentage of viability was calculated as above.

2.10.2 Trypan blue exclusion assay

The suspension cells were mixed by pipetting and 100 µL was collected into a separate eppendorf tube followed by the addition of trypan blue at appropriate ratio (1: 1 for U937 cells and 1: 10 for human monocytes) and the stained cells were counted using a hemocytometer.

2.11 Flow Cytometry

Flow cytometry gives quick analysis of numerous characteristics of single cells with both quantitative and qualitative information. Characteristics such as cell size, cell cycle, viability, cytoplasmic complexity, apoptosis nucleic contents, membrane potential and variety of membrane–bound and intracellular proteins can be measured using a flow cytometer. Flow cytometer Scatters light at various angles and distinguishes the cells based on its size and internal complexity whereas, light emitted from fluorescently labelled antibodies indicates a variety of cell surface and cytoplasmic antigens. An Accuri C6 flow cytometer (Accuri Cytometer, BD CSampler) was used to measure Propidium iodide, annexin V and TMRM probe fluorescence.

2.11.1 PI staining and cell viability

Externalization of PS (Phosphatidylserine) to the cell surface is an early marker of apoptotic cell death. PI (Propidium Iodide) a marker of membrane permeability, can be used to distinguish between early apoptosis and necrosis. Plasma membrane integrity is lost during both primary and secondary necrosis (necrosis occurs after apoptosis when apoptotic cells are not removed by phagocytosis), allowing Propidium Iodide to enter the cell and stain the nuclear material.

Sample preparation: 500 µL of U937 suspension cells were seeded at concentration 2.5 × 10^6 cells / mL into 24 well suspension plates and were directly treated with 8 µL of 1 mg/mL PI to obtain the final concentration of 1.5 µg/mL and incubated in dark for 10–15 minutes. After the incubation, the cells were analyzed using flow cytometer.

Data Collection and gating: Data on U937 was collected by setting the flow rate at 66 uL/minute with core size of 30 µm and a minimum 10,000 events into the gated area. The gate contained healthy cells, cell debris and early necrotic cells to determine the cell viability. FL3 filter was used which has excitation at (535 nm) and emission at (617 nm). Size was detected by forward scatter (FSC) and granularity by side scatter (SSC) using a dot plot by selecting a linear scale. Exclusion gates were set up based on FSC and SSC dot plot, cellular debris was excluded and a histogram was plotted to detect PI using a log scale. The data was collected using a CFlow plus software and analyzed. All the data was collected and examined using CFlow Plus software.

2.11.2 TMRM staining and mitochondria membrane potential

Apoptosis can be indicated by loss of mitochondrial membrane potential which can be measured by cationic redistribution fluorescent dyes such as tetramethylrhodamine methyl ester (TMRM) (Merck Darmstadt, Germany) (Scaduto & Grotyohann, 1999; Shapiro, 1994). Carbonyl cyanide m-chlorophenyl hydrazone (CCCP) is a protonophore that depolarizes mitochondria, acting as a positive control for loss of membrane potential which eventually results in reduced TMRM staining. TMRM dye is lipophilic in nature and its molecular structure bear a positive charge which helps it to penetrate in negatively charged mitochondria. Upon its accumulation, it exhibits orange fluorescence. Non–apoptotic cell or a healthy cell will exhibit a higher level of orange fluorescence as compared to the apoptotic cells.

Sample preparation: 1 mL of U937 suspension cells were seeded at concentration 0.5×10^6 cells / mL into 24 well suspension plates and apoptosis was induced by desirable method. Positive control cells were treated only with 1 µL of 50 mM CCCP to obtain the final concentration of 50 µM. Control and apoptosis–induced cells were treated with 5 µL 10 µM TMRM to obtain the final concentration of 50 nM. The samples were incubated in dark for 20 minutes and were analyzed using flow cytometer.

Data Collection and gating: Data on U937 cells was collected using following settings: Flow rate, 66 uL/minute; core size, 30 µm and volume, 30 µL with minimum 10,000 events to be recorded. FL2 laser filter was used as TMRM maximally excites at ~550 nm and emits maximally at 575 nm (Lisa C. Crowley). Size was detected by forward scatter (FSC) and granularity by side scatter (SSC) using a dot plot by selecting a linear scale. Exclusion gates were set up based on FSC and SSC dot plot, cellular debris was excluded and a histogram was plotted to detect TMRM using a log scale. The data was collected using a CFlow plus software and analyzed.

2.12 Western blotting

2.12.1 Solutions for western blot

Cracker buffer: 125 mM Tris–HCl, 1% SDS (w/v), 20% glycerol (w/v), 0.1% bromophenol blue (w/v) were mixed in nanopure water and pH was adjusted to 6.8 using concentrated HCl. Prior to use 2% (v/v) β–mercaptoethanol and 0.5 mM EDTA was added to 1 mL of the above solution.

Triton–X100 for cell lysis: The solution consisted of 1% triton X100, 7x minitab protease inhibitor cocktail and nanopure water. The cell lysis solution was prepared fresh prior to experiment and was stored in 4^0C until addition to samples to initiate cell lysis.

MOPS buffer: A 10X stock solution of MOPS was prepared with 500 mM MOPs, 500 mM Tris base 1% SDS (w/v) and 10 mM EDTA in water with pH adjusted to 7.7. This 10X concentration was further diluted in nanopure water to 1X prior to use.

Transfer buffer: Transfer buffer consisted of 25 mM Tris, 200 mM Glycine, and 20% methanol (v/v) in nanopure water and was stored at 4^0C for further use.

Tris buffered saline (TBS): 1X Tris buffered saline was prepared from 10X stock for nitrocellulose washing consisted of 40 mM Tris–HCl, 150 mM NaCl at pH 7.5, 0.1% Tween20 (w/v) and 0.01% thimerosal (w/v) (contains Hg, toxic) dissolved in nanopure water.

Non–fat milk in TBS (TBSM): Nitrocellulose membrane was blocked with 5% (w/v) non–fat milk powder (Anchor, New Zealand) made in 1X TBS and was stored at 4^0C for up to 1 week.

Ponceau S stain: The Ponceau S stain consisted of 0.01% Ponceau S (w/v) in 5% acetic acid.

2.12.2 Antibodies

Antibodies were stored at 4^0C and was added directly to the incubation solution. A table of antibodies and concentrations used is listed below.

Table 1: Antibodies and usage conditions.

Agent	Raised in	Dilution	Medium	Incubation Time	Supplier	Conjugation	Clonality
GADD-153	Mouse	1: 50	2.5% TBSM	Overnight at 4^0C	Santa Cruz	-	Monoclonal
m-IgGκ	Mouse	1: 2000	2.5% TBSM	1 h	Santa Cruz	HRP	
B-actin	Mouse	1: 10,000	1% TBSM	1.5 h	Sigma Aldrich	-	Monoclonal
m-IgGκ	Mouse	1: 1000	2% TBSM	1.5 h	Santa Cruz	HRP	

2.12.3 Sample Preparation

Cell lysate preparation: U937 suspension cell samples were transferred from wells to 1.5 mL centrifuge tubes after an appropriate incubation time and were centrifuged at 15,000 g for 5 minutes at 4^0C. The supernatant was discarded and the pellet was washed twice with cold PBS at 15,000 g for 5 minutes at 4^0C. The supernatant was discarded and pellet was resuspended in 200 µL of ice–cold lysis buffer containing protease inhibitor and were kept on ice for 2 minutes to ensure lysis. The samples were subjected to determine the protein concentration or were frozen at -20^0C for later use.

2.12.4 SDS-polyacrylamide gel electrophoresis.

A required volume of sample containing 100 ug of protein concentration was considered appropriate to be used for SDS–PAGE and western blot analysis. The required volume was aliquoted in to 1.5 mL centrifuge tube, was suspended into 400 µL of ice–cold Acetone and was centrifuged at 15,000 g for 10 minutes at 0^0C. The supernatant was discarded and tubes were left in fume hood for 15–30 minutes for remaining acetone to evaporate. The pellet was resuspended in 25 µL cracker buffer containing 2% β–mercaptoethanol to final the protein concentration at 2–5 ug protein per µL. The samples were vortexed and heated in a heating block at 95^0C for 3 minutes to denature the protein. After denaturation, the samples were centrifuged at 15,000 g for 5 minutes at 4^0C. 5 µL of prestained molecular weight marker mix (Thermo Scientific, Lithuania) and 23 µL/well (Depending upon the required protein content) of samples were loaded into the wells. The samples were subjected to electrophoresis on the gradient polyacrylamide gel, (4–

12% Bis–Tris gel, Invitrogen, Carslband, CA, USA) in 1X MOPS buffer. The gel was run at 100 V and was later switched to 200 V after the dye front eluted from the wells.

2.12.5 Immunoblotting

After SDS–PAGE, the gel was transferred on to nitrocellulose membrane using a transblot turbo transfer pack (Bio–rad) preparing sandwich according to manufacturer's instructions. The sandwich was enclosed into the cassette and was placed in Transblot turbo® transfer system (Bid–rad). The transfer system was set to 2.5 A, 25V and 10 minutes to transfer proteins on to the nitrocellulose membrane. Once the transfer was completed the NC was rinsed with nanopure water and was stained with 0.01% Ponceau S stain for 1–2 minutes to examine the transfer efficiency. Pink protein bands were visible with Ponceau S stain.

The following procedures were done on rocking platform mixer (Ratek Instruments, Australia and WiseMix, Wisd Laboratories Instrument). The membrane was given a quick rinse with water and was blocked in 5% non–fat milk in TBS (TBSM) for 1 hour with TBSM changing every 20 minutes. The membrane was washed with TBS for 25 minutes (TBS was changed every 5 minutes). The membrane was probed with GADD-153 (CHOP) monoclonal antibody (Santa Cruz Biotechnology Inc, USA) in 2.5% TBSM in 1: 50 dilutions and was incubated overnight at 4^0C. The membrane was given a quick wash with TBS and was washed again for 25 minutes (TBS was changed every 5 minutes) prior to secondary antibody incubation. The membrane was incubated with m-IgGκ BP-HRP secondary antibody (Sigma Aldrich, USA) in 1: 2000 dilution in 2.5% TBSM for 1 hour at room temperature. TBSM containing secondary antibody was discarded and membrane was washed with TBS for 25 minutes. After the wash, TBS was removed, the membrane was rinsed with nanopure water and kept in nanopure water for visualization. After visualization, the membrane was kept in nanopure water at 4^0C until re–probing. The membrane was stripped off the anti–GADD–153 antibodies before probing it for β–actin. The membrane was incubated in stripping buffer (2% SDS, 50 M tris, 400 µL β–mercaptoethanol, pH 6.8 heated to 50^0C on a water bath) for 20–30 minutes. This was followed by 25 minutes TBS wash (TBS changed every 5 minute) and was directly incubated with β–actin primary antibody without blocking.

Visualization: The Chemiluminescence signal corresponding to the position of hydrogen peroxidase (HRP)–conjugated secondary antibody was detected by incubating membrane with Supersignal West Dura Chemiluminescence substrates (ThermoScientific, USA), which were mixed in ratio 1: 1. The images were recorded after 2.5 minutes after the application of visualization of HRP substrate solution according to the manufacturer's instructions. The images were obtained at high resolution, without filter or light using Syngene Chemigenius–2 bioimaging system (Logue, Cleary, Saveljeva, & Samali). Exposure time varied for different antibodies – from few seconds for β–actin (25 milliseconds-5 seconds) detection to 5–7 minutes (with EDR function ticked) or 20-30 minutes (without ERD function ticked) in on Syngene Chemigenius-2 bioimaging system for GADD–153 (CHOP) detection (Clicking EDR). The images were analyzed for band intensity with GeneSnap (Syngene, USA) and ImageJ.

2.13 Statistical analysis

Statistical analysis was performed using GraphPad Prism Version 7.03 for Windows 10 (GraphPad software, San Diego, California, USA), All experiments were performed in triplet and each data point was replicated at least thrice within an experiment. Unless stated, otherwise the results are displayed as Mean ± SEM of mean values from **A)** single experiment and **B)** Combined mean values from three separate experiments. Statistical significance was tested using one and two-factor analysis of variance (ANOVA), t-tests with 95% confidence intervals and linear regression. One factor ANOVA was followed by Dunnett's post test, Bonferroni post test or Turkey's multiple comparison test, where appropriate. A two-tailed t-test with 95% confidence interval was used when two sets of values were compared. The type of statistical test used in each experiment is indicated in the figure caption and the statistical significance is denoted by *, $p < 0.05$, **, $p < 0.01$ and $p < 0.001$ respectively.

CHAPTER 3

3 RESULTS

3.1 Effect of oxLDL toxicity on U937 cells.

The research first examined oxLDL toxicity to U937 cells. U937 cells were treated with increasing concentrations of oxLDL (0.05 mg/mL–1.0 mg/mL) by incubation at 37^0C under standard incubation time of 24 hours. Cell viability was measured using PI-flow cytometry and MTT colorimetric assay. Cell morphology was assessed using an inverted light microscope (**Figure 10A**). Morphologically control cells (no oxLDL added) appeared round and circular which is a classical feature of U937 cells and resembling the monocytes. Cells treated with 0.05 mg/ mL, 0.1 mg/mL and 0.2 mg/mL oxLDL illustrated swelling or foamy appearance along with disruption of internal organelles. However, cells treated with 0.5 mg/mL or above a concentration of oxLDL indicated cell debris and distorted cell membranes, causing significant damage to their cell membranes and loss of cellular contents which are some common characteristic of necrotic cell death (**as described in 1.3.2**). Final oxLDL concentrations of 0.05, 0.1, 0.2, 0.5 and 1.0 mg/mL reduced U937 cell viability (PI Negative cells) by 92.35%, 88.02%, 55.64%, 16.11% and 4.37% respectively (compared to control) (**Figure 10B**). Therefore, the LC_{50} concentration obtained was 0.393 mg/mL, and the cell death percentage also elevated with increasing oxLDL concentrations (PI Positive cells) (**Figure 10B**). On the other hand, MTT assay showed results identical to that of PI-flow cytometry analysis. Cells treated with 0.05 and 0.1 mg/mL oxLDL yielded higher cell viability, 0.05 mg/mL oxLDL treated cells illustrated 116.12% viable cells and 0.1 mg/mL oxLDL treated cells resulted in 109.58% viability (**Figure 11**). Cells treated with 0.2, 0.5 and 1.0 mg/mL oxLDL showed a rapid and significant decrease in cell viability. 0.2 mg/mL oxLDL treated samples depicted 69.58% cell viability compared to cell only control. However, 0.5 mg/mL and 1.0 mg/mL oxLDL treated samples demonstrated a greater loss in viable cells which was about 17.49% and 3.18% compared to cell only control (**Figure 11**).

PI negative plus PI positive cells always added up to a value lower than 100% due to a number of cells that had completely lysed to became cellular debris demarcating them into a category of neither PI negative nor PI positive population. It is also important to note that the LC_{50} concentrations of oxLDL differed from batch–to–batch, but the toxicity remained somewhere between 0.1–0.5 mg/mL as determined using PI-Flow cytometry. However, in some rare situations the oxLDL toxicity was above 0.5 mg/mL. Later, it was also confirmed that the oxLDL toxicity varied within few weeks to few months which was shown by previous work (Sean ,2016).

A)

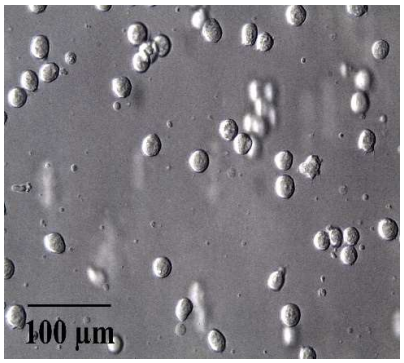

Cell only control

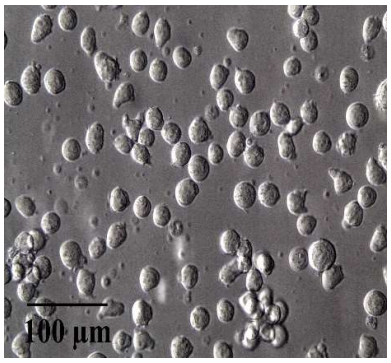

0.05 mg/mL

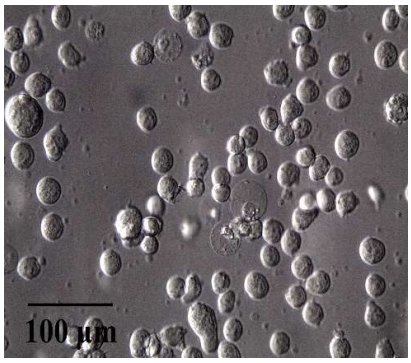

0.1 mg/mL

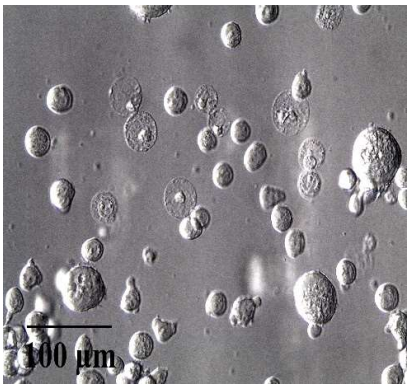

0.2 mg/mL

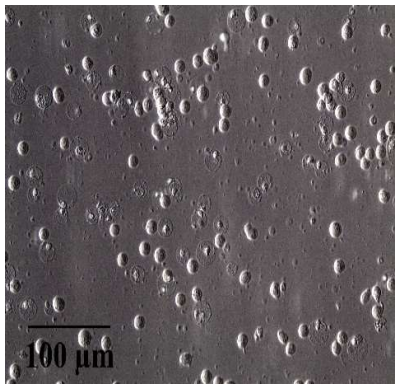

0.5 mg/mL

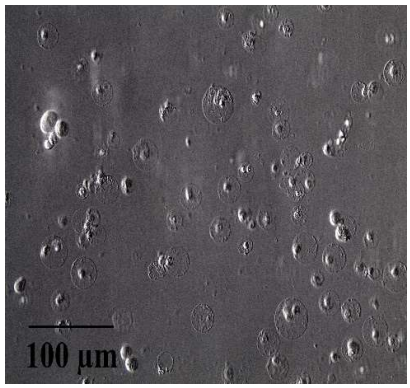

1.0 mg/mL

B)

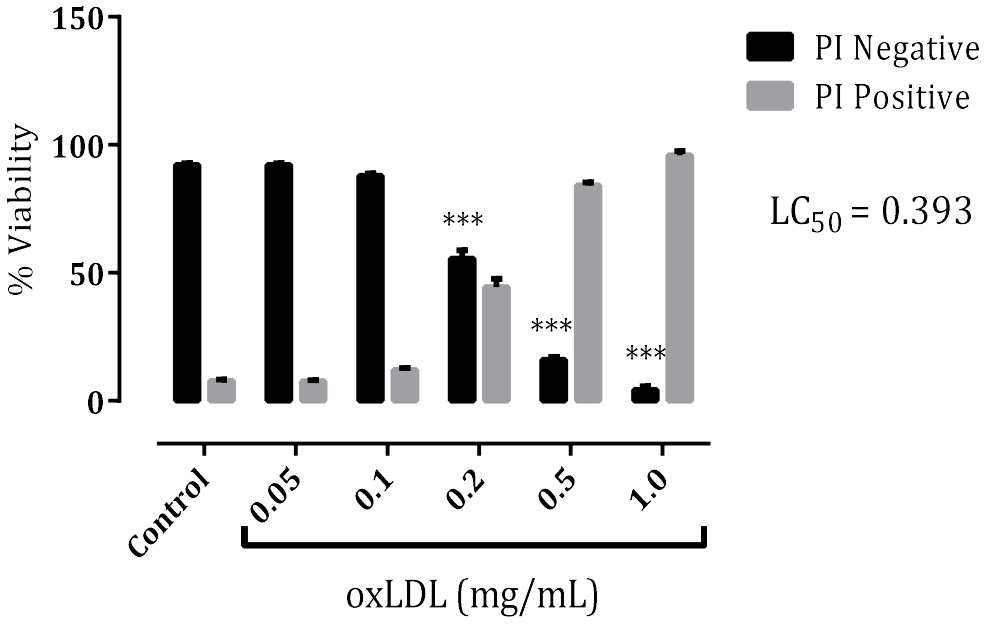

Figure 10: Effect of oxLDL toxicity on U937 cell Viability by PI Flow cytometry

U937 cells (0.5 X 10^6 cells/ml) were incubated at 37^0C in RPMI 1640 and 5% FBS with no phenol red and increasing concentrations of Cu-oxLDL for 24 hours in 24 well suspension culture plate. A) Cells were examined *in situ* using an inverted microscope (400X magnification) after 24 hours incubation with various oxLDL concentrations. Images were captured using a Leica C-Mount camera and processed using Leica Application suit software. B) Cell viability was determined using PI–Flow cytometry assay. Data are expressed as a percentage of total cell count in cell control only samples. Results are shown in mean ± SEM of technical replicates from a representative experiment. Statistical significance (two-way ANOVA, Sidak's multiple comparison tests) is indicated by PI negative cell only control vs. PI-negative oxLDL treatments. Significance levels are shown as (*), $p < 0.05$ (***), $p < 0.001$.

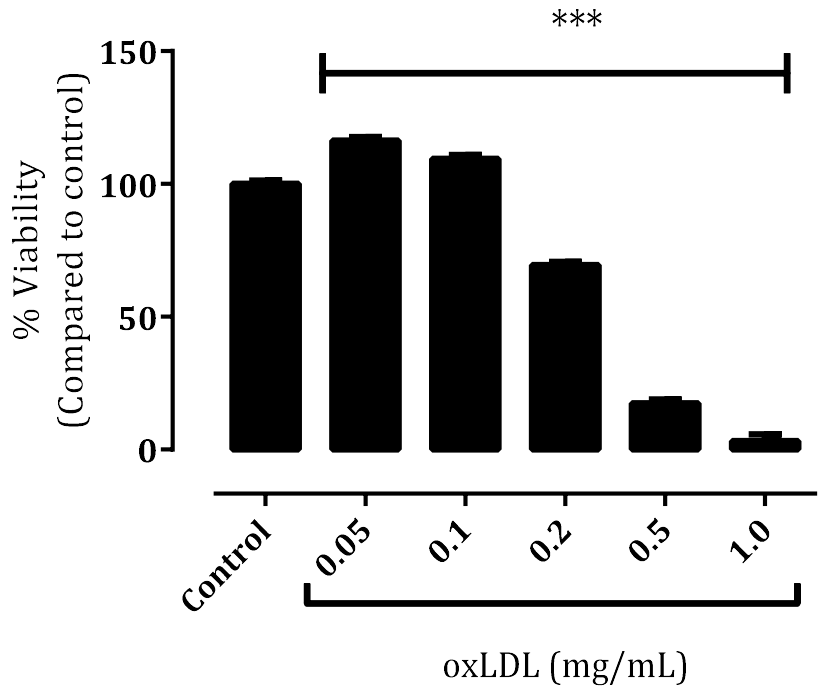

Figure 11: Effect of oxLDL toxicity on U937 cell viability by MTT assay

U937 cells (0.5 X 10^6 cells/mL) were incubated at 37^0C in RPMI and 5% FBS with no phenol red with increasing concentrations of oxLDL for 24 hours in 24 well suspension culture plates. Cell viability is determined using MTT assay. Cells were incubated with 100 µL MTT reagent at 37^0 C for 2 hours. Purple crystals were formed and were dissolved in 1 mL 10% SDS. Absorbance was recorded using Agilent UV–Visible Spectrophotometer at 570 nm wavelength. Data are expressed as the percentage of living cells in control only samples. Results are shown in mean ± SEM of technical replicates from a representative experiment. Statistical significance (one-way ANOVA, Sidak's multiple comparison tests) is represented by cell only control vs oxLDL treatments. Significance levels are indicated as (*) $p < 0.05$, (***) $p < 0.001$.

3.2 Effect of Thapsigargin (TG) on U937 cells

Thapsigargin, a potent ER–stress inducer through its action as a non–competitive inhibitor of sarco/endoplasmic reticulum Ca^{2+} ATPase (SERCA) (Inesi & Sagara, 1994). The inhibitor elevates explicitly the intracellular Ca^{2+} influx and restricts the calcium pumping ability of cell into the endoplasmic reticulum. Previous work led by Izani (2015) focused on Thapsigargin-induced Ca^{2+} influx in the U937 cells. Thapsigargin is known to inhibit the fusion of autophagosome and lysosomes, which causes stress on endoplasmic reticulum causing cellular death (Ganley, Wong, Gammoh, & Jiang, 2011). Thapsigargin is also known to trigger apoptotic cell death by activating CHOP through ATF4 expression when the cell undergoes ER–stress (Hiroki Matsumoto et al., 2013). In the current experiment, we explored Thapsigargin-induced cytotoxicity in U937 cells.

U937 cells were treated with the increasing concentrations of Thapsigargin (25 nM–100 nM) and were incubated at 37^0C under standard incubation time of 24 hours. Cell viability was measured using PI–flow cytometry and MTT colorimetric assay. Cell morphology was assessed using an inverted light microscope. Morphologically, control cells (no TG added) appeared round and spherical which is a classical feature of U937 cells (**Figure 12A**). Cells treated with 25 nM and illustrated swelling appearance and some amount of cell debris (**Figure 12A**). However, cells treated with 50 nM or above caused cell debris and distorted cell membranes, indicating significant damage to their cell membranes and loss of cellular contents which are some common characteristic of necrotic cell death (**Figure 12A**). Final TG concentrations of 25, 50, 75 and 100 nM reduced U937 cell viability (PI Negative cells) by 51%, 37%, 31%, and 30%, respectively (compared to control). Therefore, the LC_{50} concentration was obtained at 44.55 nM (**Figure 12B**). As with the oxLDL, sum of PI negative and PI positive cells was always lower than 100% due to a number of cells that had completely lysed to became cellular debris and were neither counted as PI negative nor PI positive population. The results obtained by MTT colorimetric assay followed a similar trend of decreasing cell viability with increasing concentrations of TG. It was observed that the final concentrations of 25, 50, 75 and 100 nM lessened the viability by 78.60%, 66.50%, 56.49% and 53.30% respectively compared to the cell only control (**Figure 13**). The data obtained suggests that ER–stress inducer, TG is toxic to U937 cells.

A)

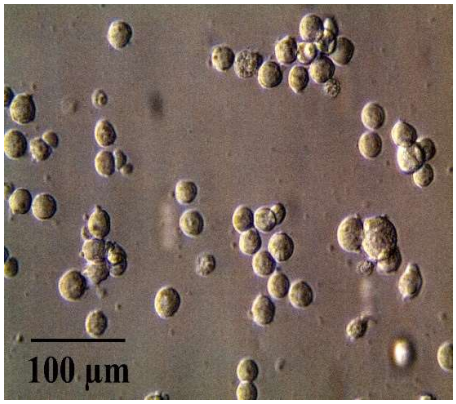

Cell only control

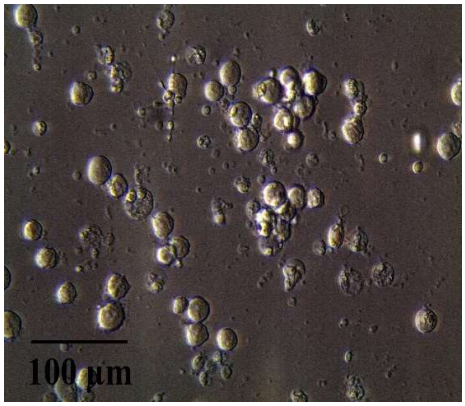

25 nM TG

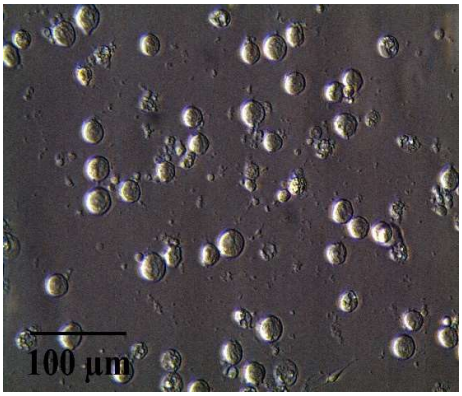

50 nM TG

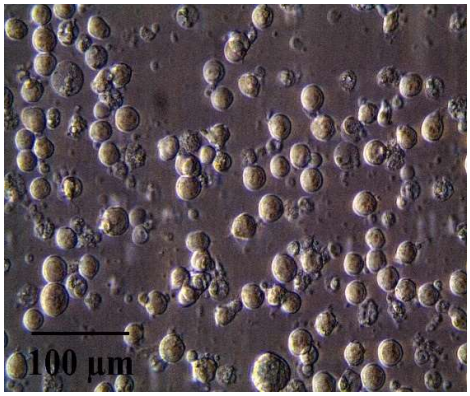

75 nM TG

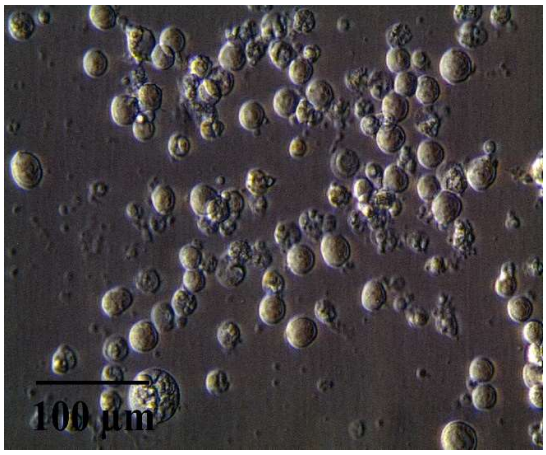

100 nM TG

B)

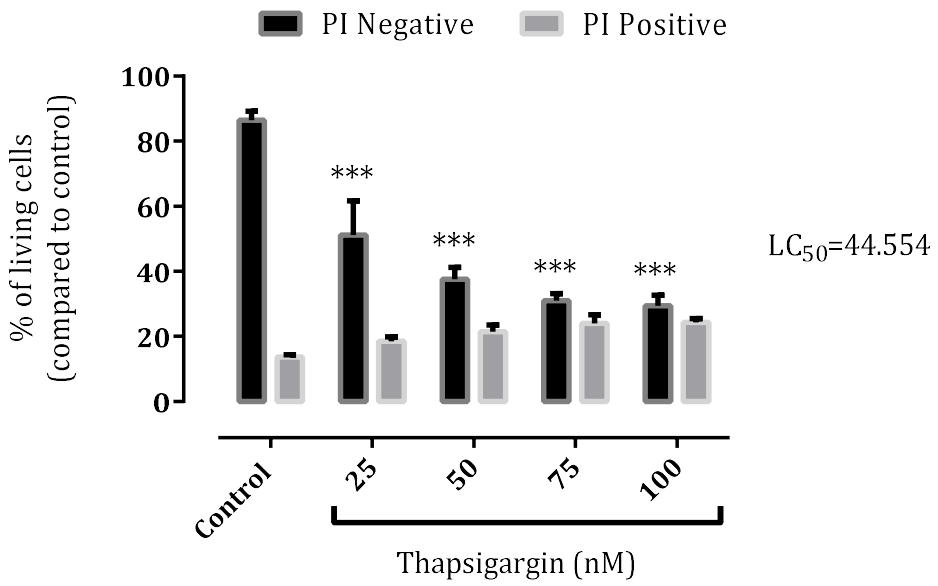

Figure 12: Effect of TG on U937 cell viability measured by PI-flow cytometry.

U937 cells (0.5 X 10^6 cells/ml) were incubated at 37^0C in RPMI 1640 and 5% FBS with no phenol red with the increasing concentrations of TG for 24 hours in 24 well suspension culture plate. A) Cells were examined *in situ* using an inverted microscope (400X magnification) after 24 hours incubation with various TG concentrations. Images were captured using a Leica C-Mount camera and processed using Leica Application suit software. B) Cell viability was determined using PI–Flow cytometry assay. Data are expressed as a percentage of total cell count in cell control only samples. Results are shown in mean ± SEM of technical replicates from a representative experiment. Statistical significance (two-way ANOVA, Sidak's multiple comparison tests) is indicated by PI negative cell only control vs. PI-negative TG treatments. Significance levels are shown as (***), $p < 0.001$.

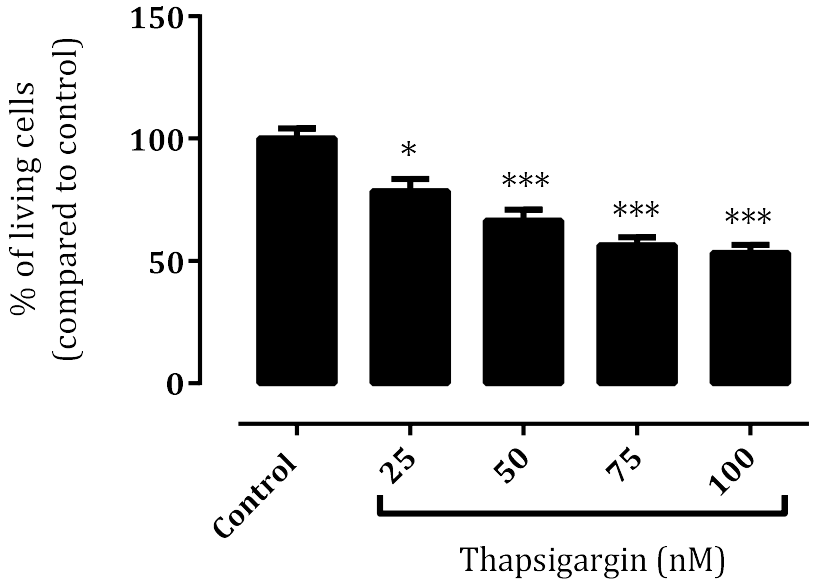

Figure 13: Effect of TG on U937 cell viability measured by MTT colorimetric assay.

U937 cells (0.5 X 10^6 cells/mL) were incubated at 37^0C in RPMI 1640 and 5% FBS with no phenol red with increasing concentrations of TG for 24 hours in 24 well suspension culture plates. Cell viability is determined using MTT assay. Cells were incubated with 100 µL MTT reagent at 37^0C for 2 hours. Purple crystals were formed and were dissolved in 1 mL 10% SDS. Absorbance was recorded using Shimadzu UV 1601PC UV-Visible Spectrophotometer at 570 nm wavelength. Data are expressed as the percentage of living cells in control only samples. Results are shown in mean ± SEM of technical replicates from a representative experiment. Cell only control vs represent statistical significance (one-way ANOVA, Sidak's multiple comparison tests). TG treatments. Significance levels are indicated as (*) $p < 0.05$, (***) $p < 0.001$.

3.3 Effect of Thapsigargin on Mitochondrial membrane potential (ΔΨm) in U937 cells.

Changes in the mitochondrial membrane potential is directly linked to cell death. TG induced U937 cell death appeared more necrosis rather than apoptosis. The cell morphology indicated internal organelle structure degradation, cell swelling, disruption of nuclear membrane and rupture of the plasma membrane as seen in **(Figure 15A)**. 25 nM and 50 nM TG treated cells illustrated cell swelling compared to untreated cell only control **(Figure 15A)**. The cells treated with 75 nM and 100 nM TG not only indicated cell swelling but degradation in internal organellar structures compared to healthy cell only control suggesting the evidence of necrotic cell death. Henceforth, it was necessary to observe whether these changes are linked the loss of mitochondrial membrane potential (ΔΨm).

U937 cells were treated with increasing concentrations of Thapsigargin (25 nM–100 nM) and incubated at 37^0C for 24 hours. Sample preparation was done as described in 2.11.2 and mitochondrial membrane potential was measured using TMRM dye and flow cytometry. CCCP (Carbonyl cyanide m-chlorophenyl hydrazone) was used as a positive control for loss of membrane potential for the experiment. It was observed that cell only control resulted in higher cell viability (**Figure 14 and Figure 15)** (76.37% compared to CCCP control cells) and low mitochondrial membrane potential **(Figure 15)**. However, the changes in the mitochondrial membrane potential increased with the increasing TG concentration in the system. Cells treated with 25 nM TG showed an increase in membrane potential **(Figure 15B)** and decrease in the number of cells (60.78% compared to CCCP control) **(Figure 16)**. Fluorescent intensity increased significantly with 50 nM and 75 nM **(Figure 14 C and D)** with decrease in the number of cells (48.09% and 47.43% compared to CCCP control cells) **(Figure 16)**. Whereas, the fluorescent intensity decreased slightly when cells were treated with 100 nM TG **(Figure 14E)** along with a decrease in cell number (24.34% compared to CCCP treated control cells) **(Figure 15B)**. This increase in the fluorescent intensity and decrease in the cell number suggests heavy lysis.

Overall the results indicate the potential of TG induced cell death in U937 cells is mediated by the increase in ΔΨm with increasing TG suggesting that the cell have lysed before the ΔΨm can be measured. TG introduces Ca^{2+} efflux in the mitochondria, resulting in the opening of mitochondrial permeability transition pore leading to a loss in membrane potential.

A)

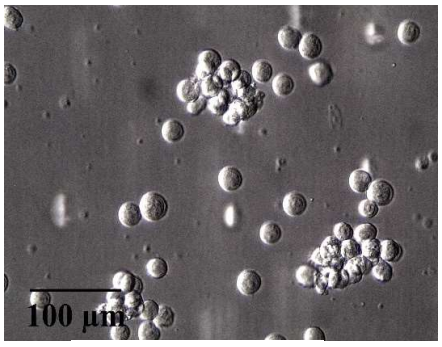

Cell only control

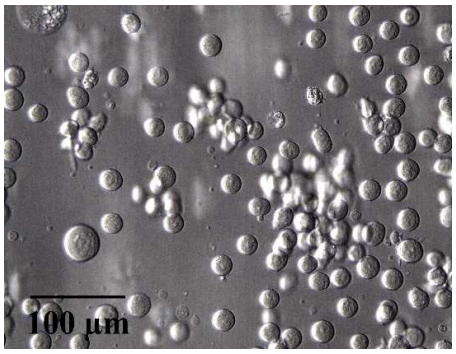

25 nM TG

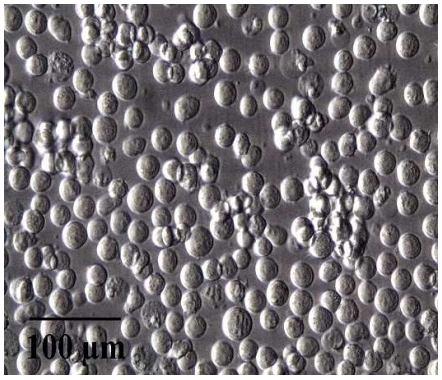

50 nM TG

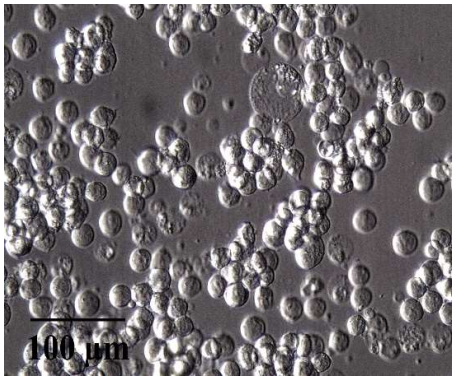

75 nM TG

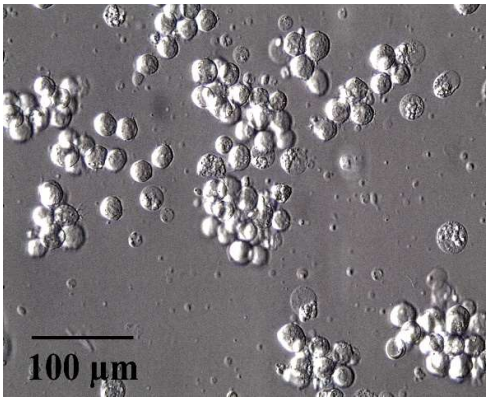

100 nM TG

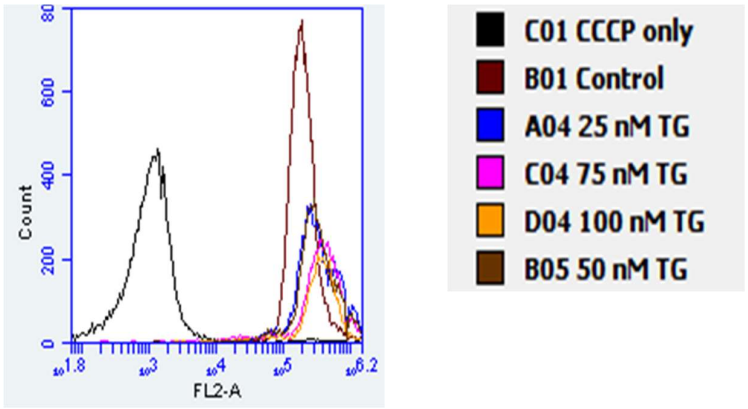

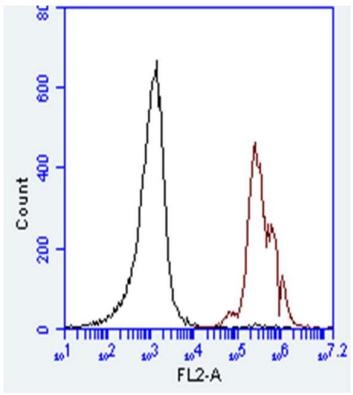

A) Cell only control

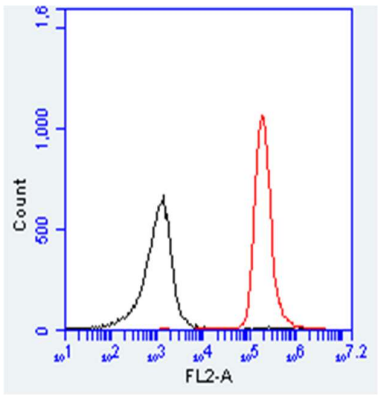

B) 25 nM TG

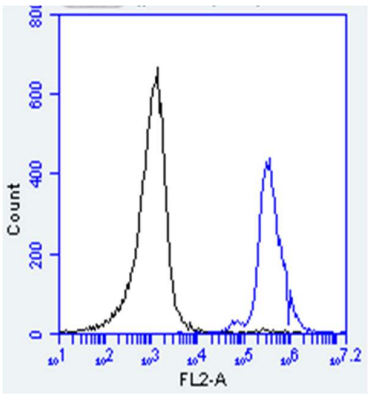

C) 50 nM TG

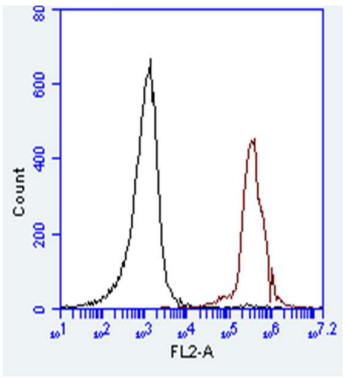

D) 75 nM TG

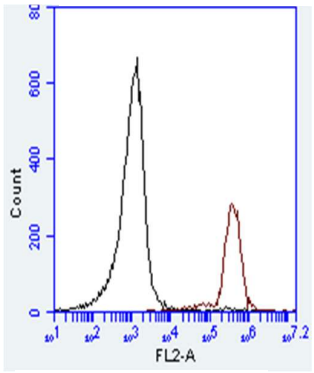

E) 100 nM TG

Figure 14: Mitochondrial membrane potential (ΔΨm) fluorescence intensity measurement by TMRM flow cytometry.

U937 cells (0.5×10^6 cells/mL) were incubated at 37^0C in RPMI 1640 without phenol red and increasing concentration of TG for 24 hours in 24 well suspension culture plate. Treatments were incubated with 50 nM CCCP alone and 50 µM TMRM alone for 20 minutes in the dark. Mitochondrial membrane potential was measured using FL–2 filter

by flow cytometer. Data is expressed as cell count vs mean cellular fluorescence. Each data expressed **(A-E)** is combined with CCCP control samples (black peak on the left side of each garph) and individual samples (colored peak on the right).

B)

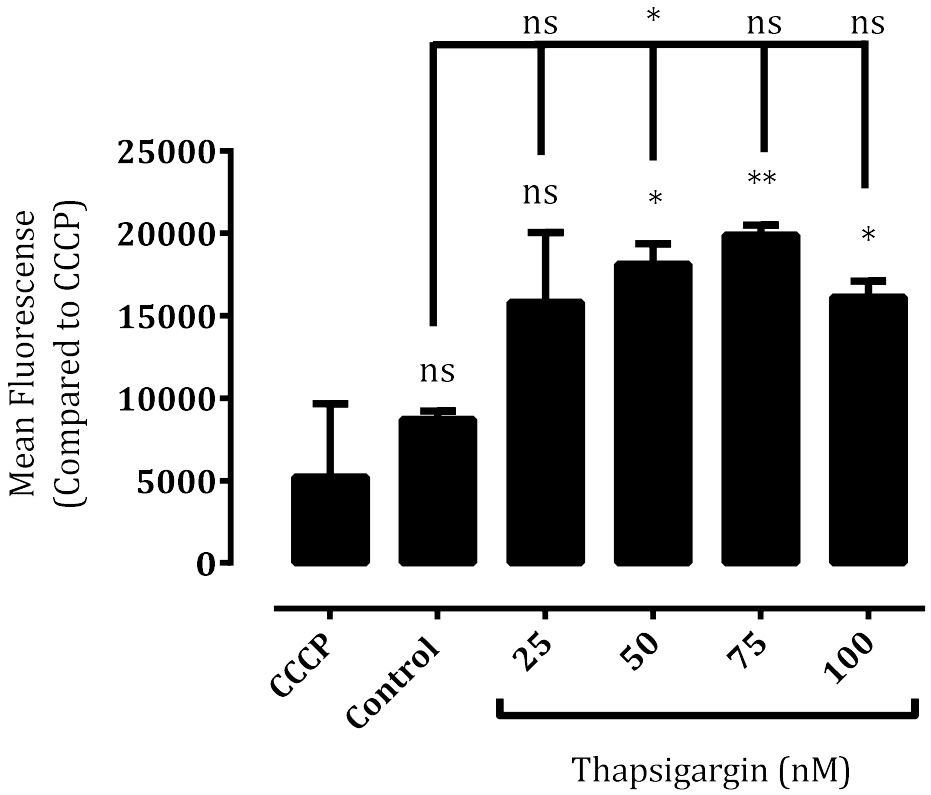

Figure 15: Effect of TG on mitochondrial membrane potential (ΔΨm) using TMRM staining.

U937 cells (0.5×10^6 cells/mL) were incubated at 37^0C in RPMI 1640 without phenol red and increasing concentration of TG for 24 hours in 24 well suspension culture plate. Treatments were incubated with 50 nM CCCP alone and 50 µM TMRM alone for 20 minutes in the dark. Mitochondrial membrane potential was measured using FL–2 filter by flow cytometer. Data is expressed as the mean cellular fluorescence intensity. **A)** Cells were examined *in situ* using an inverted microscope (400X magnification) after 24 hours incubation with various TG concentrations. Images were captured using a Leica C-Mount camera and processed using Leica Application suit software. **B)** Results are shown in mean ± SEM of technical replicates from a representative experiment. Statistical significance (one–way ANOVA, Dunnett's multiple comparison tests) is indicated by CCCP vs treatments. Significant levels are shown (*), $p < 0.05$, (**), $p < 0.01$ and (***), $p < 0.001$.

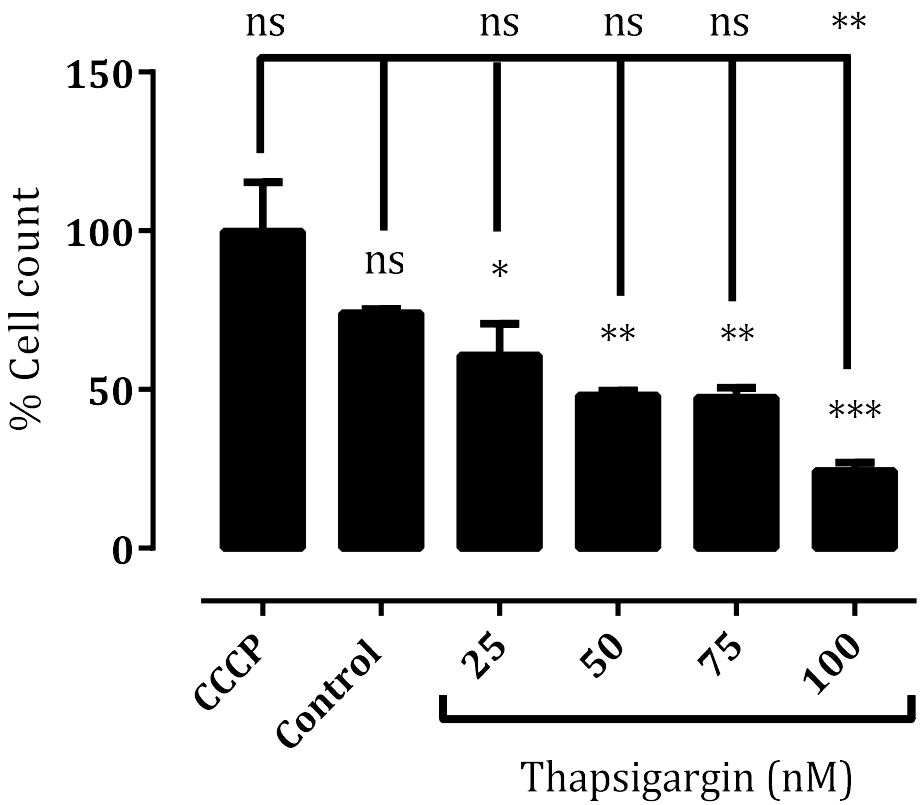

Figure 16: Effect of TG on cell viability using TMRM staining.

U937 cells (0.5×10^6 cells/mL) were incubated at 37^0C in RPMI 1640 without phenol red and increasing concentration of TG for 24 hours in 24 well suspension culture plate. Treatments were incubated with 50 nM CCCP alone and 50 µM TMRM alone for 20 minutes in the dark. Mitochondrial membrane potential was measured using FL-2 filter by flow cytometer. Data is expressed as percentage of cell viability. Results are shown in mean ± SEM of technical replicates from a representative experiment. Statistical significance (one-way ANOVA, Dunnett's multiple comparison tests) is indicated by CCCP vs treatments. Significant levels are shown (**), $p < 0.01$ and (***), $p < 0.001$.

3.4 Thapsigargin (TG)–induced CHOP activation in U937 cells.

CHOP, a marker of ER–stress, is a 29 kDa protein is expressed when the cells undergo endoplasmic reticulum stress. A dose-dependent study to investigate CHOP activation by TG in U937 cells treated with increasing concentration of (TG) 10, 25, 50, 75 and 100 nM was carried out.

After 24 hour incubation cells were extracted and lysed. The lysate was immunoblotted for CHOP protein activation with β-actin used as a loading control. CHOP expression was seen at 25 nM concentration (50.07% of control) **(Figure 17B)**. The expression increased as the TG concentration increased. The CHOP activation was observed maximum at TG concentration at 50 nM concentration (92.63% of control). A significant decrease can be seen in the expression of TG at 75 nM concentration (46.55% of control) **(Figure 17B)**. The expression again showed an elevation at a concentration of 100 nM TG (84.44% of control). Overall, the results suggest that U937 undergo ER stress when exposed to increasing concentrations of TG.

A)

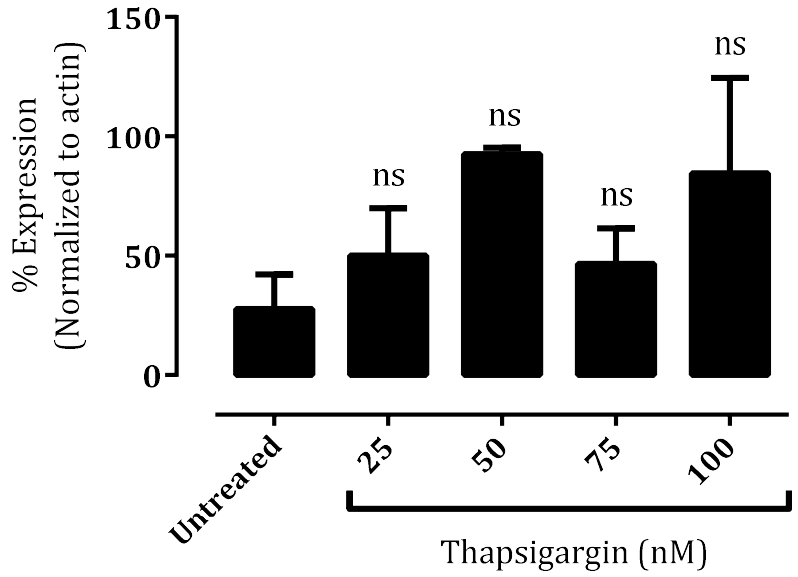

B)

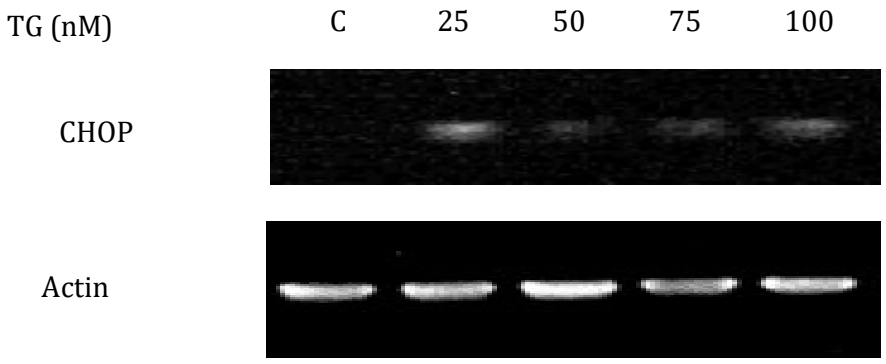

Figure 17: Thapsigargin-induced CHOP activation in U937 cells.

U937 cells (0.5×10^6 cells/mL) were treated with increasing Thapsigargin concentration (25 nM-100 nM) at 37^0C for 24 hours in RPMI 1640 containing 5% FBS and phenol red. The cell lysate was assessed for CHOP expression by western blot. **A)** Results were normalised by β–Actin and displayed as mean ± SEM of technical replicate experiment. Data is expressed as the percentage of respective control (cell only control), and significance is indicated from this control. **B)** Quantitative densitometry of western blots shows CHOP expression with increasing levels of Thapsigargin using ImageJ.

3.5 Effect of 7, 8–dihydroneopterin (7, 8–DNP) and Thapsigargin (TG) on CHOP activation in U937 cells.

Another goal this research investigated was to determine whether macrophage synthesised antioxidant 7, 8–dihydroneopterin (7, 8-DNP) has any direct role in CHOP induction. Our research group previously investigated the role of 7,8–DNP on CD36 expression, one of the primary scavenger receptor that uptake oxLDL. It has been found that 7,8–DNP downregulates CD36 expression levels in U937 cells and HMDM cells.

Some preliminary experiments performed with 7,8–DNP and TG indicated LPS contamination due to which the CHOP activation was observed with negative control 7,8–DNP and cell only control alone **(Figure 18)**. Based the observation, it was known that LPS is considered to be one of the prime factors that activate CHOP without activating apoptotic ER–stress pathways (Nakayama et al., 2010). The experiment was performed on U937 cells (0.5×10^6 cells/mL) in phenol red free RPMI 1640 containing 5% FBS for 24 hours at 37^0C. The cells were incubated with LC_{50} TG concentration of 44.55 nM alone (positive control), 7,8-DNP alone (negative control) and in combination with 7,8–DNP and TG. It was observed that the negative control and the cell only control activated CHOP on its own (38.89% and 42.80% compared to cell only control) (**Figure 18**). This problem was overcome by heat treatment on the materials that are often used to weigh up 7, 8–DNP. The spatulas was preheated at 220^0C for 2-3 hours prior weighing up 7, 8-DNP. With the preheat treatment the experiment was repeated to observe the effectiveness of pre-heating the materials and weighing up 7, 8-DNP and can be observed in **(Figure 19)** where no CHOP activation is seen with the 7, 8-DNP alone.

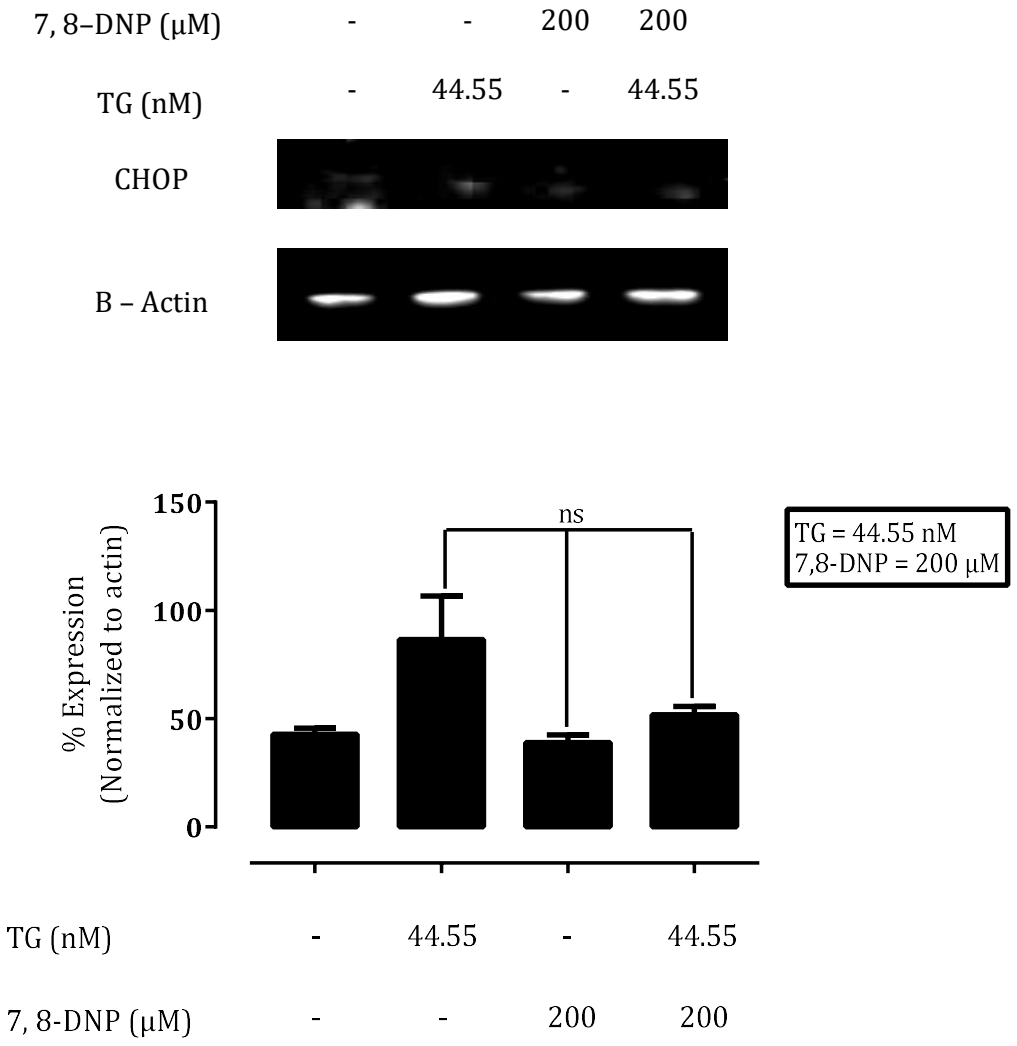

Figure 18: LPS is activating CHOP but not killing the cells.

Continuing the current objective, U937 cells were incubated with no treatments (cell only control), 75 nM TG alone as a positive control, 200 μM 7,8–DNP as negative control and in combination with varying 7,8-DNP concentrations (50, 100, 150 and 200 μM) and 75nM TG in RPMI 1640 with 5% FBS at 37^0C for 24 hours. The cells were extracted, lysed, and the lysate was immunoblotted for CHOP and β–actin was used as a loading control. The cell only control and 7, 8–DNP (negative control) has no CHOP activation **(Figure 19B).** 75 nM TG (positive control) expressed CHOP (121.95% of cell-only control). 50 μM 7,8-DNP and TG treated sample resulted in 71.91% expression compared to cell only control. The significant decrease in CHOP expression can be observed as the 7,8-DNP concentration in the cellular system increases. When the cells were incubated with TG

and 100 µM 7,8-DNP the level of CHOP expression decreased gradually from 71.91% to 68.87% compared to cell only control. A very slight fall in CHOP expression (68.64% compared to cell control) can be seen when the cells were treated with TG and 150 µM. However, when the cells were treated with TG and highest concentration of 200 µM 7,8-DNP, a substantial decrease in CHOP expression, 57.67% compared to cell only control was observed, apparently suggesting that 7,8-DNP is effective in downregulating CHOP during TG induced ER-stress in U937 cells.

A)

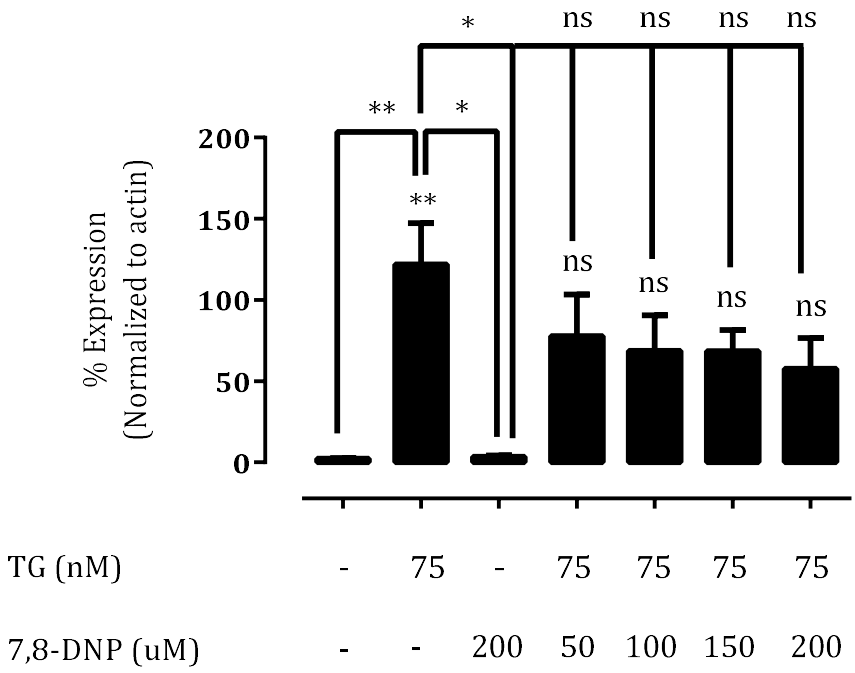

B)

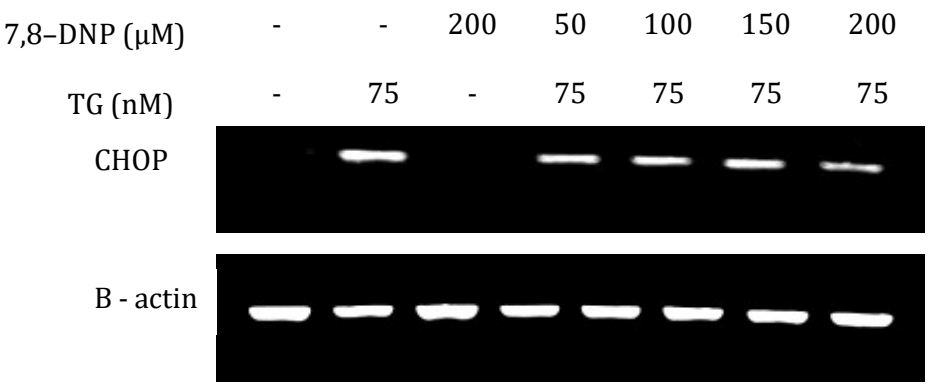

Figure 19: Effect of 7, 8-DNP on TG-induced CHOP activation in U937 cells.

U937 cells (0.5×10^6 cells/mL) were incubated with 200 μM 7, 8-DNP, 75 nM TG alone and in combination with 75 nM TG and varying 7, 8-DNP concentrations (50, 100, 150 and 200 μM) for 24 hours at 37^0C in RPMI 1640 without phenol red and containing 5% FBS. The cell lysate was assessed for CHOP expression using western blot. **A)** Results were normalised by β-Actin and displayed as mean ± SEM of technical replicates from a representative experiment. Data is expressed as the percentage of respective control (cell only control). Statistical significance (one-way ANOVA, Dunnett's multiple comparison tests) is indicated by cell only control vs treatments. Significant levels are shown (*), $p < 0.05$ and (**), $p < 0.01$. **B)** Quantitative densitometry of western blots showed CHOP expression with increasing concentrations of TG and fixed 7, 8-DNP concentration.

3.6 Dose-dependent oxLDL–induced CHOP activation in U937 cells.

With the confirmation of TG inducing CHOP expression in U937 cells, the primary aim of the project was to observe whether oxLDL is exhibiting CHOP to initiate cell death response pathways.

U937 cells were incubated with varying concentrations of oxLDL; 0.1, 0.2, 0.3, 0.4, 0.5 mg/mL and 100 nM (used as positive control) respectively for 24 hours. The cells were extracted, lysed and subjected to immunoblotting for CHOP expression with β-actin as a loading control. TG elevated CHOP expression (74.58% of control) while cell only control, 0.1 and 0.2 mg/mL oxLDL treated samples did not activate CHOP. In contrast, CHOP expression was first observed in 0.3 mg/mL oxLDL treated samples (37.31% of control). The CHOP expression initially increased with the 0.4 mg/mL oxLDL treated sample (59.41% of control) and was maximum with 0.5 mg/mL oxLDL treated sample (128.5% of control).

We also found out that different batch of oxLDL may or may not trigger CHOP activation in U937 cells. In one such batch, we observed CHOP activation through TG only positive control whereas no activation was observed with higher treated oxLDL samples. However, the results mentioned above confirm that U937 cells do exhibit CHOP and undergo ER stress to trigger cell death mechanisms.

A)

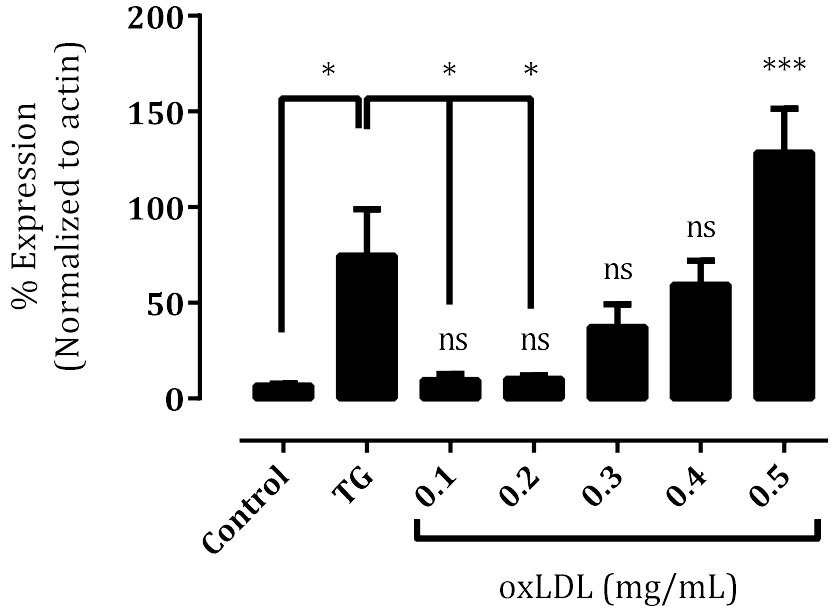

B)

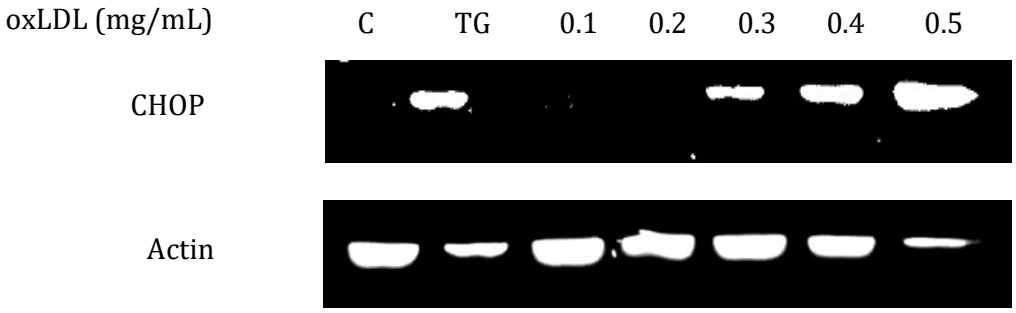

Figure 20: Dose–dependent effect of oxLDL on CHOP activation in U937 cells.

U937 cells (0.5×10^6 cells/mL) were treated with TG only (100 nM) and increasing oxLDL concentration (0.1 mg/mL–0.5 mg/mL) at 37^0C for 24 hours in RPMI 1640 containing 5% FBS without phenol red. The cell lysate was assessed for CHOP expression by western blot. **A)** Results were normalised with β-Actin and displayed as mean ± SEM of technical replicates of the representative experiment. Data are expressed as the percentage of respective control (cell only control). Statistical significance (one-way ANOVA, Dunnett's

multiple comparison tests) is indicated by cell only vs treatments. Significant levels are shown (*), $p < 0.05$ and (***), $p < 0.001$. **B)** Quantitative densitometry of western blots shows CHOP expression with increasing concentrations of oxLDL.

3.7 Time-dependent oxLDL induced CHOP activation in U937 cells.

Based on the results obtained by dose dependent treatment of oxLDL (**section 3.6**), a time dependent study was followed as to see at what time point can CHOP activation be seen with a fixed oxLDL concentration.

U937 cells were incubated with 0.4 mg/mL oxLDL for 0, 3, 6, 12 and 24 hours respectively, followed by the incubation of 100 nM TG alone for 12 and 24 hours as a positive control for the experiments. At each time point mentioned the cells were extracted, lysed. The lysate was immunoblotted for CHOP activation with β-actin as a loading control. 0.4 mg/mL oxLDL did not show any CHOP activation at 0 hour time points **(Figure 21B)**. A CHOP activation band can be observed at 3 hour (30.70% of control) with the increased expression at 6 hour 12 hour which nearly doubled at 24 hour time point (33.51%, 42.01% and 100.46% of control) **(Figure 21B)**. In correspondence to oxLDL treatment, positive control 100 nM TG also exhibited CHOP expression at 12 hour and 24 hour time points (45.75% and 104.16% of control) **(Figure 21B)**. It can also be observed that nearly 50% CHOP is activated at 12 hour time point with the expression doubling at 24 hour time point **(Figure 21B)**. It is also important to note that the β-actin bands seen in this particular experiment gave the similar results when performed in technical replicates. The intensity of actin bands deteorated with the time in oxLDL treated and TG treated control samples. The intensity of actin bands reduced at 12H and 24H oxLDL treatments whereas it was barely visible in 12H and 24H TG controls. We do not know the reason as to why there was reduction in actin band intensity, especially in 12H and 24H TG controls **(Figure 21B)**. There are some possibilities we suspect; might be due to TG effecting β-actin or high concentrations of TG which is killing the cells in higher amount or insufficient protein loading or some error in BCA protein determination assay.

The following result obtained suggests that a minimum of 3 hours is required by U937 cells to trigger CHOP activation by 0.4 mg/mL oxLDL to further initiate cell death mechanisms via CHOP activated ER–stress pathway.

A)

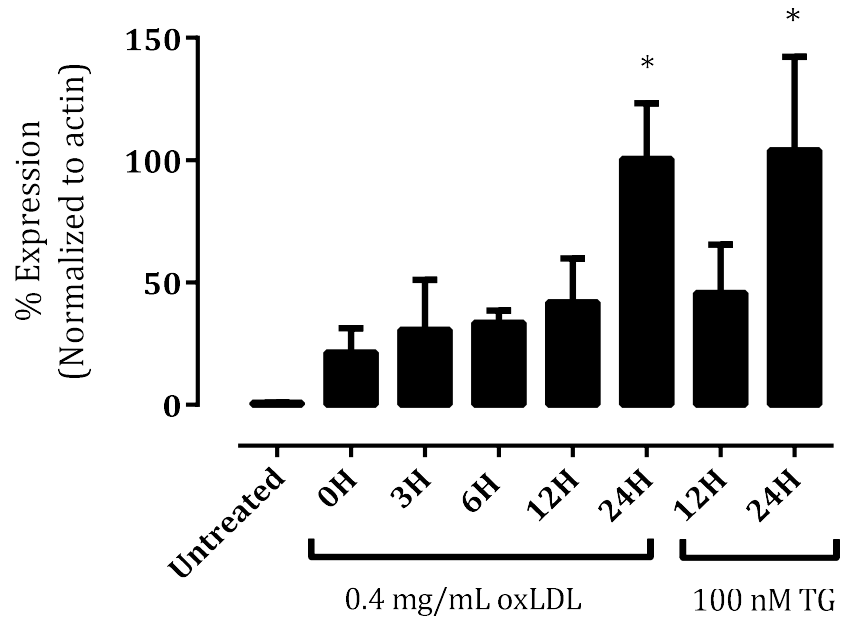

B)

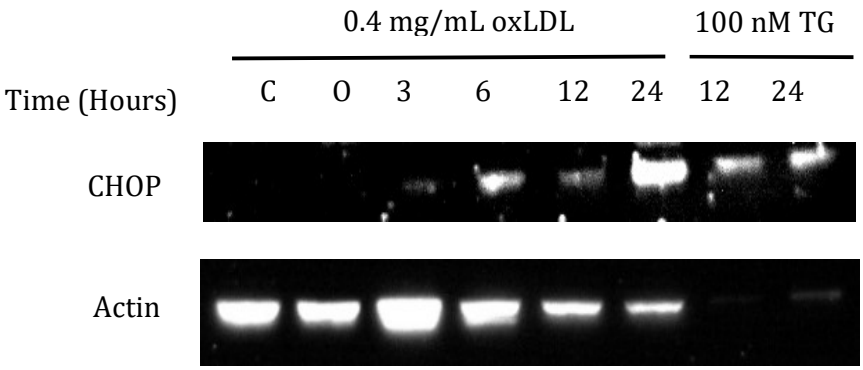

Figure 21: Time dependent activation effect of oxLDL on CHOP activation in U937 cells.

U937 cells (0.5×10^6 cells/mL) were treated with 0.4 mg/mL oxLDL and 100 nM TG for varying time points at 37^0C for 24 hours in RPMI 1640 containing 5% FBS without phenol red. The cell lysate was assessed for CHOP expression via western blot. **A)** Results were normalised by β-Actin and displayed as mean ± SEM of technical replicates of

representative experiments. Data are expressed as the percentage of individual control (cell only control), and significance is indicated from this control. Statistical significance (one-way ANOVA, Dunnett's multiple comparison tests) is indicated by cell only control vs treatments. Significant levels are shown (*), $p < 0.05$. **B)** Quantitative densitometry of western blots shows CHOP expression with increasing concentrations of oxLDL.

3.8 Effect of ACAT inhibitor (Sandoz 580–35) and oxLDL on cell viability.

U937 cells were incubated with 0.1 mg/mL and 0.2 mg/mL oxLDL alone, 10 μg/mL ACAT inhibitor, combination with 0.1 mg/mL oxLDL and 10 ug/mL ACAT inhibitor and 0.2 mg/mL and 10 μg/mL ACAT inhibitor for 24 hours at 37^0C. Cell viability was measured using PI flow cytometry and morphology was assessed with inverted light microscope. 0.1 mg/mL oxLDL control had minimum or no effect on the U937 cells as compared to 0.2 mg/mL oxLDL control indicating 89% and 68% viable cells respectively **(Figure 22)**. The oxLDL concentration used is below the known lethal concentration. 10 μg/mL ACAT inhibitor control alone prooves to be toxic to U937 cells resulting in only 35.5% viable cells. However, the combination treatment of 0.1 mg/mL oxLDL and 10 μg/mL accounts for 92% cell viability. The combine treated group elevated the cell viability by almost 2% and 57% compared to 0.1 mg/mL oxLDL control and ACAT inhibitor alone treated cells. Combine treatment of 0.2 mg/mL oxLDL and 10 μg/mL ACAT also raised the cell vaibility when compared with 0.2 mg/mL oxLDL and 10 μg/mL ACAT inhibitor alone control. In 0.2 mg/mL oxLDL and ACAT inhibitor treated cells showed 25% and 58% increase in vaibility respectively when compared to 0.2 mg/mL oxLDL and 10 μg/mL ACAT inhibitor alone **(Figure 22)**.

MTT contrasting results compared to the viability results obtained via PI-flow cytometry. Untreated samples, 0.1 mg/mL and 0.2 mg/mL oxLDL treated samples showed a increase in viable cells. Cell only control resulted in 100% cell viability whereas 0.1 mg/mL and 0.2 mg/mL oxLDL treated samples yielded 106.89% and 112.79% cell viability respectively, compared to cell only control **(Figure 23)**. The oxLDL concentration used is below the known lethal concentration. These results were in contrast to PI data which illustrated a significant decrease in cell viability (PI negative cells) when the cells were treated with 0.1 and 0.2 mg/mL oxLDL. However, a slight drop in cell viability was observed when the cells were treated with 10 μg/mL S 58-035 resulting in 102.05% cell viability to cell only control which is almost 30-fold higher than that of PI-flow cytometer data. Nevertheless, the results are quite similar to PI data **(Figure 22)** when the cells were incubated in combination with oxLDL and ACAT inhibitor. 0.1 mg/mL, 0.2 mg/mL

oxLDL and 10 μg/mL ACAT resulted in 134.70% and 135.18% cell viability compared to cell only control suggesting that ACAT inhibitor is having a protective effect on U937 cell viability. In conclusion, these results suggest that ACAT inhibitor protects the cells from oxLDL toxicity.

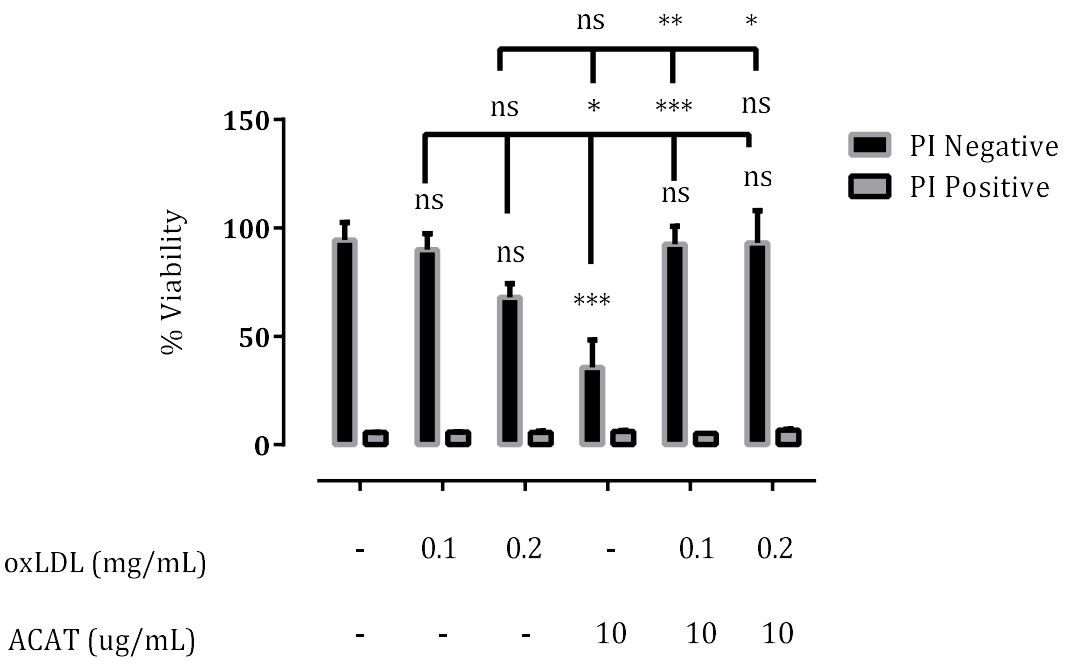

Figure 22: Effect of ACAT inhibitor (Sandoz 580-35) and oxLDL on cell viability measured by PI-flow cytometry.

U937 cells (0.5 X 10^6 cells/ml) were incubated at 37^0C in RPMI 1640 and 5% FBS without phenol red with 10 µg/mL of ACAT inhibitor (Sandoz 58–035) and 0.1 mg/mL and 0.2 mg/mL oxLDL for 24 hours in 24 well suspension culture plate. Cell viability was determined using PI–Flow cytometry assay. Data are expressed as a percentage of total cell count in cell control only samples. Results are shown in mean ± SEM of technical replicates from a representative experiment. Statistical significance (two-way ANOVA, Dunnett's multiple comparison tests) is indicated by PI negative cell only control vs. PI-negative ACAT inhibitor treatments. Significance levels are shown as (*), $p < 0.05$, (**),$p < 0.01$ and (***), $p < 0.001$.

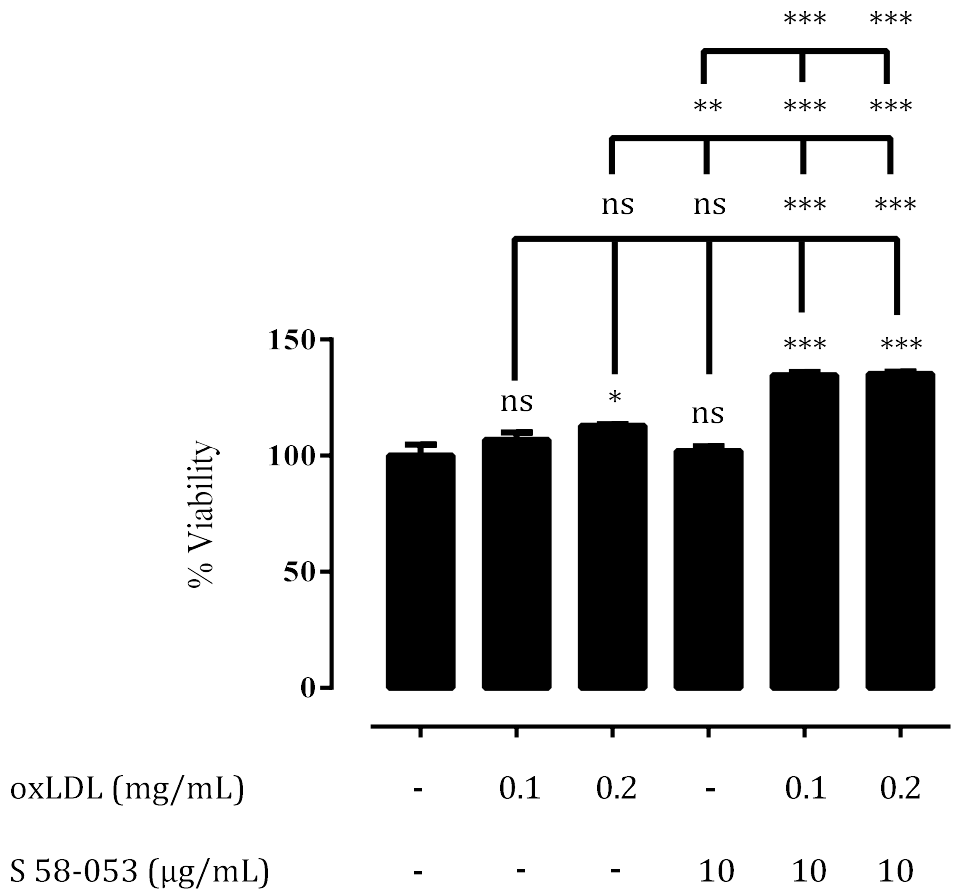

Figure 23: Effect of ACAT inhibitor S 58-035 and oxLDL on U937 cell viability by MTT colorimetric assay.

U937 cells (0.5 X 106 cells/mL) were incubated at 37^0C in RPMI 1640 and 5% FBS with no phenol red with 0.1 mg/mL, 0.2 mg/mL oxLDL and 10 µg/mL ACAT inhibitor S 58-035 alone and in combination with oxLDL and S 58-035 for 24 hours in 24 well suspension culture plates. Cell viability is determined using MTT assay. Cells were incubated with 50 µL MTT reagent at 37^0C for 2 hours. Purple crystals were formed and were dissolved in 500 µL 10% SDS. Absorbance was recorded using Shimadzu UV 1601PC UV-Visible Spectrophotometer at 570 nm wavelength. Data are expressed as the percentage of living cells in control only samples. Results are shown in mean ± SEM of technical replicates from a representative experiment. Cell only control vs TG treatments represent statistical significance (one-way ANOVA, Sidak's multiple comparison tests). Significance levels are indicated as (*) $p < 0.05$, (**) $p < 0.01$ and (***) $p < 0.001$.

3.9 Effect of ACAT inhibitor (Sandoz 580-35) on U937 cells.

The data presented in **3.8** indicated that 10 ug/mL ACAT alone was toxic to U937 cells. Therefore, it was important to analyse the cytotoxicity of ACAT inhibitor on U937 cells.

U937 cells were treated with increasing concentrations of ACAT inhibitor (Sandoz 580-35) (10 µg/mL-100 µg/mL) and were incubated at 37^0C for 24 hours. Cell viability was measured by PI flow cytometry, and cell morphology was assessed by an inverted light microscope. Increasing concentrations of ACAT inhibitor 10, 25, 50, 75 and 100 µg/mL reduced the cell viability (PI Negative cells) and increased dead cell population (PI Positive cells). As the ACAT concentration increased, the cell viability (PI Negative cells) decreased to 19%, 17%, 26%, 56% and 80% respectively. The LC_{50} of ACAT inhibitor was determined using linear regression and was calculated to be 60.215 µg/mL. The sum of PI Positive and PI Negative cells was always lower than 100% due to the number of cells that completely lysed to became the part of cellular debris which was considered neither of PI negative nor PI positive cell population.

On the other hand, MTT assay yielded 100% cell viability with 10 µg/mL of ACAT inhibitor compared to cell only control. The cell viability decreased very slightly resulting in 94.18% viable cells compared to cell only control when the cells were incubated with 25 µg/mL of ACAT inhibitor which is 14.46% higher compared to the what observed in PI. The viability decreased significantly when the concentration of ACAT inhibitor increased. 50 µg/mL concentration reduced the cell viability to 87.64% compared to cell only control. The cell viability suddenly dropped to 69.38% followed by 53.18% when the cells were treated with 75 µg/mL and highest concentration of 100 µg/mL of ACAT inhibitor. This sudden drop in cell viability with 75 µg/mL and 100 µg/mL can also be seen when analysed by PI flow cytometry.

Overall the data obtained suggest that ACAT inhibitor is toxic to U937 cells when given in higher concentrations above 25 µg/mL. However, concentrations ranging between 1-10 µg/mL of ACAT inhibitor (S 58-035) would be ideal to study its effects in atherosclerosis studies

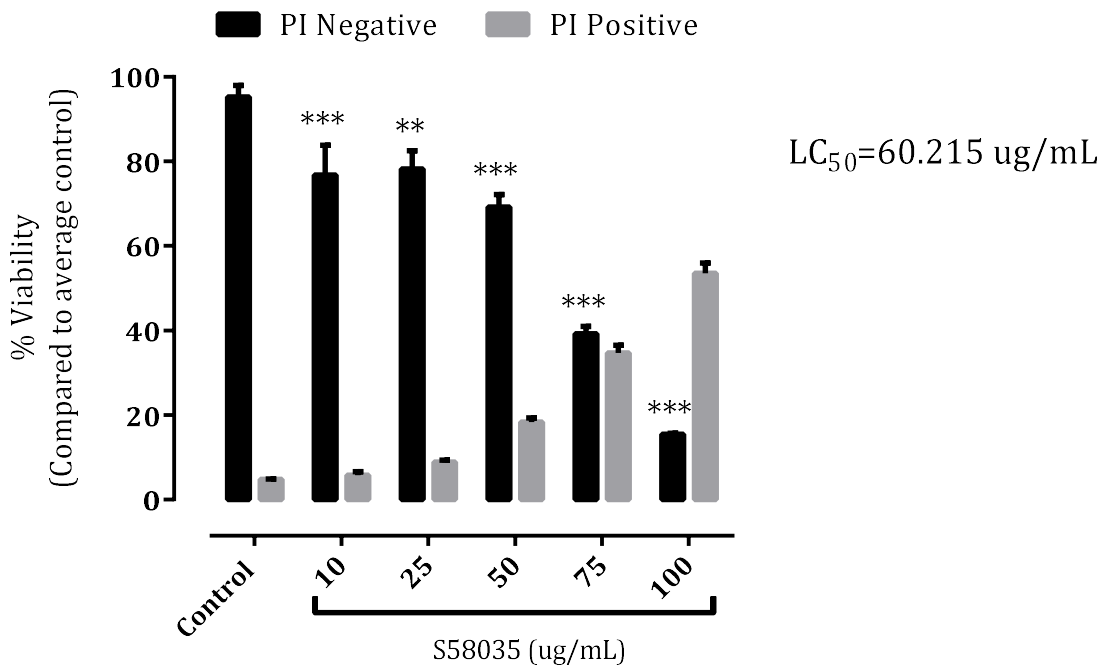

Figure 24: Effect of ACAT inhibitor on U937 cell viability by Flow cytometry

U937 cells (0.5 X 10^6 cells/ml) were incubated at 37^0C in RPMI 1640 with 5% FBS without phenol red and increasing concentrations of ACAT inhibitor for 24 hours in 24 well suspension culture plate. Cell viability was determined using PI-Flow cytometry assay. Data are expressed as a percentage of total cell count in cell control only samples. Results are shown in mean ± SEM of technical replicates from a representative experiment. Statistical significance (two-way ANOVA, Sidak's multiple comparison tests) is indicated by PI negative cell only control vs. PI-negative ACAT inhibitor treatments. Significance levels are shown as (**), $p < 0.01$ and (***), $p < 0.001$.

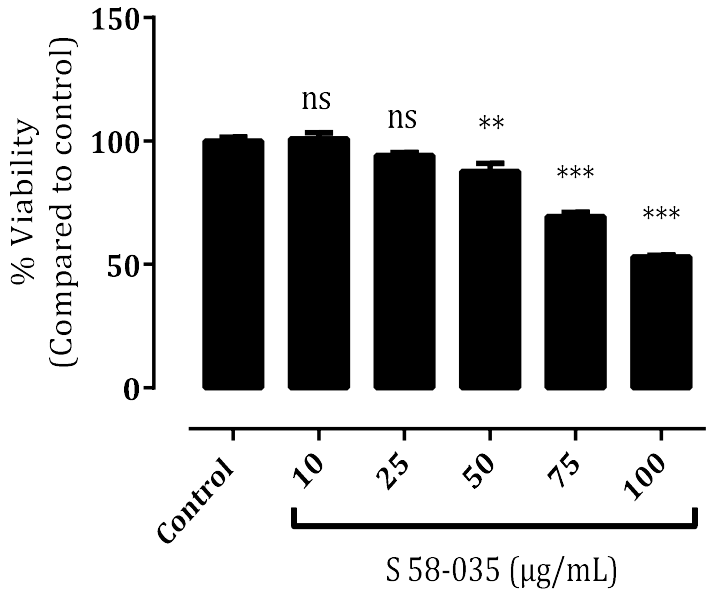

Figure 25: Effect of ACAT Inhibitor (S 58-035) on U937 cells by MTT colorimetric assay.

U937 cells (0.5 X 10^6 cells/mL) were incubated at 37^0C in RPMI 1640 and 5% FBS without phenol red and increasing concentrations of ACAT Inhibitor (S 58-035) for 24 hours in 24 well suspension culture plates. Cell viability is determined using MTT assay. Cells were incubated with 50 µL MTT reagent at 37^0C for 2 hours. Purple crystals were formed and were dissolved in 500 µL 10% SDS. Absorbance was recorded using Shimadzu UV 1601PC UV–Visible Spectrophotometer at 570 nm wavelength. Data are expressed as the percentage of living cells in control only samples. Results are shown in mean ± SEM of technical replicates from a representative experiment. Cell only control vs represent statistical significance (one-way ANOVA, Sidak's multiple comparison tests). TG treatments. Significance levels are indicated as (**) $p < 0.01$, (***) $p < 0.001$.

3.10 Effect of oxLDL on human monocytes.

Human monocytes react to oxLDL in a similar way to U937 cells. Preliminary experiments were performed on human monocytes treated with increasing concentrations of oxLDL (0.2, 0.4, 0.6, 0.8, 1.0 and 1.2 mg/mL) in phenol red free RPMI 1640 containing 10% human serum at 37^0C for 24 hours. Cell viability was measured using PI flow cytometry and MTT colorimetric assay. Cells treated with 0.2 mg/mL oxLDL showed a higher percentage of cell viability (PI negative cells) resulting for 119.23% of cell-only control which can be seen same when assayed with MTT assay (117.99% of cell-only control). Cells treated with 0.4 mg/mL oxLDL reduced the cell viability to 85.20% compared to cell only control and MTT resulted in 107.69% viable cells compared to cell only control. Cells treated with 0.6 mg/mL oxLDL deduced the viability by 50.05% compared to cell only control whereas this sudden drop in cell viability (PI negative cells) was not observed with MTT colorimetric assay (101.66% of control). Cells treated with 0.8, 1.0 and 1.2 mg/mL oxLDL showed the increase in viability (93.60% for 0.8 mg/mL compared to control) (PI negative cells) and again decreased as the concentration of oxLDL increased; 75.83% for 1.0 mg/mL oxLDL compared to control and 50.85% for 1.2 mg/mL oxLDL compared to control (PI Negative cells).

However, MTT did not follow the same trend in viability as compared to PI flow cytometry. The percentage of viable cells diminished with increasing concentration of oxLDL. Cells treated with 0.8 mg/mL oxLDL gave 99.66% viable cells compared to control;1.0 mg/mL oxLDL gave 88.85% viable cells and 1.2 mg/mL oxLDL gave 84.50% viability compared to cell only control. However, it was not possible to determine the LC_{50} concentration of oxLDL for human monocytes due to variation in cell viability and insufficient oxLDL in the cellular system.

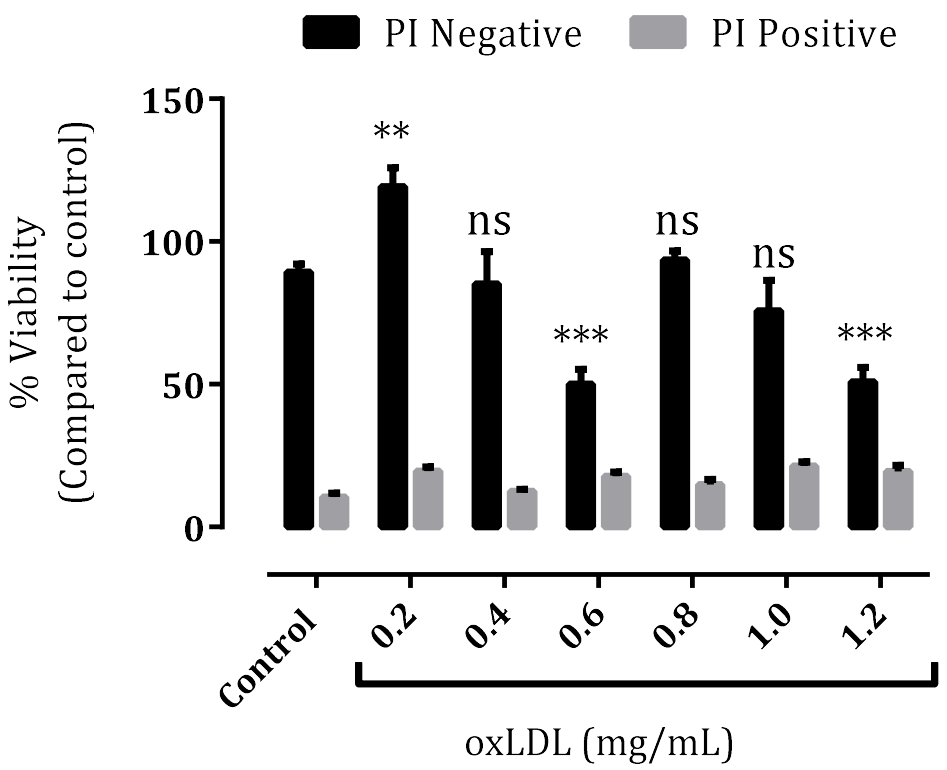

Figure 26: Effect of oxLDL on Human Monocytes using PI Flow cytometry.

Human monocytes (1 X 10^6 cells/ml) were incubated at 37^0C in RPMI 1640 and 10% human serum with no phenol red and increasing concentrations of oxLDL for 24 hours in 24 well suspension culture plate. Cell viability was determined using PI-Flow cytometry assay. Data are expressed as a percentage of average cell count in cell control only samples. Results are shown in mean ± SEM of technical replicates from a representative experiment. Statistical significance (two-way ANOVA, Sidak's multiple comparison tests) is indicated by PI negative cell only control vs. PI-negative TG treatments. Significance levels are shown as (**), $p < 0.01$ and (***), $p < 0.001$.

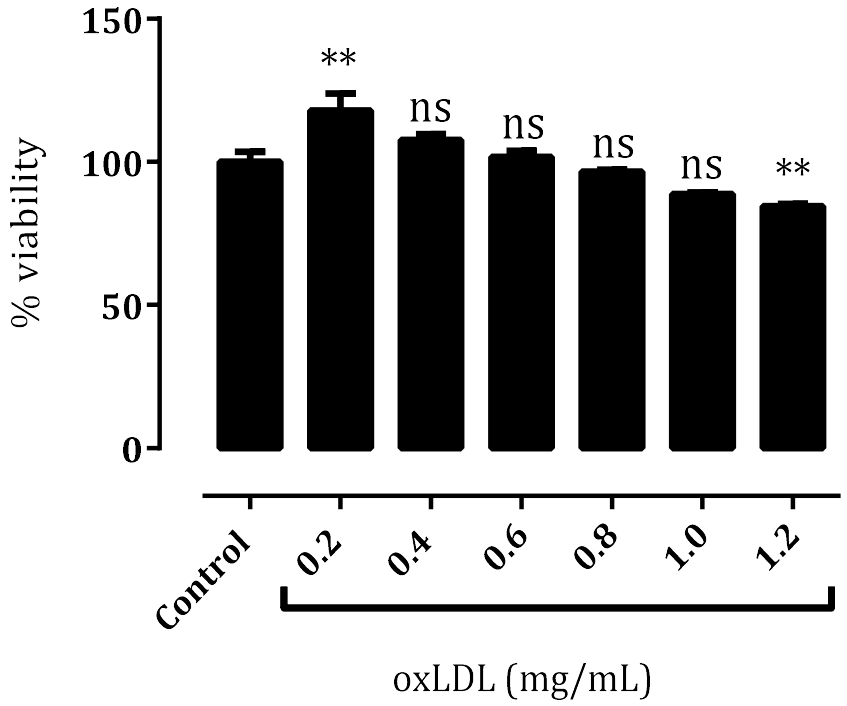

Figure 27: Effect of oxLDL on Human monocytes by MTT colorimetric assay.

Human monocytes (1 X 10^6 cells/mL) were incubated at 37^0C in RPMI 1640 and 5% FBS with no phenol red and increasing concentrations of oxLDL for 24 hours in 24 well suspension culture plates. Cell viability is determined using MTT assay. Cells were incubated with 50 µL MTT reagent at 37^0 C for 2 hours. Purple crystals were formed and were dissolved in 500 µL 10% SDS. Absorbance was recorded using Shimadzu UV 1601PC UV-Visible Spectrophotometer at 570 nm wavelength. Data are expressed as the percentage of living cells in control only samples. Results are shown in mean ± SEM of technical replicates from a representative experiment. Statistical significance (one-way ANOVA, Sidak's multiple comparison tests) is represented by cell only control vs oxLDL treatments. Significance levels are indicated as (**) $p < 0.01$.

3.11 Effect of Thapsigargin on human monocytes.

Preliminary experiments were performed on human monocytes (1×10^6 cells/mL) treated with increasing concentrations of TG (50, 100, 150, 200, 250, 300 and 350 nM) incubated in phenol red free RPMI 1640 with 10% human serum at 37^0C for 24 hours. Cell viability was measured using PI flow cytometry and MTT colorimetric assay. Cells treated with 50 nM TG resulted in 99.89% viable (PI negative) as compared to a cell control, whereas MTT showed 105.32% viable cells as compared to PI flow cytometry. The viability decreased with increase in TG concentration 100 nM treated cells depicted 96.53% cell viability; 150 nM treated cells resulted in 87.01% cell viability; 200 nM treated cells gave 64.53% cell viability; 250 nM TG treated cells resulted in slight rise in viability accounting for 79.31%; 300 nM TG treated sample resulted in viability almost equal to that of 200 nM TG treated sample giving 60.83% viable cells and highest treatment of 350 nM TG resulted in the least percentage of viable cells illustrating 58.05% viable cells compared to cell only control.

This suggests that TG is toxic to human monocytes. It can also be seen that monocyte's response to TG is not as sensitive as that observed in U937 cells .However, due to insufficient TG concentration to the cells LC_{50} could not be determined.

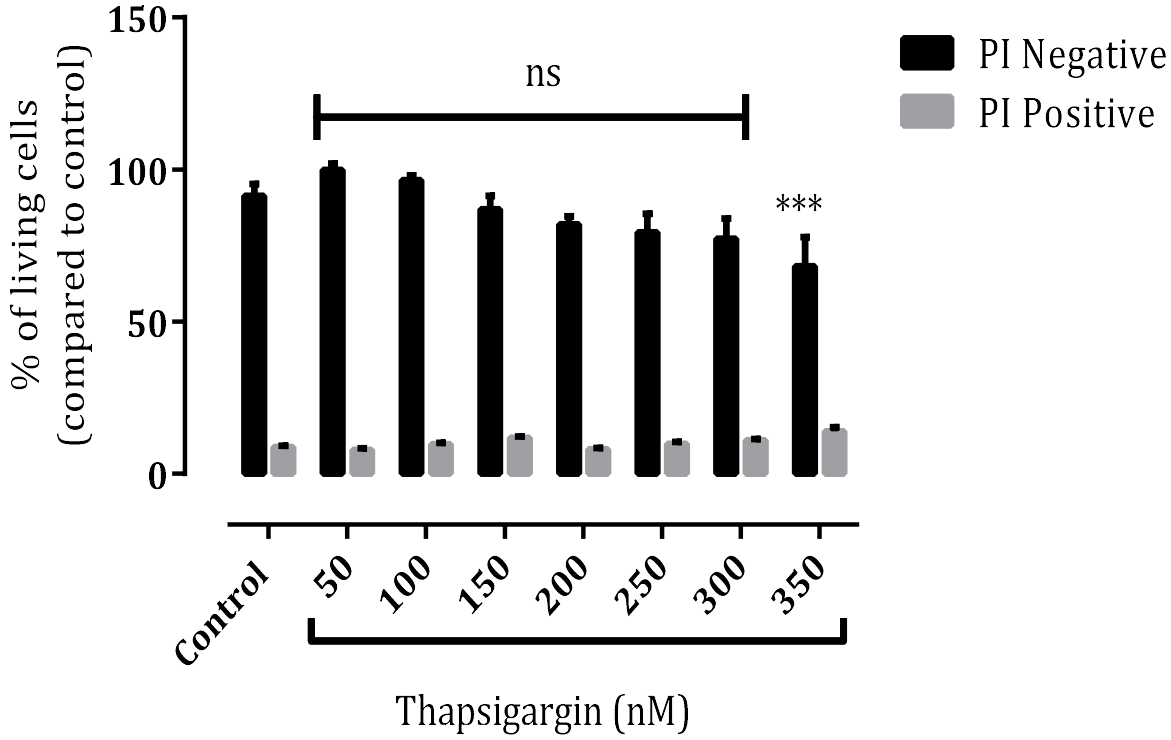

Figure 28: Effect of TG on Human monocytes by PI flow cytometry.

Human monocytes (1 X 10^6 cells/ml) were incubated at 37^0C in RPMI 1640 containing 10% human serum without phenol red and increasing concentrations of TG for 24 hours in 24 well suspension culture plate. Cell viability was determined using PI–Flow cytometry assay. Data are expressed as a percentage of average cell count in cell only control samples. Results are shown in mean ± SEM of technical replicates from a representative experiment. Statistical significance (two-way ANOVA, Sidak's multiple comparison tests) is indicated by PI negative cell only control vs. PI-negative TG treatments. Significance levels are shown as (***), $p < 0.001$.

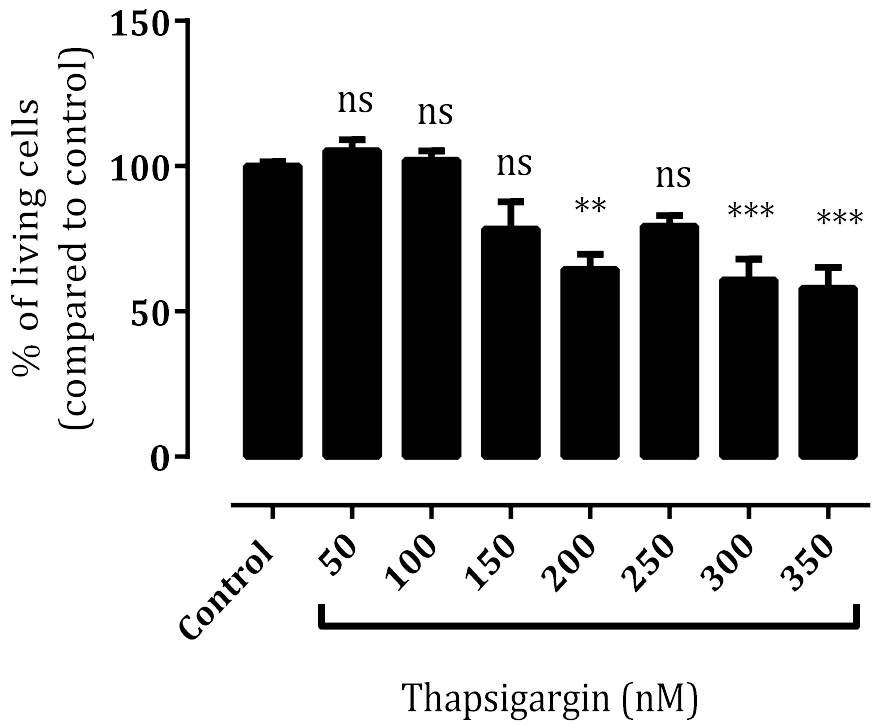

Figure 29: Effect of TG on Human monocytes by MTT colorimetric assay.

Human monocytes (1 X 10^6 cells/mL) were incubated at 37^0C in RPMI 1640 containing 10% human serum without phenol red and increasing concentrations of TG for 24 hours in 24 well suspension culture plates. Cell viability is determined using MTT assay. Cells were incubated with 50 µL MTT reagent at 37^0C for 2 hours. Purple crystals were formed and were dissolved in 500 µL 10% SDS. Absorbance was recorded using Agilent UV–Visible Spectrophotometer at 570 nm wavelength. Data are expressed as the percentage of living cells in control only samples. Results are shown in mean ± SEM of triplicates from a representative experiment. Statistical significance (one-way ANOVA, Sidak's multiple comparison tests) is represented by cell only control vs oxLDL treatments. Significance levels are indicated as (**) $p < 0.01$, (***) $p < 0.001$.

CHAPTER 4

4 Discussion

4.1 General discussion, conclusion and future work.

This research explores the critical role of oxidized LDL in endoplasmic reticulum stress-induced cell death by the activation of one of the critical ER stress markers CHOP. The research also examined the potential of the macrophage antioxidant 7, 8-DNP to downregulate CHOP expression induced by oxLDL and determining its ability in the prevention of macrophage cell death processes in later stages of atherosclerosis progression.

4.1.1 Oxidized low density proteins induced cell death.

OxLDL is believed to be the primary contributor to macrophage cell death. LDL gets modified into oxidized LDL by the ROS such as H_2O_2, HOCl and NO that are present in the intima of the artery and are readily taken up by the macrophages converting them into the cholesterol loaden foam cells which is the hallmark of atherosclerosis. Excess of free radicals that are derived from oxygen, nitrogen and other chemical substances in the body causes lipids and proteins to be oxidized through the terminal process of oxidative stress. Oxidative stress leads to crucial events like cell death and proliferation as atherosclerosis progresses. It is quite intriguing that mild oxidation can trigger cellular stress and initiate apoptosis, however, severe oxidative stress can trigger cell death, and intense stress may result in the cells to undergo necrotic death (Circu & Aw, 2010).

In the current research, we have utilized $CuCl_2$ as a mediator to heavily oxidize the native LDL for prolonged periods (more than 24 hours) (Steven P Gieseg, Crone, & Amit, 2009). This heavily oxidized Cu-oxLDL was used to study the mechanism and kinetics of oxLDL (precisely Cu–oxLDL). Alternatively, LDL can also be oxidized by acetylation (acLDL), aggregation (agLDL), minimal oxidation (mLDL) or be oxidized using hypochlorite (HOCl–oxLDL) depending upon the type and research to be carried out. Evidences

suggests that macrophage undergo foam cell formation when treated with agLDL, but it has also been seen that apoptosis is suppressed by downregulating caspase-1 and -3 with upregulation of γ-interferon at the same time (Kubo et al., 1997). Apoptotic cell death caused by agLDL is p53 dependent process (Kinscherf et al., 1998) and hence it is involved in events such as cell loss, the formation of a lipid core and other thrombotic events. It has also been evidenced that short oxLDL treatment (4-6 hours) with 0.1 mg/mL Cu-oxLDL leads to cell survival, enhanced response to GM-CSF and DNA synthesis (Hamilton et al., 1999; C.-Y. Han & Pak, 1999). We observed the similar results with cell survival when the U937 cells were treated with 0.1 mg/mL Cu-oxLDL for 24 hours. One of the critical evidence also suggested that exposing cells to 0.1 mg/mL mLDL induced cell proliferation and macrophage activation, however, highly oxidized LDL at same concentration induced cell death. Whereas, 0.2 mg/mL Cu-oxLDL resulted in cell death regardless of the oxidation degree of oxLDL (C.-Y. Han & Pak, 1999). We confirmed the similar results with highly oxidized oxLDL (Cu-oxLDL) where we observed the reduction in cell viability when the cells were incubated with 0.2 mg/mL Cu-oxLDL and higher concentrations **(Figure 10 and Figure 11)**.

Preliminary experiments with Cu-oxLDL on human monocytes suggested that Cu-oxLDL is toxic to monocytes in same ways as that of U937 cells. However, we could not determine the LC_{50} for monocytes due to an insufficient concentration of oxLDL in the system **(Figure 26 and Figure 27)**. We assume that monocytes are not as sensitive as that of U937 cells irrespective of same cell concentration. However, the cytotoxicity is dependent on the toxic nature of oxLDL.

Previous studies have shown that oxLDL either induce apoptotic or necrotic cell death depending upon the type of cells treated. When treated with increasing concentrations of Cu–oxLDL, cells undergo oxidative stress as it was sufficient to block caspase-3 activation and suppress apoptotic process further activating necrosis in U937 cells (Baird et al., 2004). However, THP-1 cells underwent apoptosis through caspase-3 activation (Baird et al., 2004). Our current study was initiated by treating U937 cells with varying concentrations of Cu-oxLDL and we found out that U937 cells are highly sensitive as the concentration increases. As a result, the cells undergo cell death by necrosis when assessed by inverted light microscope **(Figure 10A).** The cells showed swelling followed

by the degradation of internal organelle structure, disruption of nuclear and plasma membrane. We observed that cell only control appeared round which is classical feature of U937 cells. Although, cells treated with 0.1 mg/ mL and 0.2 mg/mL oxLDL illustrated swelling or foamy appearance. In contrast cells treated with higher concentration of Cu-oxLDL (concentrations above 0.3 mg/mL) illustrated cell debris with distorted cell membranes, resulting a significant damage to their cell membranes and loss of cellular contents which are some common characteristic of necrotic cell death (Syntichaki & Tavernarakis, 2003). The decrease in cell viability was observed with elevating oxLDL concentrations (PI Negative cells) **(Figure 10B)** with increase in the percentage of dead cells (PI Positive cells) **(Figure 10B)** when assessed by PI flow cytometry**.** The research also utilized MTT colorimetric assay as a measure to determine cell viability. MTT is a soluble tetrazolium salt which accepts electrons from oxidized substrates such as NADH and NADPH by the viable cells converting tetrazolium into an insoluble formazan; transforming yellow tetrazolium salts into blue colored formazan crystals that can be spectrophotometrically determined. Hence the viable cells produced more amount of insoluble formazan as compared to dead cells. In case of oxLDL, the viability decreased as the oxLDL concentration increased **(Figure 11)** and illustrated the similar trend in decrease as seen PI Flow cytometry. Overall these findings suggest that oxLDL induced cell death is cell's response to oxLDL which depends on the degree of oxidation, aggregation status, the concentration of oxLDL and exposure time.

4.1.2 OxLDL induces Endoplasmic reticulum stress pathway to initiate cell death by CHOP pathway.

The next objective of the research was to investigate the potential role of oxLDL in triggering ER stress and CHOP-induced cell death in U937 cells. Scavenger receptors are responsible for the uptake of oxLDL. Among these SR-A, SR-B (CD36), LOX-1 and TLR4 are the prominent receptors that gather oxLDL and results in the foam cell formation (Levitan et al., 2010). The increasing concentration of oxLDL in the cells activates various mechanism such as oxidative stress, calcium homeostasis imbalance and inflammation that dysfunctions ER leading to the misfolding of proteins and activating UPR to reduce the load of misfolded proteins (Hotamisligil, 2010). There are plenty of evidences that suggests that scavenger receptors and oxLDL are involved in triggering ER stress through

various ER proteins and CHOP induction (**Figure 30**). It has been previously shown that both minimally modified oxLDL (mm-oxLDL) and oxLDL can activate ER-stress during foam cell formation. Shutong Yao *et al*. (2012) shown that mm-LDL increased the expressions of ER membrane proteins p-IRE1, XBP1 and GRP78 in dose-dependent manner (Yao et al., 2012). The study also suggested that TLR4 which is among the major transmembrane receptor responsible for foam cell formation, not only alleviated FC trafficking in ER by mm-oxLDL but it also inhibited ER-stress response by reducing the nuclear translocation of ATF6, IRE1 and XBP1 and GRP78 downregulation. Notably, when TLR4 was transfected by siRNA, it upregulated the expression of p-IRE1, GRP78 and ATF6 induced by mm-LDL suggesting the crucial role played by TLR4 in mediating mm-LDL induced macrophage ER-stress (Yao et al., 2012). Research led by Hua *et al.* (2010), concluded that ER–stressor Tunicamycin elevates CD36 protein levels in human macrophages suggesting the potential role of ER–stress in the expression of scavenger receptors during atherosclerosis progression (Hua, Kandadi, Zhu, Ren, & Sreejayan, 2010).

Another important research carried by Shutong Yao *et. al*. not only showed that oxLDL upregulates CHOP expression but also illustrated that ATF6 (**discussed in 1.2.2.3**) which regulates CHOP expression, was activated by oxLDL in time and dose-dependent manner. This was followed by the upregulation of oxLDL induced CHOP activation, macrophage cell death by apoptosis when ATF6 was knocked out by siRNA transfection indicating the role of ATF6 in ER–stress pathway. This finding showed that oxLDL induced CHOP upregulation and apoptotic cell death by ATF6-siRNA transfection was only partial effect. Overall the results suggested that ATF6 play a crucial role in mediating oxLDL induced cholesterol accumulation and macrophage cell death by upregulating CHOP expression (Yao et al., 2013).

The primary motive of our research project was to determine whether Cu–oxLDL activate CHOP driven cell death mechanism in U937 cells. A significant finding mentioned above did explain the potential role played by oxLDL in CHOP activation through scavenger receptors and ER-membrane proteins. We investigated CHOP activation using a potent ER–stress inducer Thapsigargin (TG) which is a SERCA inhibitor. It was seen that CHOP was upregulated in a dose-dependent manner (**Figure 17**). Not only it showed that U937

express TG induced CHOP upregulation, but it also showed that U937 cells undergo necrotic cell death rather than apoptotic cell death. This was evident by TMRM staining by flow cytometry. TMRM dye measures the change in mitochondrial membrane potential. It was observed that the TMRM fluorescence increased with increasing TG concentration with the reduction in cell number. This suggests that the cell experienced heavy lysis right before the membrane potential was measured.

We know that oxLDL is a main contributing factor resulting in foam cell formation and macrophage cell death. The oxidized form of LDL is known to trigger cell death one of the prominent and well-studied pathways of ER-stress and CHOP-mediated cell death in a variety of cell lines **(see APPENDIX)**. Here we investigated the potential role of oxLDL in mediating cell death in U937 cells through activation of CHOP which is among the leading markers of ER-stress. The results we obtained suggested that oxLDL initiated CHOP-mediated cell death is dependent on the concentration of oxLDL and time it gets activated. We observed that oxLDL triggered CHOP activation at 0.3 mg/mL oxLDL and the expression upregulated as the concentration of oxLDL in the cells increased. At the highest concentration of 0.5 mg/mL CHOP expression was observed to be maximum killing almost all cells. The time-dependent CHOP expression was also observed which suggested that oxLDL-induced CHOP activation was first observed at 3-hour time point when the cells were treated with 0.4 mg/mL oxLDL. The expression appeared maximum at 12 and 24-hour time point suggesting that 3-hour time is the initiation point for oxLDL induced CHOP mediated cell death in U937 cells. We also observed TG (positive control) activating CHOP at 12 hour and maximum expression was followed by 24 hours acting as a control for our time-course experiment. However, it is imperative to note that we observed CHOP activation only with one batch of oxLDL prepared. We suppose that oxLDL induced CHOP activation varies from batch-to-batch of oxLDL prepared as we know that oxLDL toxicity also changes with new batch prepared. However, we do not know the reason behind different batches of oxLDL activating CHOP expression in U937 cells.

NOX activation is among the critical factors that are responsible for CHOP mediated cell death. There are several mechanisms by which NOX activates CHOP-induced cell death in cells. One of the critical mechanism reported by Li et al., (2010) suggested that NOX plays

a fundamental role in formation of excessive ROS by which the cell undergoes oxidative stress and activates calcium signalling pathways by triggering CHOP through ER-oxidase 1α (ERO1α), initiating the calcium release through a calcium channel, IP3R (**Figure 30**). This calcium channel then triggers cytoplasmic calcium to activate calcium-sensing enzyme CaMKII which causes the activation of downstream apoptotic pathways leading to Fas-mediated apoptosis (**Figure 30**). Hence, it would be beneficial to explore the role of NOX in Cu-oxLDL induced CHOP mediated cell death in U937 cells and human monocytes/macrophages.

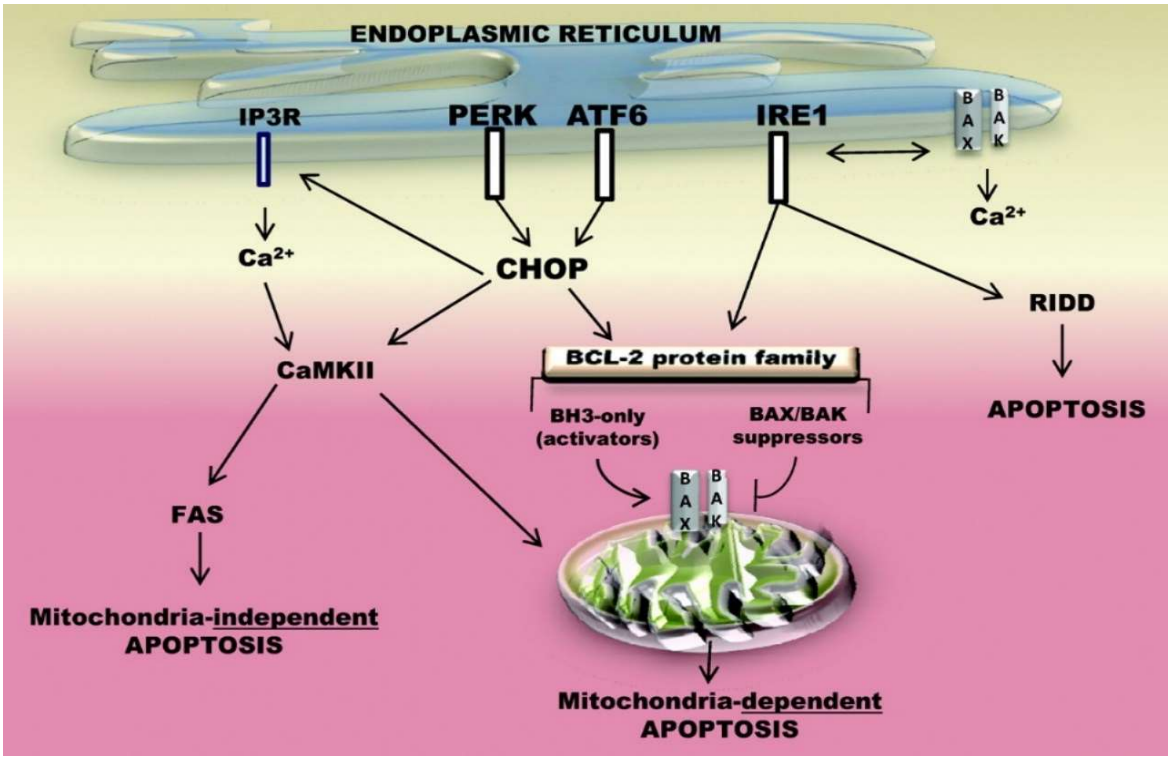

Figure 30: ER - stress-induced apoptotic pathways taken from (Scull & Tabas, 2011)

Another important mechanism by which CHOP facilitates cell death is through ER-stress and ER transmembrane proteins that take part in UPR process. Imbalances in the homeostasis process in ER such as oxidative stress, calcium homeostasis imbalance results ER-stress and prolonged ER-stress results in the failure of UPR which activates CHOP as a downstream effector of ER transmembrane proteins, i.e. PERK, ATF6 and IRE1 (**Figure 30**). These proteins ubiquitously express CHOP, and when the unfolded protein

response triggered by the ER is not resolved, these transmembrane proteins activates CHOP and initiates apoptotic cells death through interacting with the different members of BCL-2 family proteins (**Figure 30**). One of the prominent BCL-2 family protein is BH-3 only protein which further activate BAX and BAK apoptotic proteins that initiates apoptosis through caspase-12 activation. However, we suspect that U937 cells might not follow this pathway as the caspase-3 (which is an executioner caspase) gets oxidized and inactivated which is later followed by necrotic cell death as demonstrated previously (Baird et al., 2005).

4.1.2.1 Problems associated with oxLDL induced CHOP activation

Through our entire project, the main aim was to observe CHOP activation in U937 cells. We initiated the objective with TG as a positive treatment to obtain CHOP activation. Since CHOP related work was never done in this research group before, the first task was to perform western blot with the right amount of cell concentration, antibody blocking solution concentrations.

We initiated work by using U937 cells at 0.5×10^6 cell/mL concentration. The cells were lysed, and protein was extracted (**as described in 2.12.3**). Protein concentration was determined using BCA assay **(as described in 2.9.1**) and 150 µg of protein was used to perform immunoblot. The SDS-PAGE gel was run, and the proteins were transferred to a nitrocellulose membrane using Transblot turbo mini transfer packs (Bio-Rad). The membrane was blocked with 5% for an hour, washed with 1X TBS containing 0.05% tween20 and was probed with CHOP antibody for an hour with 1: 1000 antibody dilution in 1% TBSM. The membranes were washed again with 1X TBS and probed with secondary antibody in 2% TBSM for 1 hour. The antibody was discarded, washed with TBS and visualized. Upon visualization no CHOP activation was seen. The procedure mentioned above was very successful for CD36 determination but was not optimized for determining CHOP activation.

Another critical problem that we encountered was oxLDL induced CHOP activation. We found that only certain batch (s) of oxLDL induced CHOP in U937 cells. Out of 3 batches of oxLDL prepared, we observed CHOP activation in only one batch. Therefore, this had been a significant problem throughout the project suggesting that Cu-oxLDL is tricky on its own to fire up CHOP as previously mentioned the toxicity differs from batch to batch

so does the CHOP activation. However, we do not know as of why CHOP activation differs from batch to batch of oxLDL.

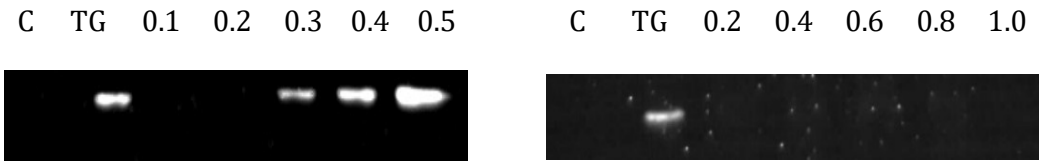

4.1.2.2 Western blotting developmental method for CHOP activation.

After failure with the method previously used for CD36 determination as a basis for CHOP determination, it was quite difficult to optimize the entire protocol. With several methodological reviews, we developed a draft with numerous changes. The main changes included antibody dilutions, durations and concentrations of blocking solutions, duration of antibody incubation and temperature at which the antibody is being incubated at. We decided not to change the cell concentration. So, the cell concentration was kept constant at 0.5×10^6 cells/mL. The cells were lysed as described in 2.12.3 and the protein concentration was determined as described in 2.9.1 and 100 µg protein was used, gel electrophoresed and was transferred onto a nitrocellulose membrane using a transblot turbo mini transfer packs (Bio-Rad). We did not change the procedure of blocking membrane with 5% TBSM. After blocking, the membrane was washed 5 times for 25 minutes with 1X TBS containing 0.1% Tween. The next step was very crucial with antibody dilution and use of an appropriate amount of TBSM. So, this step was done incubating membrane in 2.5% TBSM in CHOP antibody with antibody diluted at 1: 750 dilution. This was followed by incubating membrane overnight on a shaker at 4^0C (approximately 12-14 hours of incubation). The next day antibody was discarded followed by a quick 1X TBST wash and later 5X washing for 25 minutes before secondary antibody incubation. The secondary antibody incubation was again done in 2.5% TBSM at 1: 1000 dilution for 1 hour at RT; washed with 1X TBS, 5X for 25 minutes and visualized. Various exposure time was tried to observe CHOP activation and a barely visible band around 29 KDa could be spotted when the membrane was exposed for 5 minutes 30 seconds and more. The possible reason for barely visible CHOP was due to lower antibody concentration. This assumption was confirmed when the CHOP antibody was used at highest dilution, i.e. at 1: 250 without changing any other step. At this concentration, the CHOP band was sharp and clear as seen in Figure 20. The entire

protocol was optimized based on these observations and is described in detail in section 2.12.5.

4.1.2.3 Future work

Future work can be done on CHOP activation using acLDL instead of Cu-oxLDL as there are plenty of evidences **(see APPENDIX)** suggesting the better signal in CHOP activation in various cell lines. This work can be further carried on U937 cells or THP-1 or human monocytes to study ER-stress. Alternately work can also be carried out by siRNA transfection to determine the different mechanisms in the cells. We also think that cell might undergo necroptosis through IRE1-dependent RIDD-MLKL pathway that can be studied further.

4.1.3 The potential role of ACAT in diminishing atherosclerosis development.

Until now we have been looking the relationship between scavenger receptors, oxLDL, oxidative stress and ER-stress. It is not only that oxLDL alone contributes to cellular death process but, there is another factor that is equally responsible for cell death and its survival. This vital factor is the maintenance of cholesterol homeostasis in the cell. The cholesterol imbalance in the cells is maintained by an enzyme known as acyl-coenzyme A: cholesterol acyltransferase (ACAT) (C. Chang et al., 2006; Leon, Hill, & Wasan, 2005). The main enzyme that is responsible for esterification of free cholesterol (FC) and long chain fatty acids to cholesterol esters (CE) with ATP and coenzyme A (CoA) required as cofactors (Goodman, Deykin, & Shiratori, 1964; Mukherjee, Kunitake, & Alfin-Slater, 1958). ACAT is known to occur in 2 isoforms; ACAT-1 expressed only in macrophages and smooth muscles cells (SMCs) whereas liver and intestine express ACAT-1 and ACAT-2 (Buhman et al., 2000).

Based on its distribution ACAT play its part quite efficiently. Liver maintains regulation of plasma lipoprotein concentration; however, synthesis and processing cholesterol is maintained by both liver and brain. After triglyceride core of cholesterol is being lipolyzed by lipoprotein lipase, the remaining VLDL particles are either removed by the liver or are converted to LDL particles which are later taken up by the peripheral tissues via LDL receptor (Leon et al., 2005). Reverse cholesterol transport occurs when the

cholesterol is taken up by the peripheral tissues and is transferred back to the liver. In this situation, HDL is known to have a role in reverse cholesterol transport where cholesterol is secreted into bile and excreted in faeces. The presence of these two processes leads to cholesterol regulation in liver (Leon et al., 2005).

In macrophages, the excess cholesterol present in the foam cells undergoes efflux on HDL by ATP binding cassette A1 and G1 (ABCA1 And G1) transporters and is then transported to the liver for further excretion. 7-KC being a major oxysterol in oxLDL is also known to impair ABCA1 transporter as a result, FC is prevented from moving out of the cell. This causes membrane vesicles which are filled with CE to accumulate in the cytoplasm. With the progression of the atherosclerotic lesion, ACAT, ABCA1 and ABCG1 transporter malfunction (Moore & Tabas, 2011) as a result the intracellular accumulation of excess FC causes macrophage death via endoplasmic reticulum-mediated cell apoptosis (Bo Feng et al., 2003; I Tabas, 2004).

Many pieces of evidence suggests that ACAT inhibitors play a pivotal role in atherosclerosis and lipoprotein mechanism. However, different inhibitors have a different mode of action. ACAT inhibitor Pfizer CI-1011 decreased the lesional area and foam cell content from rich aorta by 35 and 27% suggesting its direct inhibitory within the vessel when studied on New Zealand white rabbits (Bocan et al., 2000). Another ACAT inhibitor Sandoz 58-035 has been widely used in the ACAT inhibition and atherosclerosis. Studies were done on the human macrophages in the presence of acLDL and foam cell formation with Sandoz 58-035 decreased cholesterol accumulation by lowering high-affinity binding of ^{125}I-acLDL and improving the efflux of cholesterol (Rodriguez, Bachorik, & Wee, 1999). The study also showed that the inhibitor at lower concentrations is not cytotoxic to the cells (Rodriguez et al., 1999). Based on the study on ACAT inhibitor Sandoz 58-035, we also obtained the similar results with U937 cells. The inhibitor at lower concentrations (10 µg/mL) protected the cells from further cell death when the cells were incubated with 0.1 and 0.2 mg/mL Cu-oxLDL for 24 hours. However, in that particular experiment the ACAT inhibitor alone control resulted in less than 50% viable cells which is not suppose to happen with the inhibitor, so we further planned to observe the cytotoxic effect of the inhibitor on cells and found that the cytotoxicity inhibitor is maximum as the concentration is increased with LC_{50} to be 60.12 ug/mL. This suggests

that ACAT inhibitor can be used at lower concentrations ranging from 1 μg/mL–10 μg/mL.

4.1.3.1 Possible Problems

Possible problems that could further affect the work could be the changing toxicity of oxLDL. Sean (2016) during his studies reported that oxLDL toxicity is changed over few weeks after it is prepared. In the current research we observed that the toxicity changes with every new batch prepared, however, the toxicity remains between 0.1-0.5 mg/mL. In some rare cases, the Cu-oxLDL toxicity was also observed to be above 1mg/mL. Due to this variation in oxLDL toxicity over the period of times and batches prepared there are high chances that results may vary as well.

4.1.3.2 Future Work

The future implications of this novel ACAT inhibitor can be used to see its direct effect on human monocytes and macrophages to confirm its protective action. Alternatively, its potency can also be analysed by feeding the cells (U937, THP-1, human monocytes and macrophages) with FC complexed with methyl-β-cyclodextrin (M-β-CD), a compound known to form stable complexes with FC and is highly suitable FC and ACAT inhibition studies.

4.1.4 Role of macrophage antioxidant 7,8–dihydroneopterin on CHOP expression.

7,8-DNP is synthesized by γ-interferon activated macrophages and is known to be a potent antioxidant to prevent lipid oxidation and macrophage cell death (S. P. Gieseg et al., 2010; Müller et al., 1991). Based on the effectiveness and potency of 7,8-DNP in the prevention of lipid oxidation and macrophage cells death, we thought on looking its antioxidant aspect on CHOP activation. As NOX also play an essential role in CHOP activation and is also known as an important mediator of ROS we thought of looking its effect on CHOP. 7,8-DNP can downregulate TG induced CHOP expression in U937 cells as seen in Figure 19. Based on densitometry images and statistical data it was observed that 7,8-DNP is effective in downregulating TG-induced CHOP expression in U937 cells. However, due to variability in oxLDL toxicity, oxLDL-induced CHOP expression by different batches, time limitations and delayed arrival of materials we could not achieve

our final goal to see the effect of 7, 8-DNP on Cu-oxLDL induced-CHOP expression. But, we suspect that 7, 8-DNP will downregulate oxLDL induced CHOP expression. Uptake of oxLDL is mainly regulated by CD36, and it has been previously shown that 7, 8-DNP downregulates CD36 in presence of sub-lethal dose of oxLDL (Nooshin, 2017). Therefore, if 7, 8-DNP is effective in downregulating CD36 in presence of oxLDL, there are possibilities that the antioxidant might downregulate oxLDL-induced CHOP expression in U937 cells.

5 References

Abou-Sleiman, P. M., Muqit, M. M., & Wood, N. W. (2006). Expanding insights of mitochondrial dysfunction in Parkinson's disease. *Nature Reviews Neuroscience, 7*(3), 207-219.

Acosta-Alvear, D., Zhou, Y., Blais, A., Tsikitis, M., Lents, N. H., Arias, C., . . . Dynlacht, B. D. (2007). XBP1 controls diverse cell type-and condition-specific transcriptional regulatory networks. *Molecular cell, 27*(1), 53-66.

Acton, S., Rigotti, A., Landschulz, K. T., Xu, S., Hobbs, H. H., & Krieger, M. (1996). Identification of scavenger receptor SR-BI as a high density lipoprotein receptor. *Science, 271*(5248), 518-520.

Acton, S. L., Scherer, P. E., Lodish, H. F., & Krieger, M. (1994). Expression cloning of SR-BI, a CD36-related class B scavenger receptor. *Journal of Biological Chemistry, 269*(33), 21003-21009.

Anderson, T. J. (1999). Assessment and treatment of endothelial dysfunction in humans. *Journal of the American College of Cardiology, 34*(3), 631-638. doi:10.1016/s0735-1097(99)00259-4

ANTONSSON, B., MONTESSUIT, S., LAUPER, S., ESKES, R., & MARTINOU, J.-C. (2000). Bax oligomerization is required for channel-forming activity in liposomes and to

trigger cytochrome c release from mitochondria. *Biochemical Journal, 345*(2), 271-278.

Baird, S. K., Hampton, M. B., & Gieseg, S. P. (2004). Oxidized LDL triggers phosphatidylserine exposure in human monocyte cell lines by both caspase-dependent and -independent mechanisms. *FEBS Lett, 578*(1-2), 169-174. doi:10.1016/j.febslet.2004.11.007

Baird, S. K., Reid, L., Hampton, M. B., & Gieseg, S. P. (2005). OxLDL induced cell death is inhibited by the macrophage synthesised pterin, 7,8-dihydroneopterin, in U937 cells but not THP-1 cells. *Biochim Biophys Acta, 1745*(3), 361-369. doi:10.1016/j.bbamcr.2005.07.001

Bernardi, P. (1996). The permeability transition pore. Control points of a cyclosporin A-sensitive mitochondrial channel involved in cell death. *Biochimica et Biophysica Acta (BBA)-Bioenergetics, 1275*(1-2), 5-9.

Bernardi, P., Vassanelli, S., Veronese, P., Colonna, R., Szabo, I., & Zoratti, M. (1992). Modulation of the mitochondrial permeability transition pore. Effect of protons and divalent cations. *Journal of Biological Chemistry, 267*(5), 2934-2939.

Bocan, T. M., Krause, B. R., Rosebury, W. S., Mueller, S. B., Lu, X., Dagle, C., . . . Lee, H. (2000). The ACAT inhibitor avasimibe reduces macrophages and matrix metalloproteinase expression in atherosclerotic lesions of hypercholesterolemic rabbits. *Arteriosclerosis, thrombosis, and vascular biology, 20*(1), 70-79.

Bocan, T. M., Mueller, S. B., Uhlendorf, P. D., Brown, E. Q., Mazur, M. J., & Black, A. E. (1993). Inhibition of acyl-CoA cholesterol O-acyltransferase reduces the cholesteryl ester enrichment of atherosclerotic lesions in the Yucatan micropig. *Atherosclerosis, 99*(2), 175-186.

Boullier, A., Bird, D. A., CHANG, M. K., Dennis, E. A., Friedman, P., GILLOTTE-TAYLOR, K., . . . Shaw, P. (2001). Scavenger receptors, oxidized LDL, and atherosclerosis. *Annals of the New York Academy of Sciences, 947*(1), 214-223.

Bratslavska, O., Platace, D., Miklaševičs, E., Fuchs, D., & Martinsons, A. (2007). Influence of neopterin and 7, 8-dihydroneopterin on the replication of Coxsackie type B5 and influenza A viruses. *Medical microbiology and immunology, 196*(1), 23-29.

Brown, A. J., & Jessup, W. (1999). Oxysterols and atherosclerosis. *Atherosclerosis, 142*(1), 1-28.

Brustovetsky, N., Brustovetsky, T., Jemmerson, R., & Dubinsky, J. M. (2002). Calcium-induced Cytochrome c release from CNS mitochondria is associated with the permeability transition and rupture of the outer membrane. *Journal of neurochemistry, 80*(2), 207-218.

Buhman, K. F., Accad, M., & Farese, R. V. (2000). Mammalian acyl-CoA: cholesterol acyltransferases. *Biochimica et Biophysica Acta (BBA)-Molecular and Cell Biology of Lipids, 1529*(1), 142-154.

Cawley, K., Deegan, S., Samali, A., & Gupta, S. (2011). 2 Assays for Detecting the Unfolded Protein Response. *Methods in enzymology, 490*, 31.

Chang, C., Dong, R., Miyazaki, A., Sakashita, N., Zhang, Y., Liu, J., . . . CHANG, T. Y. (2006). Human acyl-CoA: cholesterol acyltransferase (ACAT) and its potential as a target for pharmaceutical intervention against atherosclerosis. *Acta biochimica et biophysica Sinica, 38*(3), 151-156.

Chang, T., Chang, a., Catherine CY, & Cheng, D. (1997). Acyl-coenzyme A: cholesterol acyltransferase. *Annual review of biochemistry, 66*(1), 613-638.

Chen, W., Silver, D. L., Smith, J. D., & Tall, A. R. (2000). Scavenger receptor-BI inhibits ATP-binding cassette transporter 1-mediated cholesterol efflux in macrophages. *Journal of Biological Chemistry, 275*(40), 30794-30800.

Circu, M. L., & Aw, T. Y. (2010). Reactive oxygen species, cellular redox systems, and apoptosis. *Free radical biology and medicine, 48*(6), 749-762.

Collot-Teixeira, S., Martin, J., McDermott-Roe, C., Poston, R., & McGregor, J. L. (2007). CD36 and macrophages in atherosclerosis. *Cardiovascular research, 75*(3), 468-477.

Crompton, M. (1999). The mitochondrial permeability transition pore and its role in cell death. *Biochemical Journal, 341*(2), 233-249.

Cullinan, S. B., Zhang, D., Hannink, M., Arvisais, E., Kaufman, R. J., & Diehl, J. A. (2003). Nrf2 is a direct PERK substrate and effector of PERK-dependent cell survival. *Molecular and cellular biology, 23*(20), 7198-7209.

De Giorgi, F., Lartigue, L., Bauer, M. K., Schubert, A., Grimm, S., Hanson, G. T., . . . Ichas, F. (2002). The permeability transition pore signals apoptosis by directing Bax translocation and multimerization. *The FASEB journal, 16*(6), 607-609.

De Stefani, D., Raffaello, A., Teardo, E., Szabò, I., & Rizzuto, R. (2011). A forty-kilodalton protein of the inner membrane is the mitochondrial calcium uniporter. *Nature, 476*(7360), 336-340.

DeVries-Seimon, T., Li, Y., Yao, P. M., Stone, E., Wang, Y., Davis, R. J., . . . Tabas, I. (2005). Cholesterol-induced macrophage apoptosis requires ER stress pathways and engagement of the type A scavenger receptor. *The Journal of cell biology, 171*(1), 61-73.

Di Sano, F., Ferraro, E., Tufi, R., Achsel, T., Piacentini, M., & Cecconi, F. (2006). Endoplasmic reticulum stress induces apoptosis by an apoptosome-dependent but caspase 12-independent mechanism. *Journal of Biological Chemistry, 281*(5), 2693-2700.

Ding, W.-X., Shen, H.-M., & Ong, C.-N. (2002). Calpain activation after mitochondrial permeability transition in microcystin-induced cell death in rat hepatocytes. *Biochemical and biophysical research communications, 291*(2), 321-331.

Dobmeyer, J., Lohrmann, J., & Feussner, G. (1996). Prevalence and association of atherosclerosis at three different arterial sites in patients with type III hyperlipoproteinemia. *Atherosclerosis, 119*(1), 89-98. doi:10.1016/0021-9150(95)05633-5

Draude, G., Hrboticky, N., & Lorenz, R. L. (1999). The expression of the lectin-like oxidized low-density lipoprotein receptor (LOX-1) on human vascular smooth muscle cells and monocytes and its down-regulation by lovastatin. *Biochemical pharmacology, 57*(4), 383-386.

Duggan, S., Rait, C., Platt, A., & Gieseg, S. (2002). Protein and thiol oxidation in cells exposed to peroxyl radicals is inhibited by the macrophage synthesised pterin 7,8-dihydroneopterin. *Biochim Biophys Acta, 1591*(1-3), 139-145.

Dworakowski, R., Anilkumar, N., Zhang, M., & Shah, A. (2006). Redox signalling involving NADPH oxidase-derived reactive oxygen species. In: Portland Press Limited.

Eguchi, Y., Shimizu, S., & Tsujimoto, Y. (1997). Intracellular ATP levels determine cell death fate by apoptosis or necrosis. *Cancer research, 57*(10), 1835-1840.

Evanko, S. P., Raines, E. W., Ross, R., Gold, L. I., & Wight, T. N. (1998). Proteoglycan distribution in lesions of atherosclerosis depends on lesion severity, structural characteristics, and the proximity of platelet-derived growth factor and transforming growth factor-beta. *The American journal of pathology, 152*(2), 533.

Febbraio, M., Hajjar, D. P., & Silverstein, R. L. (2001). CD36: a class B scavenger receptor involved in angiogenesis, atherosclerosis, inflammation, and lipid metabolism. *Journal of Clinical Investigation, 108*(6), 785.

Febbraio, M., Podrez, E. A., Smith, J. D., Hajjar, D. P., Hazen, S. L., Hoff, H. F., . . . Silverstein, R. L. (2000). Targeted disruption of the class B scavenger receptor CD36 protects against atherosclerotic lesion development in mice. *Journal of Clinical Investigation, 105*(8), 1049.

Feng, B., Yao, P. M., Li, Y., Devlin, C. M., Zhang, D., Harding, H. P., . . . Fisher, E. A. (2003). The endoplasmic reticulum is the site of cholesterol-induced cytotoxicity in macrophages. *Nature cell biology, 5*(9), 781-792.

Feng, B., Yao, P. M., Li, Y., Devlin, C. M., Zhang, D., Harding, H. P., . . . Tabas, I. (2003). The endoplasmic reticulum is the site of cholesterol-induced cytotoxicity in macrophages. *Nat Cell Biol, 5*(9), 781-792. doi:10.1038/ncb1035

Firth, C. A., Crone, E. M., Flavall, E. A., Roake, J. A., & Gieseg, S. P. (2008). Macrophage mediated protein hydroperoxide formation and lipid oxidation in low density lipoprotein are inhibited by the inflammation marker 7, 8-dihydroneopterin. *Biochimica et Biophysica Acta (BBA)-Molecular Cell Research, 1783*(6), 1095-1101.

Ganley, I. G., Wong, P.-M., Gammoh, N., & Jiang, X. (2011). Distinct autophagosomal-lysosomal fusion mechanism revealed by thapsigargin-induced autophagy arrest. *Molecular cell, 42*(6), 731-743.

Gieseg, S., Duggan, S., & Gebicki, J. M. (2000). Peroxidation of proteins before lipids in U937 cells exposed to peroxyl radicals. *Biochem J, 350 Pt 1*, 215-218.

Gieseg, S. P., Amit, Z., Yang, Y. T., Shchepetkina, A., & Katouah, H. (2010). Oxidant production, oxLDL uptake, and CD36 levels in human monocyte-derived macrophages are downregulated by the macrophage-generated antioxidant 7,8-dihydroneopterin. *Antioxid Redox Signal, 13*(10), 1525-1534. doi:10.1089/ars.2009.3065

Gieseg, S. P., & Cato, S. (2003). Inhibition of THP-1 cell-mediated low-density lipoprotein oxidation by the macrophage-synthesised pterin, 7,8-dihydroneopterin. *Redox Rep, 8*(2), 113-115. doi:10.1179/135100003125001396

Gieseg, S. P., Crone, E., & Amit, Z. (2009). Oxidized Low Density Lipoprotein Cytotoxicity and Vascular Disease. *Endogenous Toxins: Targets for Disease Treatment and Prevention*, 619-645.

Gieseg, S. P., Crone, E. M., Flavall, E. A., & Amit, Z. (2008). Potential to inhibit growth of atherosclerotic plaque development through modulation of macrophage neopterin/7,8-dihydroneopterin synthesis. *Br J Pharmacol, 153*(4), 627-635. doi:10.1038/sj.bjp.0707408

Gieseg, S. P., & Esterbauer, H. (1994). Low density lipoprotein is saturable by pro-oxidant copper. *FEBS Lett, 343*(3), 188-194.

Gieseg, S. P., Maghzal, G., & Glubb, D. (2001). Protection of erythrocytes by the macrophage synthesized antioxidant 7,8 dihydroneopterin. *Free Radic Res, 34*(2), 123-136.

Gieseg, S. P., Reibnegger, G., Wachter, H., & Esterbauer, H. (1995). 7,8 Dihydroneopterin inhibits low density lipoprotein oxidation in vitro. Evidence that this macrophage secreted pteridine is an anti-oxidant. *Free Radic Res, 23*(2), 123-136.

Goldstein, J. L., Ho, Y., Basu, S. K., & Brown, M. S. (1979). Binding site on macrophages that mediates uptake and degradation of acetylated low density lipoprotein, producing massive cholesterol deposition. *Proceedings of the National Academy of Sciences, 76*(1), 333-337.

Goodman, D. S., Deykin, D., & Shiratori, T. (1964). The formation of cholesterol esters with rat liver enzymes. *Journal of Biological Chemistry, 239*(5), 1335-1345.

Gottlieb, R. A. (2001). Mitochondria and apoptosis. *Neurosignals, 10*(3-4), 147-161.

Green, D. R., & Reed, J. C. (1998). Mitochondria and apoptosis. *Science-AAAS-Weekly Paper Edition, 281*(5381), 1309-1311.

Gunter, T. E., & Pfeiffer, D. R. (1990). Mechanisms by which mitochondria transport calcium. *American Journal of Physiology-Cell Physiology, 258*(5), C755-C786.

Hamilton, J. A., Myers, D., Jessup, W., Cochrane, F., Byrne, R., Whitty, G., & Moss, S. (1999). Oxidized LDL can induce macrophage survival, DNA synthesis, and enhanced proliferative response to CSF-1 and GM-CSF. *Arteriosclerosis, thrombosis, and vascular biology, 19*(1), 98-105.

Han, C.-Y., & Pak, Y. K. (1999). Oxidation-dependent effects of oxidized LDL: proliferation or cell death. *Experimental & molecular medicine, 31*(4), 165-173.

Han, J., Back, S. H., Hur, J., Lin, Y.-H., Gildersleeve, R., Shan, J., . . . Hatzoglou, M. (2013). ER-stress-induced transcriptional regulation increases protein synthesis leading to cell death. *Nature cell biology, 15*(5), 481.

Hansson, G. K. (2005). Inflammation, atherosclerosis, and coronary artery disease. *New England Journal of Medicine, 352*(16), 1685-1695.

Harding, H. P., Zhang, Y., & Ron, D. (1999). Erratum: Protein translation and folding are coupled by an endoplasmic-reticulum-resident kinase. *Nature, 398*(6722), 90.

Harding, H. P., Zhang, Y., Zeng, H., Novoa, I., Lu, P. D., Calfon, M., . . . Paules, R. (2003). An integrated stress response regulates amino acid metabolism and resistance to oxidative stress. *Molecular cell, 11*(3), 619-633.

Haworth, R. A., & Hunter, D. R. (1979). The Ca2+-induced membrane transition in mitochondria: II. Nature of the Ca2+ trigger site. *Archives of biochemistry and biophysics, 195*(2), 460-467.

Heiskanen, K. M., Bhat, M. B., Wang, H.-W., Ma, J., & Nieminen, A.-L. (1999). Mitochondrial Depolarization Accompanies Cytochrome cRelease During Apoptosis in PC6 Cells. *Journal of Biological Chemistry, 274*(9), 5654-5658.

Hetz, C., Chevet, E., & Oakes, S. A. (2015). Proteostasis control by the unfolded protein response. *Nature cell biology, 17*(7), 829.

Hiroki Matsumoto, Shuichi Miyazaki, Satoshi Matsuyama, Masayuli Takeda, Makoto Kawano, Hiroshi Nakagawa, . . . Matsuo, S. (2013). Selection of autophagy or apoptosis in cell exposed to ER-Stress depends on ATF-4 expression pattern with or without CHOP expression. doi:10.1242/bio.20135033

Hollien, J., & Weissman, J. S. (2006). Decay of endoplasmic reticulum-localized mRNAs during the unfolded protein response. *Science, 313*(5783), 104-107.

Hong, D., Bai, Y.-P., Gao, H.-C., Wang, X., Li, L.-F., Zhang, G.-G., & Hu, C.-P. (2014). Ox-LDL induces endothelial cell apoptosis via the LOX-1-dependent endoplasmic reticulum stress pathway. *Atherosclerosis, 235*(2), 310-317.

Hotamisligil, G. S. (2010). Endoplasmic reticulum stress and atherosclerosis. *Nature medicine, 16*(4), 396-399.

Hua, Y., Kandadi, M. R., Zhu, M., Ren, J., & Sreejayan, N. (2010). Tauroursodeoxycholic acid attenuates lipid accumulation in endoplasmic reticulum-stressed macrophages. *Journal of cardiovascular pharmacology, 55*(1), 49.

Huh, H., Pearce, S., Yesner, L., Schindler, J., & Silverstein, R. (1996). Regulated expression of CD36 during monocyte-to-macrophage differentiation: potential role of CD36 in foam cell formation. *Blood, 87*(5), 2020-2028.

Hunter, D. R., Haworth, R., & Southard, J. (1976). Relationship between configuration, function, and permeability in calcium-treated mitochondria. *Journal of Biological Chemistry, 251*(16), 5069-5077.

Hunter, D. R., & Haworth, R. A. (1979). The Ca2+-induced membrane transition in mitochondria: III. Transitional Ca2+ release. *Archives of biochemistry and biophysics, 195*(2), 468-477.

Ichas, F., & Mazat, J.-P. (1998). From calcium signaling to cell death: two conformations for the mitochondrial permeability transition pore. Switching from low-to high-conductance state. *Biochimica et Biophysica Acta (BBA)-Bioenergetics, 1366*(1), 33-50.

Inesi, G., & Sagara, Y. (1994). Specific inhibitors of intracellular Ca 2+ transport ATPases. *Journal of Membrane Biology, 141*(1), 1-6.

Janmale, T., Genet, R., Crone, E., Flavall, E., Firth, C., Pirker, J., . . . Gieseg, S. P. (2015). Neopterin and 7, 8-dihydroneopterin are generated within atherosclerotic plaques. *Pteridines, 26*(3), 93-103.

Jiang, Y., Wang, M., Huang, K., Zhang, Z., Shao, N., Zhang, Y., . . . Wang, S. (2012). Oxidized low-density lipoprotein induces secretion of interleukin-1β by macrophages via reactive oxygen species-dependent NLRP3 inflammasome activation. *Biochemical and biophysical research communications, 425*(2), 121-126.

Johnson, B. W., & Boise, L. H. (1999). Bcl-2 and caspase inhibition cooperate to inhibit tumor necrosis factor-α-induced cell death in a Bcl-2 cleavage-independent fashion. *Journal of Biological Chemistry, 274*(26), 18552-18558.

Jürgensmeier, J. M., Xie, Z., Deveraux, Q., Ellerby, L., Bredesen, D., & Reed, J. C. (1998). Bax directly induces release of cytochrome c from isolated mitochondria. *Proceedings of the National Academy of Sciences, 95*(9), 4997-5002.

Kataoka, H., Kume, N., Miyamoto, S., Minami, M., Moriwaki, H., Murase, T., . . . Kita, T. (1999). Expression of lectinlike oxidized low-density lipoprotein receptor-1 in human atherosclerotic lesions. *Circulation, 99*(24), 3110-3117.

Kathryn J. Moore, and, F. J. S., & Fisher, E. A. (2013). Macrophages in atherosclerosis: A dynamic Balance. *Nature Reviews Immunology, 13*, 709-721. doi:10.1038/nri3520

Kerr, J. F., Wyllie, A. H., & Currie, A. R. (1972). Apoptosis: a basic biological phenomenon with wide-ranging implications in tissue kinetics. *British journal of cancer, 26*(4), 239.

Kinscherf, R., Claus, R., Wagner, M., Gehrke, C., Kamencic, H., Hou, D., . . . Pill, J. (1998). Apoptosis caused by oxidized LDL is manganese superoxide dismutase and p53 dependent. *The FASEB journal, 12*(6), 461-467.

Kirichok, Y., Krapivinsky, G., & Clapham, D. E. (2004). The mitochondrial calcium uniporter is a highly selective ion channel. *Nature, 427*(6972), 360-364.

Kluck, R. M., Bossy-Wetzel, E., Green, D. R., & Newmeyer, D. D. (1997). The release of cytochrome c from mitochondria: a primary site for Bcl-2 regulation of apoptosis. *Science, 275*(5303), 1132-1136.

Koya, R. C., Fujita, H., Shimizu, S., Ohtsu, M., Takimoto, M., Tsujimoto, Y., & Kuzumaki, N. (2000). Gelsolin inhibits apoptosis by blocking mitochondrial membrane potential

loss and cytochrome c release. *Journal of Biological Chemistry, 275*(20), 15343-15349.

Kroemer, G. (1997). The proto-oncogene Bcl-2 and its role in regulating apoptosis. *Nature medicine, 3*(6), 614-620.

Kruman, I., Guo, Q., & Mattson, M. P. (1998). Calcium and reactive oxygen species mediate staurosporine-induced mitochondrial dysfunction and apoptosis in PC12 cells. *Journal of neuroscience research, 51*(3), 293-308.

Kruman, I. I., & Mattson, M. P. (1999). Pivotal role of mitochondrial calcium uptake in neural cell apoptosis and necrosis. *Journal of neurochemistry, 72*(2), 529-540.

Kubo, N., Kikuchi, J., Furukawa, Y., Sakai, T., Ohta, H., Iwase, S., . . . Sakurabayashi, I. (1997). Regulatory effects of aggregated LDL on apoptosis during foam cell formation of human peripheral blood monocytes. *FEBS letters, 409*(2), 177-182.

Kusunoki, J., Hansoty, D. K., Aragane, K., Fallon, J. T., Badimon, J. J., & Fisher, E. A. (2001). Acyl-CoA: cholesterol acyltransferase inhibition reduces atherosclerosis in apolipoprotein E–deficient mice. *Circulation, 103*(21), 2604-2609.

Lawrie, A. M., Rizzuto, R., Pozzan, T., & Simpson, A. W. (1996). A role for calcium influx in the regulation of mitochondrial calcium in endothelial cells. *Journal of Biological Chemistry, 271*(18), 10753-10759.

Leon, C., Hill, J. S., & Wasan, K. M. (2005). Potential Role of Acyl-Coenzyme A:Cholesterol Transferase (ACAT)

Inhibitors as Hypolipidemic and Antiatherosclerosis Drugs. *Pharmaceutical Research, 22*(10), 1578-1588. doi:10.1007/s11095-005-6306-0

Levitan, I., Volkov, S., & Subbaiah, P. V. (2010). Oxidized LDL: diversity, patterns of recognition, and pathophysiology. *Antioxidants & redox signaling, 13*(1), 39-75.

Li, A. C., & Glass, C. K. (2002). The macrophage foam cell as a target for therapeutic intervention. *Nature medicine, 8*(11), 1235-1242.

Li, E., Wang, T., Wang, F., Wang, T., Sun, L.-q., Li, L., . . . Zhang, J.-y. (2015). FGF21 protects against ox-LDL induced apoptosis through suppressing CHOP expression in THP1 macrophage derived foam cells. *BMC Cardiovascular Disorders, 15*(1), 80.

Li, G., Scull, C., Ozcan, L., & Tabas, I. (2010). NADPH oxidase links endoplasmic reticulum stress, oxidative stress, and PKR activation to induce apoptosis. *The Journal of cell biology, 191*(6), 1113-1125.

Li, Y., Ge, M., Ciani, L., Kuriakose, G., Westover, E. J., Dura, M., . . . Lytton, J. (2004). Enrichment of Endoplasmic Reticulum with Cholesterol Inhibits Sarcoplasmic-Endoplasmic Reticulum Calcium ATPase-2b Activity in Parallel with Increased Order of Membrane Lipids IMPLICATIONS FOR DEPLETION OF ENDOPLASMIC

RETICULUM CALCIUM STORES AND APOPTOSIS IN CHOLESTEROL-LOADED MACROPHAGES. *Journal of Biological Chemistry, 279*(35), 37030-37039.

Libby, P. (2006). Atherosclerosis: Disease biology affecting the coronary vasculature. *American Journal of Cardiology, 98*(12A), 3Q-9Q. doi:10.1016/j.amjcard.2006.09.020

Libby, P., Ridker, P. M., & Hansson, G. K. (2009). Inflammation in atherosclerosis: from pathophysiology to practice. *Journal of the American College of Cardiology, 54*(23), 2129-2138.

Libby, P., Ridker, P. M., & Maseri, A. (2002). Inflammation and atherosclerosis. *Circulation, 105*(9), 1135-1143.

Lisa C. Crowley, B. J. M., Adrian P. Scott, and Nigel J. Waterhouse. Measuring Mitochondrial Transmembrane Potential by TMRE staining. *Cold Spring Harbor Protocols*.

Liu, Z., & Li, Y. (2013). Relationship between serum neopterin levels and coronary heart disease. *Genet. Mol. Res, 12*(4), 4222-4229.

Logue, S. E., Cleary, P., Saveljeva, S., & Samali, A. (2013). New directions in ER stress-induced cell death. *Apoptosis, 18*(5), 537-546.

Los, M., Mozoluk, M., Ferrari, D., Stepczynska, A., Stroh, C., Renz, A., . . . Schulze-Osthoff, K. (2002). Activation and caspase-mediated inhibition of PARP: a molecular switch between fibroblast necrosis and apoptosis in death receptor signaling. *Molecular biology of the cell, 13*(3), 978-988.

Ly, J. D., Grubb, D., & Lawen, A. (2003). The mitochondrial membrane potential (ΔΨm) in apoptosis; an update. *Apoptosis, 8*(2), 115-128.

Ma, Y., & Hendershot, L. M. (2004). ER chaperone functions during normal and stress conditions. *Journal of chemical neuroanatomy, 28*(1), 51-65.

Majno, G., & Joris, I. (1995). Apoptosis, oncosis, and necrosis. An overview of cell death. *The American journal of pathology, 146*(1), 3.

Marciniak, S. J., Yun, C. Y., Oyadomari, S., Novoa, I., Zhang, Y., Jungreis, R., . . . Ron, D. (2004). CHOP induces death by promoting protein synthesis and oxidation in the stressed endoplasmic reticulum. *Genes & development, 18*(24), 3066-3077.

Marzo, I., Brenner, C., Zamzami, N., Jürgensmeier, J. M., Susin, S. A., Vieira, H. L., . . . Reed, J. C. (1998). Bax and adenine nucleotide translocator cooperate in the mitochondrial control of apoptosis. *Science, 281*(5385), 2027-2031.

Meusser, B., Hirsch, C., Jarosch, E., & Sommer, T. (2005). ERAD: the long road to destruction. *Nature cell biology, 7*(8), 766-772.

Meyer, J. W., & Schmitt, M. E. (2000). A central role for the endothelial NADPH oxidase in atherosclerosis. *FEBS letters, 472*(1), 1-4.

Moore, K. J., & Freeman, M. W. (2006). Scavenger receptors in atherosclerosis beyond lipid uptake. *Arteriosclerosis, thrombosis, and vascular biology, 26*(8), 1702-1711.

Moore, K. J., & Tabas, I. (2011). Macrophages in the pathogenesis of atherosclerosis. *Cell, 145*(3), 341-355.

Mosmann, T. (1983). Rapid colorimetric assay for cellular growth and survival: application to proliferation and cytotoxicity assays. *Journal of immunological methods, 65*(1-2), 55-63.

Mukherjee, S., Kunitake, G., & Alfin-Slater, R. B. (1958). The esterification of cholesterol with palmitic acid by rat liver homogenates. *J Biol Chem, 230*(1), 91-96.

Müller, M. M., Curtius, H.-C., Herold, M., & Huber, C. H. (1991). Neopterin in clinical practice. *Clinica Chimica Acta, 201*(1-2), 1-16.

Nagy, L., Tontonoz, P., Alvarez, J. G., Chen, H., & Evans, R. M. (1998). Oxidized LDL regulates macrophage gene expression through ligand activation of PPARγ. *Cell, 93*(2), 229-240.

Nakayama, Y., Endo, M., Tsukano, H., Mori, M., Oike, Y., & Gotoh, T. (2010). Molecular mechanisms of the LPS-induced non-apoptotic ER stress-CHOP pathway. *The journal of biochemistry, 147*(4), 471-483.

Napoli, C., D'armiento, F. P., Mancini, F. P., Postiglione, A., Witztum, J. L., Palumbo, G., & Palinski, W. (1997). Fatty streak formation occurs in human fetal aortas and is greatly enhanced by maternal hypercholesterolemia. Intimal accumulation of low density lipoprotein and its oxidation precede monocyte recruitment into early atherosclerotic lesions. *Journal of Clinical Investigation, 100*(11), 2680.

Oettl, K., Greilberger, J., Dikalov, S., & Reibnegger, G. (2004). Interference of 7, 8-dihydroneopterin with peroxynitrite-mediated reactions. *Biochemical and biophysical research communications, 321*(2), 379-385.

Oettl, K., & Reibnegger, G. (2002). Pteridine derivatives as modulators of oxidative stress. *Current Drug Metabolism, 3*(2), 203-209.

Ou, H.-C., Song, T.-Y., Yeh, Y.-C., Huang, C.-Y., Yang, S.-F., Chiu, T.-H., . . . Tsai, C.-S. (2010). EGCG protects against oxidized LDL-induced endothelial dysfunction by inhibiting LOX-1-mediated signaling. *Journal of Applied Physiology, 108*(6), 1745-1756.

Ouriel, K. (2001). Peripheral arterial disease. *The lancet, 358*(9289), 1257-1264.

Oyadomari, S., & Mori, M. (2004). Roles of CHOP/GADD153 in endoplasmic reticulum stress. *Cell Death & Differentiation, 11*(4), 381-389.

Park, Y. M. (2014). CD36, a scavenger receptor implicated in atherosclerosis. *Experimental & molecular medicine, 46*(6), e99.

Pastorino, J. G., Tafani, M., Rothman, R. J., Marcineviciute, A., Hoek, J. B., & Farber, J. L. (1999). Functional consequences of the sustained or transient activation by Bax of the mitochondrial permeability transition pore. *Journal of Biological Chemistry, 274*(44), 31734-31739.

Petit, P. X., Goubern, M., Diolez, P., Susin, S. A., Zamzami, N., & Kroemer, G. (1998). Disruption of the outer mitochondrial membrane as a result of large amplitude swelling: the impact of irreversible permeability transition. *FEBS letters, 426*(1), 111-116.

Petit, P. X., Zamzami, N., Vayssière, J.-L., Mignotte, B., Kroemer, G., & Castedo, M. (1997). Implication of mitochondria in apoptosis. In *Detection of Mitochondrial Diseases* (pp. 185-188): Springer.

Pongnimitprasert, N. (2009). Atherosclerosis and nadph oxidase. *Silpakorn University Science and Technology Journal, 3*(1), 13-24.

Puthalakath, H., O'Reilly, L. A., Gunn, P., Lee, L., Kelly, P. N., Huntington, N. D., . . . Motoyama, N. (2007). ER stress triggers apoptosis by activating BH3-only protein Bim. *Cell, 129*(7), 1337-1349.

Rahaman, S. O., Lennon, D. J., Febbraio, M., Podrez, E. A., Hazen, S. L., & Silverstein, R. L. (2006). A CD36-dependent signaling cascade is necessary for macrophage foam cell formation. *Cell metabolism, 4*(3), 211-221.

Rasola, A., & Bernardi, P. (2007). The mitochondrial permeability transition pore and its involvement in cell death and in disease pathogenesis. *Apoptosis, 12*(5), 815-833.

Rezk, B. M., Haenen, G. R., van der Vijgh, W. J., & Bast, A. (2003). Tetrahydrofolate and 5-methyltetrahydrofolate are folates with high antioxidant activity. Identification of the antioxidant pharmacophore. *FEBS letters, 555*(3), 601-605.

Rodriguez, A., Bachorik, P. S., & Wee, S.-B. (1999). Novel effects of the acyl-coenzyme A: cholesterol acyltransferase inhibitor 58-035 on foam cell development in primary human monocyte–derived macrophages. *Arteriosclerosis, thrombosis, and vascular biology, 19*(9), 2199-2206.

Ron, D., & Walter, P. (2007). Signal integration in the endoplasmic reticulum unfolded protein response. *Nature reviews. Molecular cell biology, 8*(7), 519.

Rosenfeld, M. E. (1996). Cellular mechanisms in the development of atherosclerosis 1. *Diabetes research and clinical practice, 30*, S1-S11.

Ross, R. (1993). Rous-Whipple Award Lecture. Atherosclerosis: a defense mechanism gone awry. *The American journal of pathology, 143*(4), 987.

Satchell, L., & Leake, D. S. (2012). Oxidation of low-density lipoprotein by iron at lysosomal pH: implications for atherosclerosis. *Biochemistry, 51*(18), 3767-3775.

Sawamura, T., Kume, N., Aoyama, T., Moriwaki, H., Hoshikawa, H., Aiba, Y., . . . Kita, T. (1997). An endothelial receptor for oxidized low-density lipoprotein. *Nature, 386*(6620), 73.

Scaduto, R. C., & Grotyohann, L. W. (1999). Measurement of mitochondrial membrane potential using fluorescent rhodamine derivatives. *Biophysical journal, 76*(1), 469-477.

Scarlett, J. L., & Murphy, M. P. (1997). Release of apoptogenic proteins from the mitochondrial intermembrane space during the mitochondrial permeability transition. *FEBS letters, 418*(3), 282-286.

Schiffrin, E. L., Lipman, M. L., & Mann, J. F. (2007). Chronic kidney disease. *Circulation, 116*(1), 85-97.

Schobersberger, W., Hoffmann, G., Hobisch-Hagen, P., Böck, G., Völkl, H., Baier-Bitterlich, G., . . . Fuchs, D. (1996). Neopterin and 7, 8-dihydroneopterin induce apoptosis in the rat alveolar epithelial cell line L2. *FEBS letters, 397*(2-3), 263-268.

Scorrano, L., Oakes, S. A., Opferman, J. T., Cheng, E. H., Sorcinelli, M. D., Pozzan, T., & Korsmeyer, S. J. (2003). BAX and BAK regulation of endoplasmic reticulum Ca2+: a control point for apoptosis. *Science, 300*(5616), 135-139.

Scull, C. M., & Tabas, I. (2011). Mechanisms of ER stress-induced apoptosis in atherosclerosis. *Arteriosclerosis, thrombosis, and vascular biology, 31*(12), 2792-2797.

Shapiro, H. M. (1994). Cell membrane potential analysis. *Methods in cell biology, 41*, 121-133.

Shchepetkina, A. (2013). Mechanisms of 7, 8-dihydroneopterin protection of macrophages from cytotoxicity.

Shen, J., Chen, X., Hendershot, L., & Prywes, R. (2002). ER stress regulation of ATF6 localization by dissociation of BiP/GRP78 binding and unmasking of Golgi localization signals. *Developmental cell, 3*(1), 99-111.

Shimizu, S., Ide, T., Yanagida, T., & Tsujimoto, Y. (2000). Electrophysiological study of a novel large pore formed by Bax and the voltage-dependent anion channel that is

permeable to cytochrome c. *Journal of Biological Chemistry, 275*(16), 12321-12325.

Shimizu, S., Narita, M., & Tsujimoto, Y. (1999). Bcl-2 family proteins regulate the release of apoptogenic cytochrome c by the mitochondrial channel VDAC. *Nature, 399*(6735), 483-487.

Shimizu, S., & Tsujimoto, Y. (2000). Proapoptotic BH3-only Bcl-2 family members induce cytochrome c release, but not mitochondrial membrane potential loss, and do not directly modulate voltage-dependent anion channel activity. *Proceedings of the National Academy of Sciences, 97*(2), 577-582.

Shutong Yao, C. M., Hua Tian, Hui Sang, Nana Yang, Peng Jiao, Jiju Han, Chuanlong Zong, and Shucun Qin. (2014). Endoplasmic Reticulum Stress Promotes Macrophagederived Foam Cell Formation by Up-regulating Cluster of Differentiation 36 (CD36) Expression. *The Journal Of Biological Chemistry, 289*, 4032-4042.

Sobieszczyk, P., & Beckman, J. (2006). Carotid artery disease. *Circulation, 114*(7), e244-e247.

Stacchiotti, A., Favero, G., & Rezzani, R. (2013). Endoplasmic reticulum stress in the endothelium: a contribution to athero-susceptibility. In *Current Trends in Atherogenesis*: InTech.

Stary, H. C., Chandler, A. B., Dinsmore, R. E., Fuster, V., Glagov, S., Insull, W., . . . Wissler, R. W. (1995). A DEFINITION OF ADVANCED TYPES OF ATHEROSCLEROTIC LESIONS AND A HISTOLOGICAL CLASSIFICATION OF ATHEROSCLEROSIS - A REPORT FROM THE COMMITTEE-ON-VASCULAR-LESIONS OF THE COUNCIL-ON-ARTERIOSCLEROSIS, AMERICAN-HEART-ASSOCIATION. *Arteriosclerosis Thrombosis and Vascular Biology, 15*(9), 1512-1531.

Steinberg, D. (2002). Atherogenesis in perspective: hypercholesterolemia and inflammation as partners in crime. *Nature medicine, 8*(11), 1211-1217.

Syntichaki, P., & Tavernarakis, N. (2003). The biochemistry of neuronal necrosis: rogue biology? *Nature reviews. Neuroscience, 4*(8), 672.

Tabas, I. (2004). Apoptosis and plaque destabilization in atherosclerosis: the role of macrophage apoptosis induced by cholesterol. *Cell Death & Differentiation, 11*, S12-S16.

Tabas, I., Williams, K. J., & Borén, J. (2007). Subendothelial lipoprotein retention as the initiating process in atherosclerosis update and therapeutic implications. *Circulation, 116*(16), 1832-1844.

Tait, S. W., & Green, D. R. (2010). Mitochondria and cell death: outer membrane permeabilization and beyond. *Nature reviews. Molecular cell biology, 11*(9), 621.

Tao, J. T. J.-l., Ruan, X. R. X.-z., Li, H. L. H., Li, X. L. X.-m., Moorhead, J. M., John F.); , Varghese, Z. V., Zac); , & Li, X. L. X.-w. (2009). Endoplasmic reticulum stress is involved in acetylated low-density lipoprotein induced apoptosis in THP-1 differentiated macrophages. *CHINESE MEDICAL JOURNAL, 122*(15), 1794-1799. doi:10.3760/cma.j.issn.0366-6999.2009.15.015

Taylor, R. C., Cullen, S. P., & Martin, S. J. (2008). Apoptosis: controlled demolition at the cellular level. *Nature reviews. Molecular cell biology, 9*(3), 231.

Timmins, J. M., Ozcan, L., Seimon, T. A., Li, G., Malagelada, C., Backs, J., . . . Anderson, M. E. (2009). Calcium/calmodulin-dependent protein kinase II links ER stress with Fas and mitochondrial apoptosis pathways. *The Journal of clinical investigation, 119*(10), 2925-2941.

Tontonoz, P., Nagy, L., Alvarez, J. G., Thomazy, V. A., & Evans, R. M. (1998). PPARγ promotes monocyte/macrophage differentiation and uptake of oxidized LDL. *Cell, 93*(2), 241-252.

Travers, K. J., Patil, C. K., Wodicka, L., Lockhart, D. J., Weissman, J. S., & Walter, P. (2000). Functional and genomic analyses reveal an essential coordination between the unfolded protein response and ER-associated degradation. *Cell, 101*(3), 249-258.

Tu, B. P., & Weissman, J. S. (2004). Oxidative protein folding in eukaryotes. *The Journal of cell biology, 164*(3), 341-346.

Van Eck, M., Pennings, M., Hoekstra, M., Out, R., & Van Berkel, T. J. (2005). Scavenger receptor BI and ATP-binding cassette transporter A1 in reverse cholesterol transport and atherosclerosis. *Current Opinion in Lipidology, 16*(3), 307-315.

Von Ahsen, O., Renken, C., Perkins, G., Kluck, R. M., Bossy-Wetzel, E., & Newmeyer, D. D. (2000). Preservation of mitochondrial structure and function after Bid-or Bax-mediated cytochrome c release. *The Journal of cell biology, 150*(5), 1027-1036.

Wachter, H., Fuchs, D., Hausen, A., Reibnegger, G., Weiss, G., Werner, E., & Werner-Felmayer, G. (1992). *Neopterin: biochemistry-methods-clinical application*: Walter de Gruyter.

Wang, X. Z., Harding, H. P., Zhang, Y., Jolicoeur, E. M., Kuroda, M., & Ron, D. (1998). Cloning of mammalian Ire1 reveals diversity in the ER stress responses. *The EMBO journal, 17*(19), 5708-5717.

Waring, P., & Beaver, J. (1996). Cyclosporin A rescues thymocytes from apoptosis induced by very low concentrations of thapsigargin: effects on mitochondrial function. *Experimental cell research, 227*(2), 264-276.

Webb, N. R., De Villiers, W., Connell, P. M., de Beer, F. C., & van der Westhuyzen, D. R. (1997). Alternative forms of the scavenger receptor BI (SR-BI). *Journal of lipid research, 38*(7), 1490-1495.

Weiss, G., Fuchs, D., Hausen, A., Reibnegger, G., Werner, E. R., Werner-Felmayer, G., . . . Wachter, H. (1993). Neopterin modulates toxicity mediated by reactive oxygen and chloride species. *FEBS letters, 321*(1), 89-92.

Werner-Felmayer, G., Baier-Bitterlich, G., Fuchs, D., Hausen, A., Murr, C., Reibnegger, G., . . . Wachter, H. (1995). Detection of bacterial pyrogens on the basis of their effects on gamma interferon-mediated formation of neopterin or nitrite in cultured monocyte cell lines. *Clinical and diagnostic laboratory immunology, 2*(3), 307-313.

Werner-Felmayer, G., Werner, E. R., Fuchs, D., Hausen, A., Reibnegger, G., & Wachter, H. (1990). Neopterin formation and tryptophan degradation by a human myelomonocytic cell line (THP-1) upon cytokine treatment. *Cancer research, 50*(10), 2863-2867.

Werner, E. R., Werner-Felmayer, G., Fuchs, D., Hausen, A., Reibnegger, G., Yim, J., . . . Wachter, H. (1990). Tetrahydrobiopterin biosynthetic activities in human macrophages, fibroblasts, THP-1, and T 24 cells. GTP-cyclohydrolase I is stimulated by interferon-gamma, and 6-pyruvoyl tetrahydropterin synthase and sepiapterin reductase are constitutively present. *Journal of Biological Chemistry, 265*(6), 3189-3192.

Williams, K. J., & Tabas, I. (1995). The response-to-retention hypothesis of early atherogenesis. *Arteriosclerosis, thrombosis, and vascular biology, 15*(5), 551-561.

Wirleitner, B., Baier-Bitterlich, G., Böck, G., Widner, B., & Fuchs, D. (1998). 7, 8-Dihydroneopterin-induced apoptosis in Jurkat T lymphocytes: a comparison with

anti-Fas-and hydrogen peroxide-mediated cell death. *Biochemical pharmacology, 56*(9), 1181-1187.

Wirleitner, B., Czaputa, R., Oettl, K., Böck, G., Widner, B., Reibnegger, G., . . . Baier-Bitterlich, G. (2001). Induction of Afoptosis by 7, 8-Dihydroneopterin: Involvement of Radical Formation. *Immunobiology, 203*(4), 629-641.

XIaochen Yu, Yang Wang, Wenhui Zhao, and, W. Y., & Guan, X. (2014). Toll-like receptor 7 promotes the apoptosis of THP-1-derived macrophages through CHOP dependent pathway. *International Journal of Molecular Medicine, 34*, 886-893. doi:10.3892/ijmm.2014.1833

Xu, C., Bailly-Maitre, B., & Reed, J. C. (2005). Endoplasmic reticulum stress: cell life and death decisions. *Journal of Clinical Investigation, 115*(10), 2656.

Yang, J., Liu, X., Bhalla, K., Kim, C. N., Ibrado, A. M., Cai, J., . . . Wang, X. (1997). Prevention of apoptosis by Bcl-2: release of cytochrome c from mitochondria blocked. *Science, 275*(5303), 1129-1132.

Yang, Y. T., Whiteman, M., & Gieseg, S. P. (2012). Intracellular glutathione protects human monocyte-derived macrophages from hypochlorite damage. *Life Sci, 90*(17-18), 682-688. doi:10.1016/j.lfs.2012.03.002

Yao, S., Yang, N., Song, G., Sang, H., Tian, H., Miao, C., . . . Qin, S. (2012). Minimally modified low-density lipoprotein induces macrophage endoplasmic reticulum stress via toll-like receptor 4. *Biochimica et Biophysica Acta (BBA)-Molecular and Cell Biology of Lipids, 1821*(7), 954-963.

Yao, S., Zong, C., Zhang, Y., Sang, H., Yang, M., Jiao, P., . . . Qin, S. (2013). Activating transcription factor 6 mediates oxidized LDL-induced cholesterol accumulation and apoptosis in macrophages by up-regulating CHOP expression. *Journal of atherosclerosis and thrombosis, 20*(1), 94-107.

Ye, J., Rawson, R. B., Komuro, R., Chen, X., Davé, U. P., Prywes, R., . . . Goldstein, J. L. (2000). ER stress induces cleavage of membrane-bound ATF6 by the same proteases that process SREBPs. *Molecular cell, 6*(6), 1355-1364.

Yoshida, H., Matsui, T., Yamamoto, A., Okada, T., & Mori, K. (2001). XBP1 mRNA is induced by ATF6 and spliced by IRE1 in response to ER stress to produce a highly active transcription factor. *Cell, 107*(7), 881-891.

Yoshino, T., Kishi, H., Nagata, T., Tsukada, K., Saito, S., & Muraguchi, A. (2001). Differential involvement of p38 MAP kinase pathway and Bax translocation in the mitochondria-mediated cell death in TCR-and dexamethasone-stimulated thymocytes. *European journal of immunology, 31*(9), 2702-2708.

Zamzami, N., Marchetti, P., Castedo, M., Zanin, C., Vayssiere, J.-L., Petit, P. X., & Kroemer, G. (1995). Reduction in mitochondrial potential constitutes an early irreversible step

of programmed lymphocyte death in vivo. *Journal of Experimental Medicine, 181*(5), 1661-1672.

Zhuang, J., Dinsdale, D., & Cohen, G. M. (1998). Apoptosis, in human monocytic THP. 1 cells, results in the release of cytochrome c from mitochondria prior to their ultracondensation, formation of outer membrane discontinuities and reduction in inner membrane potential. *Cell death and differentiation, 5*(11), 953-962.

Zoratti, M., & Szabò, I. (1995). The mitochondrial permeability transition. *Biochimica et Biophysica Acta (BBA)-Reviews on Biomembranes, 1241*(2), 139-176.

6 APPENDIX

Cell Line	Antagonist	Result	Assay used/Techniques used	References
THP-1	• PD98058 (P-ERK signalling specific inhibitor) • FGF21 (Fibroblast Growth Factor 21) • siRNA directed against ERK. • Cu-oxLDL	• FGF21 decreases foam cell formation with reduced lipid droplets, 7KC induced apoptosis and TC levels. • Inhibitor blocked Phospho-ERK signalling and decreased ERK1/2 levels. • FGF21 suppressed 7KC induced CHOP expression and DR5 (Death receptor 5).	• siRNA transfection • Western blotting	• (E. Li et al., 2015)
	• IVA (Influenza Virus A) • DEX (Dexamethasone, Anti-inflammatory agent, regulates T cell survival, growth, and differentiation. Inhibits the Induction of nitric oxide synthase) • IMQ (imiquimod, TLR7 agonist) • Tunicamycin • oxLDL (Purchased from supplier)	• mRNA expression of TLR7 was detected in IVA infected, and IMQ treated group indicating the activation of TLR7 by IMQ treatment and IVA infection. • Various IMQ concentrations induced apoptosis activating TLR7. • IMQ had no antiviral effect in vitro. DEX inhibited pro-inflammatory cytokine secretion without a reduction in apoptosis. • oxLDL triggered apoptosis with TLR7 activation. • IVA infection induced ER stress and that CHOP played a role in IVA-induced apoptosis. • mRNA expression of GRP78 depicted a 10 fold increase and CHOP depicted 2000 fold	• ELISA • Western Blotting • RT-PCR • Q-PCR • MTT assay • Apoptosis by flow cytometry.	• (XIaochen Yu, Yang Wang, Wenhui Zhao, and, & Guan, 2014)

		increase when cells were treated with tunicamycin.		
	• acLDL	• cells underwent apoptosis with increasing LDL concentrations. • Caspase 3, 7 activities increased with 100 ug/mL acLDL. • acLDL induced intracellular TC and CE (Total Cholesterol and Cholesteryl esters) • CHOP levels increased with increasing acLDL concentration in a time-dependent manner. • acLDL induced FC triggered apoptosis by trafficking cholesterol to ER upregulating CHOP expression.	• Oil Red O staining. • HPLC • Hoechst staining • Caspase 3, 7 assays • ER cholesterol pool assay assayed FC. • Western blotting for CHOP and Bcl-2 detection	• (Tao et al., 2009)
Peritoneal Macrophages (From C57BL6/J WT mice)	• acLDL • KN93 • KN92 • SP600125 • ACAT Inhibitor S58035 • Tunicamycin • N-acetylcysteine • Thapsigargin	• Calcium-induced CaMKII activation induces NOX and oxidative stress that are necessary for ER-stress induced apoptosis. • ER-stress – CHOP – Calcium – CaMKII – JNK apoptotic pathway is bidirectional rather than linear. • NOX2 deficiency suppressed both CaMKII activation and CHOP induction under ER-stress conditions. • Partial induction of CHOP resulted in decreased apoptosis.	• Calcium Imaging • Apoptosis assay • RT-QPCR • Immunoblotting • Mitochondrial Calcium uptake. • Mitochondrial membrane potential.	• (G. Li et al., 2010)
	• ACAT Inhibitor S58035. • Cholesterol • U18666A (Amphipathic	• Nanomolar concentrations of U18666A reduced re-esterification of ingested cholesterol by 90% but	• Apoptosis Assay (Annexin v/PI). • Whole-cell cholesterol	• (B. Feng et al., 2003)

	amine, inhibitor of multiple cholesterol trafficking pathways from late endosomes) • Androstenediol (A structurally related homolog of U18666A) • M-β-CD or CD (Methyl-Beta-Cyclodextrin). • Concavalin A • Thapsigargin • Tunicamycin • A32187 • acLDL	did not affect the accumulation of cholesterol in the plasma membrane. • acLDL induced FC uptake by macrophages in the presence of ACAT inhibitor, and U18666A protected macrophages from FC-induced apoptosis. • Androstenediol does not block cholesterol trafficking to ER in macrophages, did not block acLDL induced FC-induced cell death even at higher concentrations (1 uM). • Accumulation of excess FC (using CD: Chol) in the plasma membrane is not sufficient to induce apoptosis in FC-loaded macrophages compared with cells loaded through endocytic lipoprotein pathway (using acLDL). • Blocking cholesterol traffic to ER membranes with a low dose of U18666A blocked CHOP induction in acLDL induced FC-loaded macrophages. • CHOP induction by acLDL induced androstenediol did not block FC, and neither did U18666A blocked CHOP induction by A23187 suggesting U18666A is not a direct inhibitor of CHOP nor general induction of UPR.	esterification assay. • Cholesterol Oxidase Assay. • Immunoblotting • Assay of endoplasmic reticulum calcium pools. • In-situ hybridization. Quantitative RT-PCR • Laser Capture microdetection (LCM) and RNA extraction.	

		• The addition of nanomolar concentrations of U18666A attenuated XBP1, CHOP, ATF4, and PERK which are downstream effectors of UPR.		
	• ACAT Inhibitor S58035 • M-β-CD or CD (Methyl-B-Cyclodextrin) • acLDL • Thapsigargin (Sarcoendoplasmic reticulum calcium ATPase inhibitor) • Tunicamycin (Protein glycosylation Inhibitor) • Staurosporine (p38 activator)	• acLDL induced FC loading in macrophages induced CHOP after 10h from WT mice. • P38 phosphorylation showed a biphasic pattern; moderate expression of 2-5 hr after acLDL induced FC loading, decreased expression between 5-10 hr and increased expression by 15h. • CHOP expression was consistent after acLDL induced FC loading to 15h. • Staurosporine did not activate CHOP. • FC loading by Chol: CD did not induce apoptosis. • FC loading induced by CD-Chol lead to the induction of CHOP and Phospho-PERK.	• Cell death Assay (Apoptosis assay using annexin V/PI) • Whole cell esterification Assay. • Immunoblotting.	• (DeVries-Seimon et al., 2005)
Murine RAW264.7 macrophages	• siRNA transfection against ATF-6, IRE-1, PERK, GRP78, and CD36. • Cu-oxLDL • TM (Tunicamycin, ER-stress inducer) • PBA (4-phenylbutric	• oxLDL uptake by CD36 induced ER-stress in the cells was observed when TM promoted uptake of ox-LDL in a concentration-dependent manner (0.5 – 2 mg/L), and PBA inhibited ox-LDL uptake by TM. • TM up-regulated the levels of CD36 protein and mRNA in	• Lipid uptake assay using oil red O stain. • Immunofluorescence assay for ATF-6 nuclear relocation (ATF6 antibody 1:100 sc-22799) • Western blotting.	• (Shutong Yao, 2014)

	acid ER-stress inhibitor)	concentration and time-dependent manner. • Exposure of cells with TM and ox-LDL together or alone all induced ER-stress as determined by phosphorylation of PERK and IRE-1 and upregulation of XBP-1, GRP78 and nuclear translocation of ATF6. • GRP78 levels were higher in macrophages treated with ox-LDL and TM together as compared to macrophages treated with ox-LDL alone. • siRNA directed against ATF6, IRE-1 and GRP78 reduced oxLDL induced CD36 protein upregulation. • ER-stress inducer PBA reduced CD36 upregulation in apoE deficient mice.		
	• Cholesterol • Synthetic phospholipids • ACAT inhibitor S58035 • M-β-CD (Methyl-Beta-cyclodextrin) • Thapsigargin • acLDL	• The research study also includes mouse peritoneal macrophages from C57BL6/J WT mice, HEK293 cells, and microsomes. • acLDL induced FC-loaded macrophages, and mouse peritoneal macrophages express SERCA2b. Control mouse peritoneal macrophages express CHOP after 5h of acLDL induced FC loading. • When SERCA2b-containing microsomes were incubated with CD: Chol, it inhibited both SERCA2b calcium	• Endoplasmic reticulum membrane fractionation. • Spectrophotometric assay (For measurement of Ca2+ dependent ATPase activity). • ATP-mediated oxalate-dependent assay. • Immunoblotting • ESR spectroscopy.	• (Y. Li et al., 2004)

		ATPase activity and SERCA2b mediated calcium uptake in a dose-dependent manner.		
MCF-7 cells (Thymocytes, Peritoneal macrophages, and breast cancer derived cell line)	• Thapsigargin • Tunicamycin • TMB-8 (intracellular calcium release antagonist) • U0126 (ERK inhibitor) • **NO LIPID LOADING**	• CHOP is critical for transcriptional up-regulation of Bim. • Bim proteins and BIM mRNA increased significantly in WT thymocytes. • Peritoneal macrophages from $chop^{-/-}$ mice were reported to be abnormally resistant to apoptosis induced by the ER stressors indomethacin or Thapsigargin. • $Chop^{-/-}$ mice failed to upregulate Bim in response to treatment with Thapsigargin. • Thapsigargin upregulates Bim and CHOP expressions	• Western blotting • Northern blotting • Q-PCR	• (Puthalakath et al., 2007)
ETNA cells (Derived from striatum primordia of WT or apaf-/- embryos which are apoptosome deficient)	• Tunicamycin • Thapsigargin • Brefeldin A • **NO LIPID LOADING.**	• UPR markers CHOP, GRP78 upregulated by UPR receptors IRE1, ATF6 and PERK by the addition of Tunicamycin • Mitochondria released cytochrome c when ER-stress was induced by Er-stress inducers Tunicamycin, Thapsigargin or Brefeldin A.	• Apoptosis evaluation by Flow cytometry • CHOP was measured by Western blotting (1:1000 dilution).	• (Di Sano et al., 2006)
HepG2 Cells	• NaF • Tunicamycin • Thapsigargin • ATF4 siRNA • CHOP siRNA • **NO LIPID LOADING.**	• Cell viability decreased to 70%, 54% and 35% in NaF, Tu and Tg treatment groups respectively. • NaF and Tu resulted in autophagosome formation which was	• MTT assay • Hoechst staining • Monodasylcadaverin staining • Western Blotting.	• (Hiroki Matsumoto et al., 2013)

		assessed by MDC (mono dansylcadaverine) • Tg alone induced apoptosis. • Tg treatment increased phospho-eIF2α, ATF4, CHOP, IRE1 and GRP levels • The addition of ATF4 siRNA to Tu and NaF treated cells suppressed autophagy activated by ER-stress inducers. • The addition of CHOP siRNA to NaF and Tu treated cells did not suppress autophagy, but in turn, Tg-treated cells activated autophagy with increased ATF4 expression suppressing CHOP.		
HUVECs (Human umbilical vein endothelial cells)	• shRNA is targeting LOX-1 transcript. • Nox-4 siRNA transfection. • Ire-statin (IRE-1 inhibitor) • Salubrinal (eIF2 inhibitor) • AEBSF (ATF6 inhibitor) • oxLDL	• oxLDL activated ER-sensors IRE-1, PERK, GRP78 through LOX-1. • The inhibitors prevented oxLDL-induced EC apoptosis. • oxLDL activated proapoptotic mediators (CHOP, Bcl-2 and Caspase 12).	• siRNA transfection • Western Blotting • PCR	• (Hong et al., 2014)